Transport phenomena in correlated quantum liquids: Ultracold Fermi gases and F/N junctions

Author: Hua Li

Boston College

The Graduate School of Arts and Sciences

Department of Physics

TRANSPORT PHENOMENA IN CORRELATED QUANTUM LIQUIDS: ULTRACOLD FERMI GASES AND F/N JUNCTIONS

a dissertation

by

HUA LI

submitted in partial fulfillment of the requirements

for the degree of

Doctor of Philosophy

March 2016

TRANSPORT PHENOMENA IN CORRELATED QUANTUM LIQUIDS: ULTRACOLD FERMI GASES AND F/N JUNCTIONS

by

HUA LI

Dissertation Advisor: Prof. KEVIN S. BEDELL

ABSTRACT

Landau Fermi-liquid theory was first introduced by L. D. Landau in the effort of understanding the normal state of Fermi systems, where the application of the concept of elementary excitations to the Fermi systems has proved very fruitful in clarifying the physics of strongly correlated quantum systems at low temperatures. In this thesis, I use Landau Fermi-liquid theory to study the transport phenomena of two different correlated quantum liquids: the strongly interacting ultracold Fermi gases and the ferromagnet/normal-metal (F/N) junctions. The detailed work is presented in chapter II and chapter III of this thesis, respectively. Chapter I holds the introductory part and the background knowledge of this thesis.

In chapter II, I study the transport properties of a Fermi gas with strong attractive interactions close to the unitary limit. In particular, I compute the transport lifetimes of the Fermi gas due to superfluid fluctuations above the BCS transition temperature T_c. To calculate the transport lifetimes I need the scattering amplitudes. The scattering amplitudes are dominated by the superfluid fluctuations at temperatures just above T_c. The normal scattering amplitudes are calculated from the Landau parameters. These Landau parameters are obtained from the local version of the induced interaction model for computing Landau

parameters. I also calculate the leading order finite temperature corrections to the various transport lifetimes. A calculation of the spin diffusion coefficient is presented in comparison to the experimental findings. Upon choosing a proper value of F_0^a, I am able to present a good match between the theoretical result and the experimental measurement, which indicates the presence of the superfluid fluctuations near T_c. Calculations of the viscosity, the viscosity/entropy ratio and the thermal conductivity are also shown in support of the appearance of the superfluid fluctuations.

In chapter III, I study the spin transport in the low temperature regime (often referred to as the precession-dominated regime) between a ferromagnetic Fermi liquid (FFL) and a normal metal metallic Fermi liquid (NFL), also known as the F/N junction, which is considered as one of the most basic spintronic devices. In particular, I explore the propagation of spin waves and transport of magnetization through the interface of the F/N junction where nonequilibrium spin polarization is created on the normal metal side of the junction by electrical spin injection. I calculate the probable spin wave modes in the precession-dominated regime on both sides of the junction especially on the NFL side where the system is out of equilibrium. Proper boundary conditions at the interface are introduced to establish the transport of the spin properties through the F/N junction. A possible transmission conduction electron spin resonance (CESR) experiment is suggested on the F/N junction to see if the predicted spin wave modes could indeed propagate through the junction. Potential applications based on this novel spin transport feature of the F/N junction are proposed in the end.

Dedicated to my family

ACKNOWLEDGEMENTS

"Time flies when you are having fun." As I am writing this thesis, I can not help but think about this phrase. It almost feels like yesterday when I first joined the physics department six and a half years ago, and it has truly turned into a joyful journey ever since. I am very grateful for all the help and supports I received from the department, the faculty members and my colleagues along the way.

First and foremost, I would like to thank my advisor Professor Kevin Bedell for his guidance throughout the years I worked with him. Professor Bedell took me in as his student in my second year at Boston College, and he has been an amazing advisor since. He showed great patience walking me through the fundamentals in research when I first started working with him, and he was always there whenever I needed help. He is very intelligent, full of ideas and always encourages me to try and look into new things. The mentorship goes beyond research and academics as he would often share his life experience with me. Not only did I learn a lot of physics from him, but I also grow tremendously as a person working with him. Without him, I would not become who I am today writing up this thesis.

I would also like to thank Professor David Broido who I had worked with over the first summer I spent at Boston College. I would like to thank a lot of my colleagues who I had the pleasure to work with and learn from. In particular, Dr. Yi Zhang, Dr. Fan Ye, Dr. Yun Peng, Dr. Yuan-Ming Lu, Dr. Tian-Yi Sun, James Dusty Stokes, Dr. Daniel Walkup, Kun Jiang, Bing Ye, Matt Gochan and the list goes on. I thank the department of physics for supporting

me throughout my PhD by providing me teaching assistantships every year and I thank all the professors I had taken courses from and worked for as teaching assistants. I greatly appreciate the staff members of the physics department, Jane Carter, Nancy Chevry, Sile Power, Gisele Byda and Joyce Light, for assisting and helping me in various different ways.

In the end, I would like to express my sincere appreciation to my parents for their hard work and sacrifice in raising me and supporting me all the way through college. I attribute all my achievements to my parents and dedicate this thesis to them.

TABLE OF CONTENTS

LIST OF FIGURES

Figure

LIST OF ABBREVIATIONS

F/N ferromagnet/normal-metal

FFL ferromagnetic Fermi liquid

NFL normal metal metallic Fermi liquid

CESR conduction electron spin resonance

BEC Bose-Einstein condensation

QEQ quasiequilibrium

p-h particle-hole

ESR electron spin resonance

CHAPTER I

Introduction and Background Knowledge

Landau Fermi-liquid theory is among the many achievements of the Soviet physicist L. D. Landau in theoretical physics. The phenomenological theory of Fermi liquids concerns mainly the study of the normal state of Fermi systems. It introduces the concept of elementary excitations, which are the fermion quasiparticles for a Fermi system. When applied to the normal state of strongly interacting quantum systems, Landau Fermi-liquid theory has achieved great success in understanding the low temperature thermodynamic properties, such as specific heat, magnetic susceptibility and compressibility; transport properties including spin diffusion, viscosity and thermal conduction; as well as collective properties like spin waves. Since this thesis is largely based on the application of Landau Fermi-liquid theory to the study of the transport phenomena in correlated quantum liquids, brief introductions to a few key pieces of knowledge of Landau Fermi-liquid theory related to this work are presented in the sections to follow. For a complete review on the topic of Landau Fermi-liquid theory, the reader may refer to the books by Baym and Pethick [1], and Pines and Nozieres [2], which provide thorough illustrations of the phenomenological theory. The profundity of Landau Fermi-liquid theory goes beyond mere phenomenology as it is closely linked to the many body microscopic theory of quantum liquids. The reader may refer to the Nozieres book

[3] for a detailed derivation of Landau Fermi-liquid theory from microscopic first principles.

In order to have a continuous flow of knowledge in this thesis, the introductions to the two different correlated quantum liquids studied in this work: the strongly interacting ultracold Fermi gases and the F/N junctions, are postponed until their respective chapters.

1.1 Quasiparticles

In Landau Fermi-liquid theory, the fermion quasiparticles are the elementary excitations of a correlated Fermi system. The name "quasiparticle" itself indicates an analogy between the Fermi-liquid quasiparticles and the bare fermion particles. To understand the analogy, let us first consider an "ideal" Fermi gas — that is, a gas of noninteracting fermions — of N fermion particles, each of mass m, confined in a volume V. The quantum states of each individual fermion particle are characterized by two quantum numbers, the momentum $\mathbf{p}$ and the spin $\sigma = \pm\frac{\hbar}{2}$ of the particle. The single particle wave function takes the form of a simple plane wave:

$$\psi_{\mathbf{p}}(\mathbf{r}) = \frac{1}{\sqrt{V}} e^{i\mathbf{p}\cdot\mathbf{r}}. \tag{1.1}$$

The eigenstates of the system is the antisymmetric combinations of N such single particle states, the wave functions of which are the Slater determinants of N simple plane waves shown above. It is enough to characterize an energy eigenstate of the noninteracting Fermi gas by specifying a distribution function $n_{\mathbf{p}\sigma}$ to indicate the occupancies of different single particle states, which equals to 1 if the state $\mathbf{p}, \sigma$ is occupied and to zero otherwise. Each single particle state allows at most one fermion according to Pauli exclusion principle for fermions. The ground state of the system is formed by filling all N particles in the single particle states one by

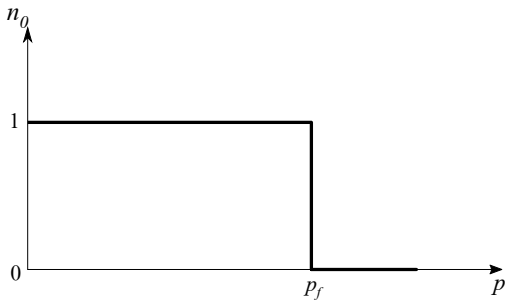

Figure 1.1: The ground state particle distribution function.

one from the lowest possible momentum state, and we end up with a state where all single particle states with momentum less than the Fermi momentum, p_f, are occupied and all other states are left empty, the Fermi momentum being given by

$$\frac{N}{V} = \frac{1}{3\pi^2}\left(\frac{p_f}{\hbar}\right)^3. \tag{1.2}$$

The ground state distribution function $n^0_{\mathbf{p}\sigma}$ takes the form shown in Fig. 1.1. The surface defined by $|\mathbf{p}| = p_f$ in the momentum space forms the so called Fermi surface, and the energy of the particles on the Fermi surface defines the chemical potential μ. At low temperatures, the energetically low-lying excited states of the system may be created by either adding a particle with momentum greater than p_f to the system, referred to as a particle-like excitation, or removing a particle with momentum less than p_f from the system, referred to as a hole-like excitation. Any excited energy eigenstaes of the system can be constructed by creating different numbers of such fermion-like elementary excitations — particles and holes — in the system.

For a real Fermi liquid where fermion particles interact with each other, the Landau theory establishes a one-to-one correspondence between the eigenstates of the real correlated Fermi liquid and the eigenstates of the ideal Fermi gas. One can imagine the eigenstates of the correlated Fermi liquid gradually evolving from the eigenstates of the ideal Fermi gas by slowly turning on the interaction

between particles. The ground state of the correlated Fermi liquid emerges from the ideal Fermi gas ground state specified by its particle distribution function $n^0_{\mathbf{p}\sigma}$. Quasiparticles and quasiholes are defined as the elementary fermion-like excitations of the correlated system analogous to the particles and holes in the ideal Fermi gas, which can be thought of as the fully dressed particle-like and hole-like motions caused by adiabatically turning on the interactions. One need to keep in mind, however, that the concept of quasiparticles is only well defined in the vicinity of the Fermi surface, as elementary excitations of the real system with energies far away from the Fermi surface decay rapidly compared to the time required for adiabatically turning on the interactions in the ideal system. The particle distribution function in the ideal Fermi gas is now referred to as the quasiparticle distribution function in the correlated Fermi liquid, and I use $n_{\mathbf{p}\sigma}$ to denote this quantity for the rest of this thesis. The ground state quasiparticle distribution function $n^0_{\mathbf{p}\sigma}$ coincides with that of the ideal Fermi gas given by Fig. 1.1. At some low temperature T, the quasiparticle distribution function is proved to be the usual Fermi-Dirac distribution function

$$n_{\mathbf{p}\sigma} = \frac{1}{e^{(\varepsilon_{\mathbf{p}\sigma}-\mu)/k_BT}+1}, \tag{1.3}$$

where $\varepsilon_{\mathbf{p}\sigma}$ is the quasiparticle energy to be defined in next section, and it reduces to $n^0_{\mathbf{p}\sigma}$ when the temperature is zero. It is worth pointing out that the real physically meaningful quantity is the departure $\delta n_{\mathbf{p}\sigma}$ from the ground state

$$\delta n_{\mathbf{p}\sigma} = n_{\mathbf{p}\sigma} - n^0_{\mathbf{p}\sigma}, \tag{1.4}$$

that measures the "excitations" — that is, the quasiparticles — of the real system rather than $n_{\mathbf{p}\sigma}$.

The study of the correlated Fermi systems using Landau Fermi-liquid theory

is formulated around the concept of quasiparticles. A few key concepts and useful results of the theory are illustrated in the following sections.

1.1.1 Quasiparticle Energy and Interactions

For an ideal Fermi gas, the total energy (per unit volume) of the system can be expressed as a simple sum of the energies of each particle. In the case of a real Fermi liquid, the total energy of the system is a functional of the quasiparticle distribution function $E[n_{\mathbf{p}\sigma}]$, which in general cannot be specified explicitly. The quasiparticle energy $\varepsilon_{\mathbf{p}\sigma}$ is defined as the small increment in the total energy when a quasiparticle with momentum $\mathbf{p}$ and spin σ is added to the system,

$$\delta E = \frac{1}{V} \sum_{\mathbf{p}\sigma} \varepsilon_{\mathbf{p}\sigma} \delta n_{\mathbf{p}\sigma}, \tag{1.5}$$

where, $\delta E = E[n_{\mathbf{p}\sigma}] - E_0$, the variation in the total energy is measured with respect to the ground state energy (per unit volume) E_0, since we are only considering the low-lying excitations of the system where well defined quasiparticles appear in the immediate vicinity of the Fermi surface. Due to the particle interactions in the real Fermi liquid, the energy of the quasiparticle in the state $\mathbf{p}\sigma$ is also dependent on the presence of quasiparticles in other states $\mathbf{p}'\sigma'$. Hence $\varepsilon_{\mathbf{p}\sigma}$ is given by

$$\varepsilon_{\mathbf{p}\sigma} = \varepsilon^0_{\mathbf{p}\sigma} + \frac{1}{V} \sum_{\mathbf{p}'\sigma'} f_{\mathbf{p}\sigma,\,\mathbf{p}'\sigma'} \delta n_{\mathbf{p}'\sigma'} + \ldots, \tag{1.6}$$

where the first term $\varepsilon^0_{\mathbf{p}\sigma}$ denotes the ground state quasiparticle energy of state $\mathbf{p}\sigma$ — that is, the energy increment of the system caused by adding a quasiparticle $(\mathbf{p}\sigma)$ to the ground state, and the second term gives the interaction effect of first order in $\delta n_{\mathbf{p}\sigma}$, where $f_{\mathbf{p}\sigma,\,\mathbf{p}'\sigma'}/V$ is defined as the interaction energy between quasiparticles $\mathbf{p}\sigma$ and $\mathbf{p}'\sigma'$ and $\delta n_{\mathbf{p}'\sigma'}$ specifies the distribution of the quasiparticle $\mathbf{p}'\sigma'$. From $\varepsilon^0_{\mathbf{p}\sigma}$, we also define various useful quantities that will be mentioned

frequently throughout this thesis. The velocity of a quasiparticle on the Fermi surface (the Fermi velocity) is given by

$$v_f = \left(\frac{\partial \varepsilon^0_{\mathbf{p}\sigma}}{\partial p} \right)_{p=p_f}. \tag{1.7}$$

The effective mass m^* of a quasiparticle is consequently defined through

$$v_f = \frac{p_f}{m^*}. \tag{1.8}$$

The notion Fermi energy $E_{_F}$ is defined as $E_{_F} = p_f^2/2m^*$, which coincides with the quasiparticle energies on the Fermi surface $\varepsilon^0_{p_f\sigma} = \mu$, in the case of an ideal Fermi gas. We can also define the density of quasiparticle states at the Fermi surface by

$$N(0) = \frac{1}{V} \sum_{\mathbf{p}\sigma} \delta(\varepsilon^0_{\mathbf{p}\sigma} - \mu) = -\frac{1}{V} \sum_{\mathbf{p}\sigma} \frac{\partial}{\partial \varepsilon_{\mathbf{p}\sigma}} n^0_{\mathbf{p}\sigma}. \tag{1.9}$$

In the absence of an external magnetic field, the density of states is found to be

$$N(0) = \frac{m^* p_f}{\pi^2 \hbar^3} = \frac{3n}{2E_{_F}}. \tag{1.10}$$

According to Eqs. (1.5) and (1.6), the total energy of the system under quasiparticle distribution $\delta n_{\mathbf{p}\sigma}$ can be expressed as

$$E[n_{\mathbf{p}\sigma}] = E_0 + \frac{1}{V} \sum_{\mathbf{p}\sigma} \varepsilon^0_{\mathbf{p}\sigma} \delta n_{\mathbf{p}\sigma} + \frac{1}{2} \frac{1}{V^2} \sum_{\mathbf{p}\sigma,\, \mathbf{p}'\sigma'} f_{\mathbf{p}\sigma,\, \mathbf{p}'\sigma'} \delta n_{\mathbf{p}\sigma} \delta n_{\mathbf{p}'\sigma'} + \ldots. \tag{1.11}$$

From Eq. (1.11), we find the quasiparticle interaction energy f is in fact a second variation of the total energy,

$$f_{\mathbf{p}\sigma,\, \mathbf{p}'\sigma'} = V^2 \frac{\delta^2 E}{\delta n_{\mathbf{p}\sigma} \delta n_{\mathbf{p}'\sigma'}}. \tag{1.12}$$

So far, the general picture of Landau Fermi-liquid theory has been drawn through the definitions of the quasiparticle energy $\varepsilon_{\mathbf{p}\sigma}$ and interaction $f_{\mathbf{p}\sigma,\,\mathbf{p}'\sigma'}$, with Eq. (1.11) serving as the foundation for developing the phenomenological theory.

The equilibrium quasiparticle distribution function $n_{\mathbf{p}\sigma}$ is further separated into a number density part $n_{\mathbf{p}}$ and a spin density part $\boldsymbol{\sigma}_{\mathbf{p}}$ through the following relation,

$$n_{\mathbf{p}\sigma} = n_{\mathbf{p}} + \boldsymbol{\sigma}_{\mathbf{p}} \cdot \boldsymbol{\tau}_{\sigma\sigma}, \tag{1.13}$$

where $\boldsymbol{\tau}$ is the 2×2 Pauli spin matrices, σ is the quasiparticle spin measured in units of $\frac{\hbar}{2}$. When all the quasiparticle spins are quantized along the z axis, σ equals 1 for spin up fermions and -1 for spin down fermions, $\boldsymbol{\tau}_{\sigma\sigma} = \sigma\mathbf{z}$. The total particle number density n and the total spin polarization (per unit volume) $\boldsymbol{\sigma}$ of the system are therefore calculated from

$$n = \frac{N}{V} = \frac{1}{V}\sum_{\mathbf{p}\sigma} n_{\mathbf{p}\sigma} = \frac{2}{V}\sum_{\mathbf{p}} n_{\mathbf{p}}, \tag{1.14}$$

$$\boldsymbol{\sigma} = \frac{1}{V}\sum_{\mathbf{p}\sigma} n_{\mathbf{p}\sigma}\boldsymbol{\tau}_{\sigma\sigma} = \frac{2}{V}\sum_{\mathbf{p}} \boldsymbol{\sigma}_{\mathbf{p}}. \tag{1.15}$$

Consequently, the quasiparticle energy $\varepsilon_{\mathbf{p}\sigma}$ can be written as

$$\varepsilon_{\mathbf{p}\sigma} = \varepsilon_{\mathbf{p}} + \mathbf{h}_{\mathbf{p}} \cdot \boldsymbol{\tau}_{\sigma\sigma}, \tag{1.16}$$

where $\varepsilon_{\mathbf{p}}$ is a mean quasiparticle energy summed up in spin indices, and $\mathbf{h}_p$ is proportional to the effective magnetic field. In the absence of spin-orbit coupling, the quasiparticle interaction energy $f_{\mathbf{p}\sigma,\,\mathbf{p}'\sigma'}$ can also be expressed as

$$f_{\mathbf{p}\sigma,\,\mathbf{p}'\sigma'} = f^{s}_{\mathbf{p}\mathbf{p}'} + f^{a}_{\mathbf{p}\mathbf{p}'}\boldsymbol{\tau}_{\sigma\sigma} \cdot \boldsymbol{\tau}_{\sigma'\sigma'}, \tag{1.17}$$

where superscripts s and a stand for symmetric and antisymmetric in terms of the

spin configurations of the interacting quasiparticle pair. Eqs. (1.6), (1.13), (1.16) and (1.17) lead to the following relations:

$$\varepsilon_{\mathbf{p}} = \varepsilon^0_{\mathbf{p}} + \frac{2}{V}\sum_{\mathbf{p}'} f^s_{\mathbf{p}\mathbf{p}'}\delta n_{\mathbf{p}'} \tag{1.18}$$

$$\mathbf{h}_{\mathbf{p}} = \mathbf{h}^0_{\mathbf{p}} + \frac{2}{V}\sum_{\mathbf{p}'} f^a_{\mathbf{p}\mathbf{p}'}\delta\boldsymbol{\sigma}_{\mathbf{p}'}, \tag{1.19}$$

where $\varepsilon^0_{\mathbf{p}}$ is the ground state spin averaged quasiparticle energy, and $\mathbf{h}^0_{\mathbf{p}} = -\frac{1}{2}\gamma\hbar\mathscr{H}$ (where γ is the gyromagnetic ratio) is the coupling to the external magnetic field $\mathscr{H}$.

1.1.2 Landau Parameters

The Landau parameters follow directly from the quasiparticle interaction energy f introduced in the previous section. Since quasiparticles are only well defined close to the Fermi surface, the magnitudes of the quasiparticle momentums can all be approximated by p_f. Therefore, $f^s_{\mathbf{p}\mathbf{p}'}$ and $f^a_{\mathbf{p}\mathbf{p}'}$ can be expanded in terms of the angle θ between $\mathbf{p}$ and $\mathbf{p}'$:

$$f^{s(a)}_{\mathbf{p}\mathbf{p}'} = \sum_{l=0}^{\infty} f^{s(a)}_l P_l(\cos\theta), \tag{1.20}$$

where P_l are the Legendre polynomials. The Landau parameters are defined by

$$F^{s(a)}_l \equiv N(0) f^{s(a)}_l, \tag{1.21}$$

which are dimensionless quantities that measure the strengths of the quasiparticle interactions at the Fermi surface.

At low temperatures, the equilibrium thermodynamics of the real Fermi liquid can be described by Landau Fermi-liquid theory with the interactions being cap-

tured by the Landau parameters. For a Galilean invariant system, the effective mass of a quasiparticle is related to the bare mass through the following equation,

$$\frac{m^*}{m} = 1 + \frac{F_1^s}{3}. \tag{1.22}$$

The low temperature entropy (per unit volume) of the real Fermi liquid is given by

$$s = \frac{\pi^2}{3} N(0) k_B^2 T, \tag{1.23}$$

and the low temperature specific heat at constant volume is calculated to be

$$c_V = \frac{\pi^2}{2} n k_B \frac{T}{T_F}, \tag{1.24}$$

where T_F is the Fermi temperature defined by $k_B T_F \equiv p_f^2/2m^*$. The zero temperature compressibility and the spin susceptibility can be expressed as

$$\mathscr{K} = \frac{1}{n^2}\left(\frac{\partial n}{\partial \mu}\right)_{T=0} = \frac{1}{n^2}\,\frac{N(0)}{1+F_0^s}, \tag{1.25}$$

and

$$\chi = \frac{\hbar^2}{4}\,\frac{\gamma^2 N(0)}{1+F_0^a}, \tag{1.26}$$

respectively. The above results recover these of the ideal Fermi gas when the interactions between quasiparticles are turned off by making the Landau parameters $F_l^{s(a)}$ go to zero.

1.1.3 Quasiparticle Scattering Amplitude

Quasiparticle scattering plays an important role in understanding the transport phenomena of correlated Fermi systems. At low temperatures where the density of the thermally excited quasiparticles are low, it is sufficient to consider only the

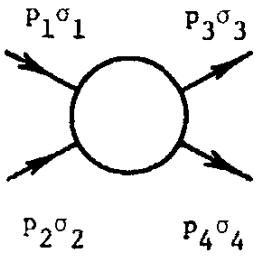

Figure 1.2: Scattering of two quasiparticles [1].

collisions between two quasiparticles. The two particle scattering process is shown in Fig. 1.2, where $|\mathbf{p}_1\sigma_1,\ \mathbf{p}_2\sigma_2\rangle$ and $|\mathbf{p}_3\sigma_3,\ \mathbf{p}_4\sigma_4\rangle$ indicate respectively the states of the incident and the scattered quasiparticles, and the scattering amplitude for such a process can be written as

$$\langle \mathbf{p}_3\sigma_3,\ \mathbf{p}_4\sigma_4|\, t\, |\mathbf{p}_1\sigma_1,\ \mathbf{p}_2\sigma_2\rangle. \tag{1.27}$$

In the normal state, the above transition amplitude is equivalent to the vertex function of particle-hole type in the microscopic quantum field theory [4]. The full scattering amplitude t can be constructed from the bare quasiparticle interaction f through repeated quasiparticle-quasihole pair creation and recombination processes. A diagrammatic representation of this construction process is presented in Fig. 1.3, where the spin indices are hidden, $(p-\frac{q}{2},\ p'+\frac{q}{2})$ and $(p+\frac{q}{2},\ p'-\frac{q}{2})$ are the four momenta — the momentum and energy, $p\equiv(\mathbf{p},\ \omega)$ — states of the incident and the scattered quasiparticle pairs, respectively. The full quasiparticle scattering amplitude can be expressed as

$$t_{\mathbf{pp}'}(\mathbf{q},\omega) = \langle \mathbf{p}+\mathbf{q}/2,\ \mathbf{p}'-\mathbf{q}/2|\, t\, |\mathbf{p}-\mathbf{q}/2,\ \mathbf{p}'+\mathbf{q}/2\rangle, \tag{1.28}$$

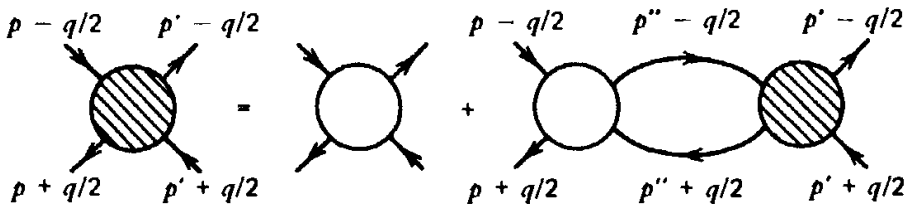

Figure 1.3: Diagram for repeated quasiparticle-quasihole scattering. The shaded circle represents the full scattering amplitude t, and the unshaded circle represents the bare quasiparticle-quasihole interaction f. The lines connecting the two circles represent the quasiparticle-quasihole propagators [1].

and

$$t_{\mathbf{pp}'}(\mathbf{q},\omega+i\eta) = f_{\mathbf{pp}'} - \sum_{\mathbf{p}''\neq\mathbf{p}'} f_{\mathbf{pp}''}\frac{\mathbf{q}\cdot\nabla_{p''}n^0_{p''}}{\omega+i\eta-\mathbf{q}\cdot\mathbf{v}_{\mathbf{p}''}}t_{\mathbf{p}''\mathbf{p}'}(\mathbf{q},\omega+i\eta), \qquad (1.29)$$

where $\mathbf{q}$ is the momentum transfer, and, $\omega = \varepsilon_{\mathbf{p}+\mathbf{q}/2} - \varepsilon_{\mathbf{p}-\mathbf{q}/2}$, is the energy transfer between the incident and scattered quasiparticles. In the low temperature limit, the energies of the quasiparticles are approximated by the Fermi energy E_F, therefore the energy transfer in the collision process is very small and we call this the low frequency limit ("k-limit") in which $qv_f \gg \omega$. The scattering processes concerned in this thesis are all studied under this limit. We can reduce the full scattering amplitude in Eq. (1.29) in the k-limit to

$$t_{\mathbf{pp}'}(\mathbf{q},0) = f_{\mathbf{pp}'} + \sum_{\mathbf{p}''\neq\mathbf{p}'} f_{\mathbf{pp}''}\frac{\partial n^0_{p''}}{\partial\varepsilon_{p''}}t_{\mathbf{p}''\mathbf{p}'}(\mathbf{q},0). \qquad (1.30)$$

Let us define a variable θ to stand for the angle between the momenta, $\mathbf{p}$ and $\mathbf{p}'$, of the incident quasiparticles, and another variable ϕ to denote the angle between the plane containing the momentum vectors of the incident quasiparticles and the plane containing the momentum vectors of the scattered quasiparticles, as shown in Fig. 1.4. The scattering amplitude can then be written as a function of the

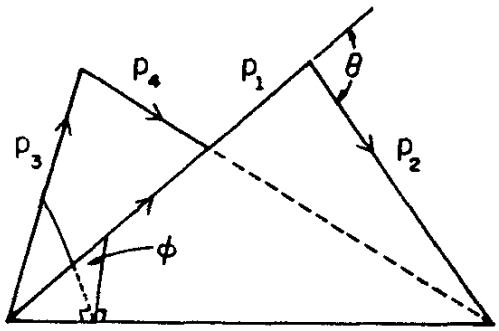

Figure 1.4: The relation of scattering angles θ and ϕ to the incident ($\mathbf{p}_1$ and $\mathbf{p}_2$) and final ($\mathbf{p}_3$ and $\mathbf{p}_4$) quasiparticle momenta [1].

angles θ and ϕ, $t_{\mathbf{pp}'}(\mathbf{q}, 0) = t(\theta, \phi)$. The spin structure of the scattering amplitude is similar to that of the functions $f_{\mathbf{p}\sigma,\,\mathbf{p}'\sigma'}$ in which the scattering amplitude is decomposed into a spin symmetric part $t^s(\theta, \phi)$ and a spin antisymmetric part $t^a(\theta, \phi)$ according to the following relation,

$$t_{\sigma\sigma'}(\theta, \phi) = t^s(\theta, \phi) + t^a(\theta, \phi)\boldsymbol{\tau}_{\sigma\sigma} \cdot \boldsymbol{\tau}_{\sigma'\sigma'}, \tag{1.31}$$

where σ and σ' are the spins of the incident quasiparticles. In the case of small momentum transfer, $q \ll p_f$, which corresponds to $\phi = 0$, there exists a simple relation between the quasiparticle scattering amplitude and the Landau parameters:

$$N(0)t^{s(a)}(\theta, \phi = 0) = \sum_l A_l^{s(a)} P_l(\cos\theta), \tag{1.32}$$

$$A_l^{s(a)} = \frac{F_l^{s(a)}}{1 + F_l^{s(a)}/(2l+1)}. \tag{1.33}$$

An additional constraint on the Landau parameters called the "forward scattering sum rule" states

$$\sum_l (A_l^s + A_l^a) = 0, \tag{1.34}$$

which is derived from Eq. (1.31) and (1.32) using the fact that $t_{\uparrow\uparrow}(\theta = 0, \phi) = 0$ due to the symmetry properties of the quasiparticle scattering process. The arrows represent the spins of the incident quasiparticles and $t_{\uparrow\uparrow}(\theta, \phi)$ corresponds to the total spin one (triplet) scattering channel denoted by

$$t_t(\theta, \phi) = t_{\uparrow\uparrow}(\theta, \phi). \tag{1.35}$$

The total spin zero (singlet) scattering channel $t_s(\theta, \phi)$ is given by

$$t_s(\theta, \phi) = 2t_{\uparrow\downarrow}(\theta, \phi) - t_{\uparrow\uparrow}(\theta, \phi). \tag{1.36}$$

For a finite momentum transfer $\phi \neq 0$ and to a simple first approximation, the singlet and triplet scattering amplitudes can be written as

$$\begin{aligned} t_s(\theta, \phi) &\simeq t_s(\theta, 0) \\ t_t(\theta, \phi) &\simeq t_t(\theta, 0) \cos\phi. \end{aligned} \tag{1.37}$$

Equivalently, we have

$$\begin{aligned} N(0)t_{\uparrow\uparrow}(\theta, \phi) &\simeq \sum_l (A_l^s + A_l^a) P_l(\cos\theta) \cos\phi \\ N(0)t_{\uparrow\downarrow}(\theta, \phi) &\simeq \sum_l \frac{1}{2} \left[(A_l^s - 3A_l^a) + (A_l^s + A_l^a) \cos\phi \right] P_l(\cos\theta), \end{aligned} \tag{1.38}$$

where the quasiparticle scattering amplitudes can be determined entirely by the Landau parameters.

The concepts introduced in this section will get referred to repeatedly throughout this thesis especially in chapter II where I calculate the quasiparticle scattering amplitudes for the strongly correlated ultra cold Fermi gas.

1.2 Transport properties

In this section, the standard Fermi-liquid theory approach in studying the transport properties of a correlated Fermi liquid is introduced. To be more specific, the calculations of the various transport lifetimes and transport coefficients are reviewed. As a brief introduction as this section is, only the key steps and the important results are presented. The complete derivation is rather tedious and it is not the purpose of this thesis to introduce the Landau theory in great details. The reader may refer to the books [1, 2] for the complete picture.

1.2.1 Landau Kinetic Equation

The study of the quasiparticle transport properties involves the study of the behavior of a nonequilibrium and inhomogeneous Fermi liquid. The quasiparticle distribution function $n_{\mathbf{p}\sigma}(\mathbf{r},t)$ varies with both position and time. The space and time evolution of the quasiparticle distribution function is governed by the Landau kinetic equation:

$$\frac{\partial n_{\mathbf{p}\sigma}(\mathbf{r},t)}{\partial t}+\nabla_p\varepsilon_{\mathbf{p}\sigma}(\mathbf{r},t)\cdot\nabla_r n_{\mathbf{p}\sigma}(\mathbf{r},t)-\nabla_r\varepsilon_{\mathbf{p}\sigma}(\mathbf{r},t)\cdot\nabla_p n_{\mathbf{p}\sigma}(\mathbf{r},t)=I\left[n_{\mathbf{p}'\sigma'}\right], \quad (1.39)$$

where $I\left[n_{\mathbf{p}'\sigma'}\right]$ is the quasiparticle collision integral, which indicates the net rate of increase in the occupation of state $\mathbf{p}\sigma$ caused by quasiparticle collisions. The collision integral can be evaluated as

$$\begin{aligned} I_1\left[n_{\mathbf{p}'\sigma'}\right] &= \frac{1}{V^2}\sum_{\mathbf{p}_2\sigma_2}\sum_{\substack{\mathbf{p}_3\sigma_3\\ \mathbf{p}_4\sigma_4}}{}'W(12;34)\delta_{\mathbf{p}_1+\mathbf{p}_2,\,\mathbf{p}_3+\mathbf{p}_4}\delta_{\sigma_1+\sigma_2,\,\sigma_3+\sigma_4}\delta(\varepsilon_1+\varepsilon_2-\varepsilon_3-\varepsilon_4) \\ &\quad\times\left[n_3n_4(1-n_1)(1-n_2)-n_1n_2(1-n_3)(1-n_4)\right], \end{aligned} \quad (1.40)$$

where the prime sign on the second sum means summing over distinguishable final states, and the quantity $W(12;34)$ is the transition probability for a two

quasiparticle scattering process on the Fermi surface. The spin averaged transition probability $W(\theta, \phi)$ is defined by

$$\sum_{\sigma_2\sigma_3\sigma_4} {}'W(12;34) = \frac{1}{2}W_{\uparrow\uparrow}(\theta,\phi) + W_{\uparrow\downarrow}(\theta,\phi) = 2W(\theta,\phi), \tag{1.41}$$

where the angles (θ, ϕ) are the same angles introduced when discussing the quasiparticle scattering amplitudes, in fact the transition probabilities are directly related to the scattering amplitudes through the following relations,

$$W_{\uparrow\uparrow}(\theta,\phi) = \frac{2\pi}{\hbar}|t_{\uparrow\uparrow}(\theta,\phi)|^2, \tag{1.42a}$$

$$W_{\uparrow\downarrow}(\theta,\phi) = \frac{2\pi}{\hbar}|t_{\uparrow\downarrow}(\theta,\phi)|^2. \tag{1.42b}$$

Therefore, the transition probabilities can be determined from the Landau parameters, and the collision integral depends directly on the Landau parameters as well.

A particle kinetic equation and a spin kinetic equation can be derived from the Landau kinetic equation, Eq. (1.39), to characterize the space and time evolution of the particle density $n_{\mathbf{p}}(\mathbf{r}, t)$ and the spin density $\boldsymbol{\sigma}_{\mathbf{p}}(\mathbf{r}, t)$, respectively. The particle kinetic equation is associated with the study of the thermal conduction and the viscosity of the system, while the spin kinetic equation becomes useful in understanding the spin diffusion.

1.2.2 Spin Diffusion

The calculations of the spin diffusion coefficient D and the spin diffusion lifetime τ_D involve solving the spin kinetic equation in the presence of a small gradient in the spin density perturbation $\nabla\left(\sigma_i(\mathbf{r}, t) - \sigma_i^0(\mathbf{r}, t)\right)$. The spin diffusion assumes the Fick form

$$\mathbf{j}_{\sigma_i}(\mathbf{r}, t) = -D\nabla\left(\sigma_i(\mathbf{r}, t) - \sigma_i^0(\mathbf{r}, t)\right), \tag{1.43}$$

where $\mathbf{j}_{\sigma_i}$ denotes the spin current polarized in the direction of the i^{th} spin component. At low temperatures, D is solved to be

$$D = \frac{1}{3} v_f^2 (1 + F_0^a) \tau_D. \tag{1.44}$$

The spin diffusion lifetime τ_D is closely related to the quasiparticle collision rate $I\left[n_{\mathbf{p}'\sigma'}\right]$. A characteristic quasiparticle relaxation time is defined from the collision integral by

$$\tau \equiv \frac{8\pi^4 \hbar^6}{m^{*3} \langle W \rangle \left(k_B T\right)^2}, \tag{1.45}$$

where $\langle W \rangle$ is the angle averaged transition probability given by

$$\langle W \rangle \equiv \int \frac{d\Omega}{4\pi} \frac{W(\theta, \phi)}{\cos(\theta/2)}. \tag{1.46}$$

The spin diffusion lifetime τ_D turns out to be proportional to the characteristic relaxation time τ through a complex quantity λ_D:

$$\frac{\tau_D}{\tau} = \frac{1}{6} + \frac{4\lambda_D}{\pi^2} \sum_{\nu_{\text{odd}}} \frac{2\nu + 1}{\nu^2 (\nu + 1)^2 \left[\nu(\nu + 1) - 2\lambda_D\right]}, \tag{1.47}$$

where λ_D is given by

$$\lambda_D = 1 - \frac{1}{\langle W \rangle} \int \frac{d\Omega}{4\pi} \frac{W_{\uparrow\downarrow}(\theta, \phi)(1 - \cos\theta)(1 - \cos\phi)}{2\cos(\theta/2)}. \tag{1.48}$$

The above results are quite textbook, and the detailed derivations can be found in the Fermi-liquid theory book [1].

1.2.3 Viscosity

The viscosity interested in this thesis is the first viscosity (or shear viscosity), and the calculations of the viscosity coefficient η and the viscous lifetime τ_η are

related with the solution of the particle kinetic equation. The low temperature first viscosity is found to be

$$\eta = \frac{1}{5} n p_f v_f \tau_\eta, \tag{1.49}$$

where a similar proportionality relation exists between τ_η and τ as in the case of the spin diffusion,

$$\frac{\tau_\eta}{\tau} = \frac{1}{6} + \frac{4\lambda_\eta}{\pi^2} \sum_{\nu_{\rm odd}} \frac{2\nu+1}{\nu^2(\nu+1)^2\left[\nu(\nu+1) - 2\lambda_\eta\right]}, \tag{1.50}$$

and λ_η is given by

$$\lambda_\eta = \frac{1}{\langle W \rangle} \int \frac{d\Omega}{4\pi} \frac{W(\theta,\phi)}{\cos(\theta/2)} \left(1 - 3\sin^4(\theta/2)\sin^2\phi\right). \tag{1.51}$$

1.2.4 Thermal Conduction

To study thermal conduction of the system, one needs to solve the particle kinetic equation subject to a small temperature gradient ∇T. The thermal conductivity K is defined through the following relation:

$$\mathbf{j}_T = -K \nabla T, \tag{1.52}$$

where $\mathbf{j}_T$ is the thermal current. The low temperature thermal conductivity K is evaluated to be

$$K = \frac{1}{3} c_V v_f^2 \tau_K, \tag{1.53}$$

where the thermal conducting lifetime τ_K is proportional to τ,

$$\frac{\tau_K}{\tau} = \frac{12 - \pi^2}{2\pi^2} + \frac{12\lambda_K}{\pi^2} \sum_{\nu_{\rm even}} \frac{2\nu+1}{\nu^2(\nu+1)^2\left[\nu(\nu+1) - 2\lambda_K\right]}. \tag{1.54}$$

The quantity λ_K is given by

$$\lambda_K = \frac{1}{\langle W \rangle} \int \frac{d\Omega}{4\pi} \frac{W(\theta, \phi)}{\cos(\theta/2)} (1 + 2\cos\theta) \,. \tag{1.55}$$

For a normal Fermi liquid, the various transport properties introduced above can all be expressed in terms of the transition probability function $W(\theta, \phi)$, which in turn is determined by the Landau parameters, therefore, it is enough to know the Landau parameters of the real Fermi liquid to understand its transport properties.

CHAPTER II

Transport Phenomena in Ultracold Fermi Gases with Superfluid Fluctuations

2.1 Introduction

In this chapter, I present my study on the transport phenomena of ultracold Fermi gases above the superfluid transition temperature T_c. Ever since the first experimental realization of Bose-Einstein condensation (BEC) in a Bose gas in 1995 [5–7], ultracold atomic gases have drawn a lot of attentions in the physics community and there has been an enormous amount of experimental and theoretical work carried out to study ultracold atomic physics [8, 9]. In addition to Bose gases, there are as well cold Fermi gases, with an interaction strength that can be tuned by the proximity of a Feshbach resonance [10, 11]. At resonance, the Fermi gas is said to be at unitarity with an infinitely large scattering length a_s, therefore the system becomes scale invariant and obeys universal thermodynamic relations [12]. The superfluid transition temperature of an ultracold Fermi gas decreases exponentially with decreasing interaction strength in the weakly attracting limit [9], $T_c \approx 0.28 T_F e^{\pi/2k_F a_s}$, where k_F is the Fermi wave vector defined as $k_F = p_f/\hbar$. At unitarity, the Fermi gas is strongly correlated, so one expects a big boost in T_c due to the increasing pairing gap approaching unitarity and thus a

significantly larger critical region above T_c compared to a nonunitary dilute Fermi gas with attractive interactions (BCS regime). The superfluid lambda transition which was once difficult to observe in a dilute Fermi gas has also been experimentally realized recently in a unitary Fermi gas [13]. Comparing to the relatively clear picture of the thermodynamics of strongly interacting Fermi gases [8, 9], the transport properties of such systems have yet to be fully understood. A string theory calculation has suggested the existence of a universal scale invariant lower bound in the viscosity of strongly interacting quantum liquids [14]. The conjectured quantum limited viscosity has since been explored in depth using different theoretical models [15–17], and such a lower bound has also been argued to exist in the spin diffusion coefficient [18]. Therefore, it is quite tentative to believe that such scale invariant universality exists in the general transport properties as it does in the thermodynamics of the strongly interacting Fermi gas. What's more, transport measurements on the spin diffusion coefficient and the viscosity coefficient in strongly interacting Fermi gases [19–21] have also shown that both the spin diffusion coefficient and the viscosity/entropy ratio saturate to some minimum values at temperatures very close to the superfluid transition temperature T_c. However, whether the measured minimums in the transport properties truly indicate a universal quantum limited lower bound in the transport properties still needs further clarification, and the idea of universal quantum limited transport in strongly interacting Fermi gases remains debatable.

Motivated by the remaining challenges in the understanding of the transport properties in ultracold unitary Fermi gases, in this work, I develop a new theoretical model using Landau Fermi-liquid theory and beyond to study the transport phenomena in an ultracold Fermi gas with strong attractive interactions close to the unitary limit. In particular, I calculate the various transport lifetimes and the corresponding transport coefficients of the ultracold Fermi gas. Most importantly,

I reveal superfluid fluctuations (sometimes referred to as the Cooper instibility) in the transport lifetimes of the unitary Fermi gas above T_c. The quasiparticle scattering amplitudes near the Fermi surface are essential in calculating the transport lifetimes according to Landau Fermi-liquid theory [1] as shown in Chapter I. At temperatures close to T_c, the scattering amplitudes are greatly affected by the formation of Cooper pairs that causes superfluid fluctuations in the system. The superfluid fluctuations dominate the quasiparticle scattering amplitudes right above T_c, and the exact form of their contributions to the scattering amplitudes are computed in section 2.2. The calculations of the low temperature transport lifetimes and transport coefficients follow the steps of Landau Fermi-liquid theory by evaluating the total quasiparticle scattering probability, and the results are adopted from section 1.2. The total scattering probability contains both a contribution from the normal Fermi-liquid scattering channel given in sections 1.1.3 and 1.2.1, and a contribution from the superfluid fluctuations. The Landau parameters needed in calculating the scattering amplitudes are computed in section 2.3 using the local induced interaction model [22, 23]. Further, in section 2.4, the leading order finite temperature corrections to the transport lifetimes and transport coefficients are added to complete the calculations of the transport properties of the strongly correlated Fermi gas. Section 2.5 shows the results of the transport calculations, where I have compared the calculated spin diffusion coefficient and viscosity/entropy ratio with their respective experimental findings in Ref. [19] and Ref. [20, 21], along with the discussions on the results. This work has been published in the journal Physical Review B [24].

2.2 Superfluid Fluctuations in the Scattering Amplitude

Superfluid fluctuations in the transport lifetimes of a unitary Fermi gas are investigated through calculating the quasiparticle scattering amplitudes of the gas

near T_c in a similar fashion as an earlier study on zero-sound attenuation in liquid ^{3}He [25]. As the temperature approaches T_c, the virtual formation of Cooper pairs starts to dominate the quasiparticle scattering process. Singularities in the scattering amplitudes are found for small total momentum quasiparticle scattering, leading to diverging scattering amplitudes at T_c for zero total momentum quasiparticle scattering. Here I consider only the s-wave (spin singlet) pairing mechanism for the Cooper pairs, thus the exact calculation of superfluid fluctuations in the scattering amplitudes is performed by evaluating the temperature vertex function of particle-particle type in the spin singlet channel using regular quantum field theory methods. The integral equation for the temperature vertex function is given by summing over the various "ladder diagrams" of the vertex function [4],

$$\begin{aligned}\mathscr{T}_s(p_1,p_2;\ p_3,p_4) &= \tilde{\mathscr{T}}_s(p_1,p_2;\ p_3,p_4) - \frac{T}{2(2\pi)^3}\sum_{\omega_n}\int \tilde{\mathscr{T}}_s(p_1,p_2;\ k,q-k) \\ &\quad \times \mathscr{G}(q-k)\mathscr{G}(k)\mathscr{T}_s(k,q-k;\ p_3,p_4)\mathrm{d}^3\mathbf{k} \qquad (2.1)\end{aligned}$$

where $\tilde{\mathscr{T}}_s$ is the temperature particle-particle irreducible vertex function, $\mathscr{G}$ is the exact temperature Green's function, $\omega_n = (2n+1)\pi T$ are the "odd" Matsubara frequencies for fermions. Here we have introduced the four-momentum $p_i \equiv (\mathbf{p}_i, \omega_i)$ to denote the momenta $\mathbf{p}_i$ and frequencies ω_i of the incident and scattered quasiparticles in the Fourier transformed momentum space, and $q \equiv (\mathbf{q}, \omega_0)$ stands for the total momentum $\mathbf{q}$ and total frequency ω_0 of the incident quasiparticles, where $\mathbf{q} = \mathbf{p}_1 + \mathbf{p}_2$ and $\omega_0 = \omega_1 + \omega_2$. For small total momentum scattering ($|\mathbf{q}| \ll k_F$) and when only quasiparticles near the Fermi surface are considered in the scattering processes, $|\mathbf{p}_i| = k_F$ for $i = 1, \cdots, 4$, $\mathscr{T}_s$ depends only on the total four-momentum q, i.e. $\mathscr{T}_s(p_1,p_2;p_3,p_4) = \mathscr{T}_s(q)$. In the diagram technique of quantum field theory, the energy is measured from the chemical potential, $\xi(\mathbf{p}) = \varepsilon^0_{\mathbf{p}} - \mu$, thus the

total frequency ω_0 is approximately zero for quasiparticle scattering at the Fermi surface. Integrate out the second term on the right side of Eq. (2.1), we have in the small q limit with $\omega_0 = 0$ the temperature vertex function,

$$\mathscr{T}_s(\mathbf{q},0) = \frac{1}{\frac{m^* p_f}{4\pi^2\hbar^3}\left[\ln\frac{T_c}{T} - \frac{1}{6}\left(\frac{v_f|\mathbf{q}|}{2\hbar\omega_D}\right)^2 - \frac{7\zeta(3)}{3\pi^2}\left(\frac{v_f|\mathbf{q}|}{4k_BT}\right)^2\right]}, \tag{2.2}$$

where the superfluid transition temperature T_c is given by

$$k_B\, T_c = \frac{2\gamma\hbar\omega_D}{\pi} e^{-4\pi^2\hbar^3/m^* p_f|\tilde{\mathscr{T}}_s|}, \tag{2.3}$$

$\mathbf{ln}\gamma$ is the Euler's constant and $\hbar\,\omega_D = 0.244\,E_F^0$ is the cutoff frequency [26]. Quasiparticles with energies deviating from the Fermi energy by a value beyond $\hbar\,\omega_D$ are neglected in the interaction. Here we have set $\tilde{\mathscr{T}}_s = \tilde{\Gamma}_s$, where $\tilde{\Gamma}_s$ is the zero temperature irreducible particle-particle vertex function, which is equivalent to the spin singlet normal Fermi-liquid scattering amplitude $t_s(\theta,\phi)$ given by Eqs. (1.36) and (1.38). The full temperature vertex function $\mathscr{T}_s(\mathbf{q},0)$ is equal to the superfluid fluctuation dominated spin singlet quasiparticle scattering amplitude. As shown by Eq. (2.2), the scattering amplitude is indeed divergent at T_c for zero total momentum $\mathbf{q}$. The detailed derivation of Eq. (2.2) from Eq. (2.1) is given in Appendix A.

In order to calculate the transport lifetimes and transport coefficients, the spin averaged transition probability $W(\theta,\phi)$ is needed as discussed in section 1.2. In the presence of the superfluid fluctuations at temperatures right above T_c, the transition probability $W(\theta,\phi)$ contains both a superfluid fluctuations part $W_{\rm f}(\theta,\phi)$, and a normal Fermi-liquid scattering part $W_{\rm n}(\theta,\phi)$, with

$$W(\theta,\phi) = W_{\rm f}(\theta,\phi) + W_{\rm n}(\theta,\phi). \tag{2.4}$$

The superfluid fluctuations are phase space limited as Cooper pairs pairing breaks down when the total momentum of the pair exceeds a certain value $|\mathbf{q}_{\max}|$, hence quasiparticle scattering processes with a total momentum greater than $|\mathbf{q}_{\max}|$ is denoted by $W_{\rm n}(\theta,\phi)$, which is equivalent to the normal Fermi-liquid transition probability derived from Eqs. (1.41) and (1.42),

$$W_{\rm n}(\theta,\phi) = \frac{2\pi}{\hbar}\left(\frac{1}{2}|t_{\uparrow\downarrow}|^2 + |t_{\uparrow\uparrow}|^2\right), \tag{2.5}$$

where $t_{\uparrow\downarrow}$ and $t_{\uparrow\uparrow}$ take the normal Fermi-liquid expression given by Eq. (1.38). Quasiparticle scattering processes with a total momentum less than $|\mathbf{q}_{\max}|$ is denoted by the superfluid fluctuations term $W_{\rm f}(\theta,\phi)$, which can be expressed in terms of the singlet (t_s) and triplet (t_t) quasiparticle scattering amplitudes in the same fashion as the normal transition probability derived from Eqs. (1.35), (1.36), (1.41) and (1.42),

$$W_{\rm f}(\theta,\phi) = \frac{2\pi}{\hbar}\left(\frac{1}{2}\left|\frac{t_s+t_t}{2}\right|^2 + |t_t|^2\right), \tag{2.6}$$

where $t_s = \mathscr{T}_s(\mathbf{q},0)$ is the singlet scattering amplitude from the superfluid fluctuations and the triplet scattering amplitude is the normal Fermi-liquid triplet scattering amplitude, because only the singlet pairing channel is considered in the superfluid fluctuations. The phase space averaged transition probability in Eq. (1.46) could then be written as

$$\begin{aligned}\langle W\rangle &= \int_0^{|\mathbf{q}_{\max}|}\frac{d\Omega}{4\pi}\frac{W_{\rm f}(\theta,\phi)}{\cos(\theta/2)} + \int_{|\mathbf{q}_{\max}|}^{2p_f}\frac{d\Omega}{4\pi}\frac{W_{\rm n}(\theta,\phi)}{\cos(\theta/2)} \\ &= \langle W\rangle_{\rm fluctuations} + \langle W\rangle_{\rm normal},\end{aligned} \tag{2.7}$$

where $\langle W\rangle_{\rm fluctuations}$ and $\langle W\rangle_{\rm normal}$ stand for the phase space averaged superfluid fluctuation and normal Fermi-liquid transition probabilities, respectively. The critical momentum $|\mathbf{q}_{\max}|$ is determined by evaluating the zero temperature particle-

particle vertex function [4],

$$\Gamma_s(q) = \tilde{\Gamma}_s(q) - \frac{i}{2(2\pi)^4}\int \tilde{\Gamma}_s(q)G(q-k)G(k)\Gamma_s(q)\mathrm{d}^4k, \tag{2.8}$$

where G is the zero temperature Green's function. Standard quantum field theory analysis [4] gives for small q the vertex function

$$\Gamma_s(\mathbf{q},\omega_0) = -\frac{4\pi^2\hbar^3}{m^*p_f}\frac{i\varpi}{\omega_0 - i\varpi + i\left(v_f^2|\mathbf{q}|^2/6\hbar\varpi\right)}, \tag{2.9}$$

where $\varpi = 2\omega_D e^{-4\pi^2\hbar^3/m^*p_f|\tilde{\Gamma}_s|}$. The maximum momentum of a Cooper pair can be determined from $v_f|\mathbf{q}_{\max}| = \sqrt{6}\hbar\varpi$ by assuring that $\Gamma_s(\mathbf{q},\omega_0)$ has a pole in the upper half plane of ω_0.

So far, I have determined the exact form of the quasiparticle scattering amplitude from the superfluid fluctuations in Eq. (2.2). The full quasiparticle scattering probability is expressed by Eq. (2.7). The Landau parameters are needed to evaluate these quantities, and I proceed to give the calculations of the Landau parameters in next section.

2.3 Local Induced Interaction Model

2.3.1 Description of The Model

The Landau parameters are calculated using the local induced interaction model. The induced interaction model was first introduced in the 1970's [27] to describe the quasiparticle interaction of liquid ^{3}He. The more general momentum dependent scattering amplitude model was developed in the 1980's [28–30]. Such a theory splits the quasiparticle interaction into two spices: the direct and the induced, as shown in Fig. 2.1. The induced term comes from the part of the interactions induced through the exchange of the collective excitations, whereas the

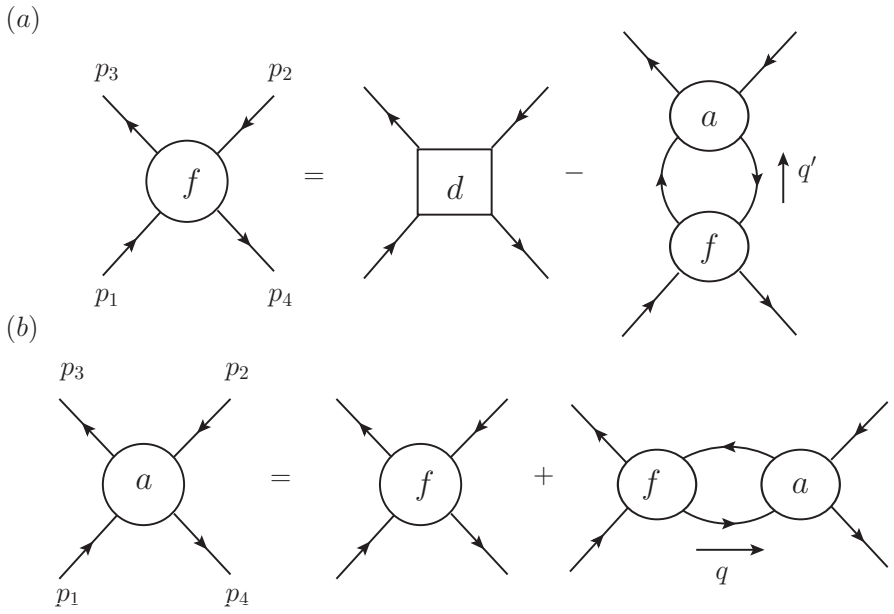

Figure 2.1: Diagrammatic representation of the integral equations for the Landau parameters F and the scattering amplitudes a. (a) represents the equation for Landau parameters decomposed into direct and induced terms; (b) sums all the reducible diagrams. It represents the equation relating F to the scattering amplitudes a.

direct term is the Fourier transform of a model dependent effective quasiparticle potential. The generalized expressions of the Landau parameters were derived diagrammatically by Ainsworth and Bedell [30]. In the local limit of a Fermi liquid, the quasiparticle interaction is independent of the momentum [22], thus Landau parameters $F_l^{s(a)}$ with $l > 0$ are all zero. Therefore, the forward scattering sum rule Eq. (1.34) is reduced to a simple summation of two terms,

$$A_0^s + A_0^a = 0. \tag{2.10}$$

Consequently, the spin triplet quasiparticle scattering amplitude given by Eqs. (1.35) and (1.38) for a normal Fermi liquid vanishes in the local limit, which means $t_t = t_{\uparrow\uparrow}(\theta, \phi) = 0$ in the local limit. The spin singlet quasiparticle scattering amplitude $t_s(\theta, \phi)$ for a normal Fermi liquid then reduces, according to Eq. (1.38)

and Eq. (2.10) in the local limit, to

$$t_s(\theta,\phi) = 2t_{\uparrow\downarrow}(\theta,\phi) = \frac{(A_0^s - 3A_0^a)}{N(0)} = -\frac{4A_0^a}{N(0)}. \tag{2.11}$$

In the local model, the set of equations for the Landau parameters $F_0^{s(a)}$ is reduced to [23, 31]

$$F_0^s = D_0^s + \frac{1}{2}F_0^s A_0^s + \frac{3}{2}F_0^a A_0^a \tag{2.12}$$

$$F_0^a = D_0^a + \frac{1}{2}F_0^s A_0^s - \frac{1}{2}F_0^a A_0^a, \tag{2.13}$$

where $D_0^{s(a)}$ are the spin symmetric and antisymmetric direct interaction terms generated by the effective quasiparticle potential, and they are fully antisymmetrized so that $D_0^{\uparrow\uparrow(\downarrow\downarrow)} = 0$, where the arrows denote the spins of the interacting quasiparticles. According to Ainsworth and Bedell [30], $D_0^s = \frac{N(0)}{2}(D_0^{\uparrow\uparrow} + D_0^{\uparrow\downarrow}) = \frac{2}{\pi}k_F a_s$ and $D_0^a = +\frac{N(0)}{2}(D_0^{\uparrow\uparrow} - D_0^{\uparrow\downarrow}) = -\frac{2}{\pi}k_F a_s$, where a_s is the quasiparticle s-wave scattering length. Together with the local limit forward scattering sum rule Eq. (2.10), I derive the expression for the scattering length a_s as a function of F_0^a from the local induced interaction model Eqs. (2.12) and (2.13),

$$\frac{-1}{k_F a_s} = \frac{8}{\pi}\frac{(1+F_0^a)(1+2F_0^a)}{F_0^a + 3F_0^a(1+2F_0^a)^2}. \tag{2.14}$$

This relation is depicted in Fig. 2.2. The quasiparticle interaction strength of a Fermi gas is characterized by the s-wave scattering length a_s. On the BCS side of the BCS-BEC crossover[32] in which I study the transport phenomena in this work, the s-wave scattering length of the Fermi gas is always negative and it goes to negative infinity at unitarity. Therefore, F_0^a of a unitary Fermi gas approaches positive infinity in the local model according to Fig. 2.2. Utilizing the local induced interaction model, I am able to calculate the Landau parameters $F_0^{s(a)}$ for Fermi gases with arbitrary quasiparticle interaction strengths. These Landau

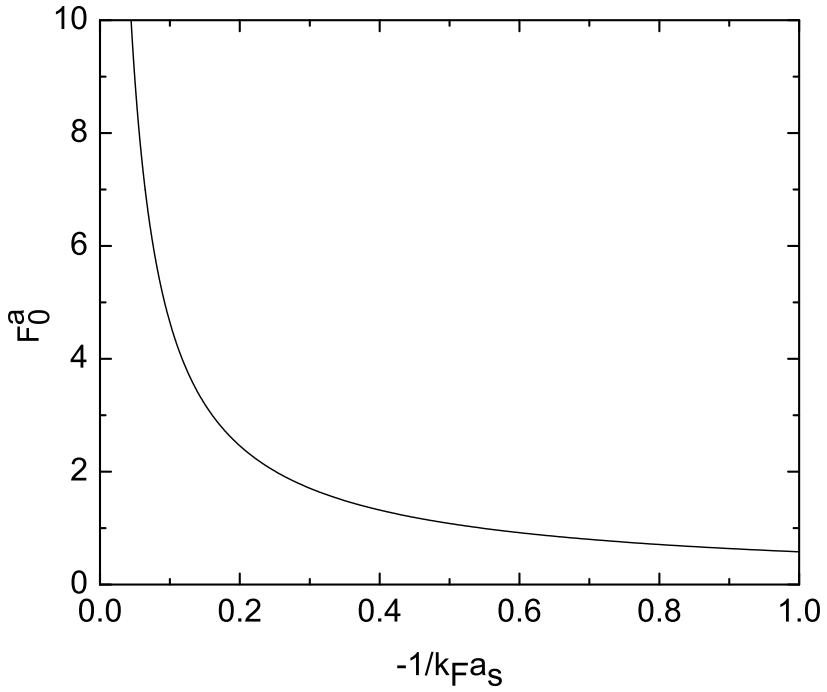

Figure 2.2: The Landau parameter F_0^a versus $-(k_F a_s)^{-1}$ curve.

parameters are then used to determine the quasiparticle scattering amplitudes in the calculations of the transport lifetimes and transport coefficients in section 2.4.

2.3.2 Universal Thermodynamics

Despite its simple structure and easy mathematics, the local induced interaction model does a good job in explaining the universal thermodynamics of the unitary Fermi gas. In a Galilean invariant system, the mass renormalization disappears for a local Fermi liquid, i.e. $m^* = m$. This is true since $F_1^s = 0$ in the local limit and Eq. (1.22) justifies the above statement. Using the local forward scattering sum rule Eq. (2.10), the Landau parameter F_0^s saturates to -0.5 at unitarity from the local model. Hence, the quasiparticle mass and the Landau parameter F_0^s are both independent of the quasiparticle density n, which makes it simple to analyze the various thermodynamic quantities of the unitary Fermi gas. I can derive the relation between the zero temperature chemical potential $\mu(n, 0)$

and the Fermi energy $E_F^0 \equiv p_f^2/2m$ of an ideal Fermi gas from the zero temperature compressibility of the normal Fermi gas given in Eq. (1.25) by integrating out both μ and n,

$$\begin{aligned} d\mu &= \frac{1+F_0^s}{N(0)}dn = \frac{2E_F(1+F_0^s)}{3n}dn \\ \Rightarrow \mu(n,0) &= (1+F_0^s)\,\frac{m}{m^*}E_F^0, \end{aligned} \tag{2.15}$$

where the ideal gas Fermi energy E_F^0 is related to the real gas Fermi energy E_F through $E_F = \frac{m}{m^*}E_F^0$. The direct proportionality between the chemical potential and the Fermi energy resembles a similar universal relation $\mu = (1+\beta)E_F^0$, existing in the unitary Fermi gases [9], where μ stands for the exact zero temperature chemical potential of the unitary Fermi gas with superfluid condensations and β is the true zero temperature Berstch parameter and is denoted by ξ in [13]. The quantity $1+F_0^s$ relates to a number ξ_n, which is the hypothetical zero temperature limit of the Berstch parameter extrapolated from the normal Fermi-liquid chemical potential [13, 33], through the relation $(1+F_0^s) = \frac{m^*}{m}\xi_n$. In the absence of the mass renormalization, $1+F_0^s$ is equivalent to ξ_n and differs from the true zero temperature Berstch parameter ξ for not considering the superfluid condensation energy. The local induced interaction model gives the value of $1+F_0^s = 0.5$ in the unitary limit, which is close to the result $\xi_n = 0.54$ from the Monte Carlo calculations for the unitary Fermi gases [33, 34].

I also study the leading order temperature dependence of several thermodynamic quantities using basic thermodynamic analysis. In the absence of spin polarization and mass renormalization, the chemical potential of a normal Fermi gas is given, according to Landau Fermi-liquid theory [1], as

$$\mu(n,T) \equiv \mu(n,0)\left[1 - \frac{\pi^2(1+F_0^s)}{12}\left(\frac{T}{T_s}\right)^2\right], \tag{2.16}$$

where I have introduced the temperature scale $T_s \equiv \frac{\mu(n,0)}{k_B}$, and T_s reduces to the Fermi temperature T_F^0 for an ideal Fermi gas. The chemical potential therefore scales the same in temperature as the ideal Fermi gas apart from a renormalization in the temperature scale. The total entropy is given according to Eq. (1.23) by

$$\frac{S}{Nk_B} = \frac{\pi^2(1+F_0^s)}{2}\frac{T}{T_s}. \tag{2.17}$$

Further, the temperature dependence of the compressibility $\mathscr{K}(n,T)$ can be derived from the definition of the compressibility, $\mathscr{K} = \frac{1}{n^2}\frac{\partial n}{\partial \mu}$, and it is given by

$$\mathscr{K}(n,T) = \mathscr{K}(n,0)\left[1 + \frac{\pi^2(1+F_0^s)}{12}\left(\frac{T}{T_s}\right)^2\right]^{-1}, \tag{2.18}$$

where the zero temperature compressibility $\mathscr{K}(n,0)$ given by Eq. (1.25) can be reexpressed in terms of n and E_F,

$$\mathscr{K}(n,0) = \frac{3}{2nE_F}\frac{1}{1+F_0^s}. \tag{2.19}$$

The compressibility function can also be expressed as

$$\mathscr{K} = -\frac{1}{V}\left(\frac{\partial V}{\partial P}\right)_T = \frac{1}{n}\left(\frac{\partial n}{\partial P}\right)_T, \tag{2.20}$$

thus the temperature dependence of the pressure $P(n,T)$ is obtained by solving the above equation,

$$\begin{aligned} dP &= \frac{2E_F(1+F_0^s)}{3}\left[1 + \frac{\pi^2(1+F_0^s)}{12}\left(\frac{T}{T_s}\right)^2\right]dn \\ \Rightarrow \quad P(n,T) &= P(n,0)\left[1 + \frac{5\pi^2(1+F_0^s)}{12}\left(\frac{T}{T_s}\right)^2\right], \end{aligned} \tag{2.21}$$

where the zero temperature pressure $P(n,0)$ is given by

$$P(n,0) = \frac{2}{5}(1+F_0^s)nE_F. \tag{2.22}$$

All the thermodynamic quantities calculated above involve universal functions of the Fermi energy E_F and the ratio T/T_s, as expected from a unitary Fermi gas [12]. The analogy between the unitary Fermi gas and the ideal Fermi gas is remarked here. Consider the unitary Fermi gas undergoing an adiabatic process (i.e. no entropy generation), the entropy function given in Eq. (2.17) implies that the ratio T/T_s remains unchanged throughout the whole process. The product $Pn^{-5/3}$ is obtained from Eq. (2.21) as

$$Pn^{-5/3} = \frac{2(1+F_0^s)}{5}\frac{\hbar^2\left(3\pi^2\right)^{2/3}}{2m^*}\left[1+\frac{5\pi^2(1+F_0^s)}{12}\left(\frac{T}{T_s}\right)^2\right]. \tag{2.23}$$

Therefore, during a reversible adiabatic process, $Pn^{-5/3} = \text{const}$, for the unitary Fermi gas, typical of noninteracting atomic gases.

2.3.3 BCS-BEC Crossover

In addition to the thermodynamic quantities calculated above, the local induced interaction model provides meaningful analysis to the physics of BCS-BEC crossover as well. An effective s-wave scattering amplitude $\tilde{a}_0$ could be defined as [4]

$$\frac{\tilde{\Gamma}_s}{2} = \frac{4\pi\hbar^2\,\tilde{a}_0}{m^*}. \tag{2.24}$$

In the local limit, $\tilde{\Gamma}_s$, which is equivalent to the singlet normal Fermi-liquid scattering amplitude $t_s(\theta,\phi)$, is given by Eq. (2.11),

$$\tilde{\Gamma}_s = t_s(\theta,\phi) = \frac{A_0^s - 3A_0^a}{N(0)} = -\frac{4A_0^a}{N(0)}. \tag{2.25}$$

Analogous to the two-body scattering problem in quantum mechanics [35], I can write down the s-wave phase shift

$$\delta_0 = k_F \tilde{a}_0 = \frac{\pi}{8}(A_0^s - 3A_0^a) = -\frac{\pi}{2}A_0^a. \tag{2.26}$$

Using the local induced interaction model result $F_0^a \to +\infty$ therefore $A_0^a = 1$ at unitarity, the s-wave phase shift δ_0 is evaluated to give $\delta_0 = -\frac{\pi}{2}$ on the BCS side of the BCS-BEC crossover. On the BEC side of the crossover, however, the scattering length a_s takes the opposite limit as it approaches positive infinity at unitarity. As a result, $F_0^s \to +\infty$ in the local induced interaction model at the crossover [31], which means $\delta_0 = \frac{\pi}{2}$ on the BEC side of the crossover. Based on Levinson's theorem [35], the increase in the phase shift by π indicates the appearance of a bound state on the BEC side of the BCS-BEC crossover, in agreement with the physics of the BCS-BEC crossover as fermion pairs start to form bounded dimers crossing over to the BEC side. A rough estimate of the molecular binding energy on the BEC side is presented based on the formula

$$E_b = \frac{-\hbar^2}{m\tilde{a}_0^2} \approx -0.8E_F. \tag{2.27}$$

The superfluid transition temperature T_c from the BCS side can be estimated using Eq. (2.3). In the local limit, Eq. (2.3) reduces to

$$T_c = 0.28\, T_F^0 e^{-1/|A_0^a|}. \tag{2.28}$$

Using $F_0^a \to \infty$ in the unitary limit of the BCS Fermi gas from the local model, the above expression gives $T_c = 0.102T_F^0$. The local model predicts a T_c value relatively close to the experimentally measured value of $T_c = 0.167T_F^0$ for the unitary Fermi gas [13]. In the later calculations, I have introduced a scaling factor $L = 1.64$ in

the exponential term of T_c, $e^{-1/|A_0^a|} \to Le^{-1/|A_0^a|}$, to artificially lift T_c at unitarity from the local model prediction to its experimental value.

2.4 Transport Lifetimes and Coefficients

The study of the transport phenomena in the strongly correlated Fermi gas in this work involves the calculation of the various transport lifetimes and transport coefficients. To be more specific, I calculate the transport lifetimes associated with the spin diffusion τ_D, the viscosity τ_η and the thermal conduction τ_K, as well as the related transport coefficients, the spin diffusion coefficient D, the viscosity coefficient η and the thermal conductivity K at low temperatures. The low temperature behaviors of the transport properties for the strongly correlated Fermi gas can still be described by Laudau Fermi-liquid theory as shown in section 1.2, except for the superfluid fluctuations effect introduced in section 2.2 when the temperature is very close to T_c from above.

In this section, I integrate the superfluid fluctuations into the normal Fermi-liquid formulas provided in section 1.2 to study the low temperature transport properties of the strongly correlated Fermi gas. I also add the leading order finite temperature corrections [36–40] to the transport lifetimes and transport coefficients in the attempt to characterize the transport phenomena at the intermediate temperature regime. The Landau parameters needed to calculate the quasiparticle scattering amplitudes are evaluated based on the local induced interaction model from section 2.3. The high temperature portion of the transport properties are sketched qualitatively to give a full temperature profile for the transport phenomena, so that the comparison between the theory and the experiments can be made.

2.4.1 Scattering Amplitudes in the Local Limit

In the local limit, the spin triplet normal Fermi-liquid scattering amplitude vanishes, $t_t = t_{\uparrow\uparrow}(\theta,\phi) = 0$, as mentioned in section 2.3.1. The spin singlet normal Fermi-liquid scattering amplitude $t_s(\theta,\phi)$ is given by Eq. (2.11). Therefore, the normal Fermi-liquid transition probability defined in Eq. (2.5) reduces to

$$W_{\rm n}(\theta,\phi) = \frac{1}{2}W_{\uparrow\downarrow}(\theta,\phi) = \frac{1}{2}\frac{2\pi}{\hbar}\left|\frac{-2A_0^a}{N(0)}\right|^2. \tag{2.29}$$

The transition probability from the superfluid fluctuations $W_{\rm f}(\theta,\phi)$ defined in Eq. (2.6) reduces to

$$W_{\rm f}(\theta,\phi) = \frac{1}{2}\frac{2\pi}{\hbar}\left|\frac{\mathscr{T}_s(\mathbf{q},0)}{2}\right|^2. \tag{2.30}$$

Performing the integrals in Eq. (2.7) in the above local limit, I have the phase space averaged transition probabilities,

$$\langle W\rangle_{\rm normal} = \frac{2\pi}{\hbar}\frac{2}{|N(0)|^2}\cdot 2(1-\frac{\sqrt{6}\pi}{4\gamma}\frac{T_c}{T_{_F}})|A_0^a|^2 \tag{2.31}$$

$$\begin{aligned}\langle W\rangle_{\rm fluctuation} &= \frac{2\pi}{\hbar}\frac{2}{|N(0)|^2} \\ &\times \left[\frac{\frac{\sqrt{6}\pi T_c}{4\gamma T_F}}{\ln\frac{T}{T_c}\left[\ln\frac{T}{T_c}+\left(\frac{\sqrt{6}\pi T_c}{4\gamma T_F}\right)^2\left(11.2+0.28\left(\frac{T_F}{T_c}\right)^2\right)\right]}\right. \\ &+ \left.\frac{\tan^{-1}\left(\sqrt{\left(\frac{\sqrt{6}\pi T_c}{4\gamma T_F}\right)^2\left(11.2+0.28\left(\frac{T_F}{T_c}\right)^2\right)}/\sqrt{\ln\frac{T}{T_c}}\right)}{\left(\ln\frac{T}{T_c}\right)^{3/2}\sqrt{11.2+0.28\left(\frac{T_F}{T_c}\right)^2}}\right],\end{aligned} \tag{2.32}$$

where the critical momentum $\mathbf{q}_{\max}$ has been expressed in terms of T_c,

$$v_f|\mathbf{q}_{\max}| = \sqrt{6}\hbar\varpi = \frac{\sqrt{6}\pi}{\gamma}k_B T_c, \tag{2.33}$$

and the critical momentum translates to the scattering angle θ in the integrals of Eq. (2.7) through $|\mathbf{q}| = 2p_f \sin\theta/2$. The total phase spaced averaged transition probability $\langle W\rangle$ follows from Eq. (2.7) directly. The characteristic relaxation time τ is then determined from Eq. (1.45) with the superfluid fluctuations effect included through $\langle W\rangle$. In the end, the various transport lifetimes and transport coefficients can be calculated from the characteristic relaxation time τ.

2.4.2 Spin Diffusion

I start off the calculation of the transport properties with the spin diffusion lifetimes τ_D. The zero temperature spin diffusion lifetime is approximated from Eq. (1.47), which I denote with τ_D^0 here,

$$\frac{\tau_D^0}{\tau} = \frac{1}{6} + \frac{4\lambda_D}{\pi^2}\frac{3}{4(2-2\lambda_D)}, \tag{2.34}$$

where it is enough to keep only the first term in the summation since the higher terms decrease rapidly. The factor λ_D is estimated from Eq. (1.48) without considering the superfluid fluctuations in the scattering amplitudes. In the local limit, the normal Fermi-liquid transition probability $W_{\rm n}(\theta,\phi)$ becomes angle independent as shown in Eq. (2.29), and λ_D turns out to be a constant, $\lambda_D = -1/3$, irrelevant of the Landau parameters. The zero temperature spin diffusion lifetime τ_D^0 is then a simple fraction of the relaxation time τ,

$$\tau_D^0 \approx 0.129\,\tau = \frac{0.129\times 16}{\hbar|N(0)|^2\langle W\rangle}\frac{\hbar}{k_B T_F}\left(\frac{T_F}{T}\right)^2, \tag{2.35}$$

where $\langle W \rangle$ is evaluated from the local induced interaction model as in section 2.4.1. The leading order finite temperature correction to τ_D^0 is computed in the local limit [36] in Appendix B,

$$\begin{aligned} \frac{1}{\tau_D} - \frac{1}{\tau_D^0} &= -\frac{3}{2}\pi\zeta(3)\frac{k_B T_F}{\hbar}\left(\frac{T}{T_F}\right)^3 \\ &\times \left[\, -2.95(A_0^a)^3 + 1.564(A_0^a)^2 + 1.278\, A_0^a F_0^a \,\right]. \end{aligned} \tag{2.36}$$

The full expression of τ_D for the low to intermediate temperatures is estimated by solving Eq. (2.36),

$$\begin{aligned} \tau_D &= \frac{\hbar}{k_B T_F}\left(\frac{T_F}{T}\right)^2 \left(\frac{\hbar|N(0)|^2}{0.129\times 16}\langle W\rangle - \frac{3}{2}\pi\zeta(3)\right. \\ &\left. \times \left[\, -2.95(A_0^a)^3 + 1.564(A_0^a)^2 + 1.278 A_0^a F_0^a \,\right]\frac{T}{T_F}\right)^{-1} \end{aligned} \tag{2.37}$$

Additionally, the spin diffusion coefficient D is calculated from τ_D using Eq. (1.44) at the low to intermediate temperatures to compare with the experiment [19]. The classical high temperature limit ($T \gg T_F$) of the spin diffusion coefficient is sketched qualitatively to present a better comparison between the theory and the experiment. The characteristic relaxation time τ scales at high temperatures as [41]

$$\tau \propto \frac{\hbar}{k_B T_F}\left(\frac{T}{T_F}\right)^{1/2}, \qquad T \gg T_F. \tag{2.38}$$

The spin diffusion lifetime τ_D assumes the same temperature dependence at high temperatures, the numerical factor in front is extrapolated from the experimental data [19] to give

$$\tau_D \approx 5.84\frac{\hbar}{k_B T_F}\left(\frac{T}{T_F}\right)^{1/2}, \qquad T \gg T_F. \tag{2.39}$$

The spin diffusion coefficient is then expressed as

$$D = \begin{cases} \frac{1}{3} v_f^2 (1 + F_0^a) \tau_D, & T \ll T_F, \\ \frac{k_B T}{m} \tau_D = 5.84 \frac{\hbar}{m} \left(\frac{T}{T_F} \right)^{3/2}, & T \gg T_F, \end{cases} \tag{2.40}$$

where τ_D is given by Eq. (2.37) at low temperatures and by Eq. (2.39) at high temperatures. Eq. (2.40) concludes the spin diffusion properties of the strongly correlated Fermi gas with superfluid fluctuations.

2.4.3 Viscosity and Viscosity/Entropy

The computation of the viscous lifetime τ_η and the viscosity coefficient η follows the same procedure as the spin diffusion case. The zero temperature viscous lifetime τ_η^0 is approximated from Eq. (1.50)

$$\frac{\tau_\eta^0}{\tau} = \frac{1}{6} + \frac{4\lambda_\eta}{\pi^2} \frac{3}{4(2 - 2\lambda_\eta)}, \tag{2.41}$$

where λ_η is evaluated in the same local normal Fermi-liquid limit as λ_D, $\lambda_\eta = 1/5$. Similar to τ_D^0, the quantity τ_η^0 is given by

$$\tau_\eta^0 \approx 0.205\, \tau = \frac{0.205 \times 16}{\hbar |N(0)|^2 \langle W \rangle} \frac{\hbar}{k_B T_F} \left(\frac{T_F}{T} \right)^2. \tag{2.42}$$

The leading order finite temperature correction to τ_η^0 is given as [36]

$$\frac{1}{\tau_\eta} - \frac{1}{\tau_\eta^0} = -3\pi\zeta(3) \frac{k_B T_F}{\hbar} \left(\frac{T}{T_F} \right)^3 \times \left[0.202 (A_0^a)^3 + 0.164 (A_0^a)^2 \right]. \tag{2.43}$$

The full expression of τ_η in the low to intermediate temperature regime is determined from the above equation to be

$$\begin{aligned}\tau_\eta &= \frac{\hbar}{k_B T_F}\left(\frac{T_F}{T}\right)^2\left(\frac{\hbar|N(0)|^2}{0.205\times 16}\langle W\rangle - 3\pi\zeta(3)\right.\\ &\left.\times\left[\,0.202(A_0^a)^3+0.164(A_0^a)^2\,\right]\frac{T}{T_F}\right)^{-1}. \end{aligned} \tag{2.44}$$

The low temperature viscosity coefficient η is then determined from τ_η according to Eq. (1.49). The high temperature limit of τ_η is fitted from the experimental measurement of the viscosity coefficient [21]

$$\tau_\eta \approx 3.4\frac{\hbar}{k_B T_F}\left(\frac{T}{T_F}\right)^{1/2}, \qquad T \gg T_F. \tag{2.45}$$

Therefore, the complete viscosity coefficient over the entire temperature regime is given as

$$\eta = \begin{cases} \frac{1}{5} n p_f v_f \tau_\eta, & T \ll T_F, \\ n k_B T \tau_\eta = 3.4 n\hbar\left(\frac{T}{T_F}\right)^{3/2}, & T \gg T_F, \end{cases} \tag{2.46}$$

where τ_η is given by Eq. (2.44) at low temperatures and by Eq. (2.45) at high temperatures. Eq. (2.46) concludes the viscous properties of the strongly correlated Fermi gas with superfluid fluctuations.

The ratio of viscosity coefficient over entropy density, η/s, is also calculated here to see whether the universal quantum limited lower bound proposed by string theory [14] truly exists in the transport properties of a unitary Fermi gas. To obtain the ratio η/s, I need to calculate the entropy density s in both the low and high temperature limit. The low temperature entropy density is given by Eq. (1.23) from Landau Fermi-liquid theory, and can be rewritten in terms of the

temperature ratio $\frac{T}{T_F}$ as

$$s = \frac{\pi^2}{2} n k_B \left(\frac{T}{T_F} \right), \qquad T \ll T_F. \tag{2.47}$$

A finite temperature correction term is also included in the calculation of the low temperature entropy density [1],

$$\Delta s = -\frac{1}{20} \pi^4 n k_B B^s \left(\frac{T}{T_f} \right)^3 \ln \left(\frac{T}{T_c} \right) \tag{2.48}$$

where

$$B^s = N(0) b^s = -\frac{1}{2} \left[(A_0^s)^2 \left(1 - \frac{\pi^2}{12} A_0^s \right) + 3 (A_0^a)^2 \left(1 - \frac{\pi^2}{12} A_0^a \right) \right]. \tag{2.49}$$

The full entropy density in the low temperature limit is therefore

$$s = \frac{\pi^2}{2} n k_B \left(\frac{T}{T_F} \right) \left[1 - \frac{\pi^2}{10} B^s \left(\frac{T}{T_f} \right)^2 \ln \left(\frac{T}{T_c} \right) \right], \qquad T \ll T_F. \tag{2.50}$$

In the high temperature limit, the total entropy S assumes that of a classical Fermi gas based on regular statistical mechanics analysis [42],

$$S = N k_B \left\{ \frac{5}{2} - \ln \left(\frac{n \lambda^3}{g} \right) \right\}, \qquad T \gg T_F, \tag{2.51}$$

where $\lambda = h / \left(2 \pi m k_B T \right)^{1/2}$ is the thermal wave length, and $g = 2$ for the two component Fermi gases. In the local limit, the mass renormalization disappears, i.e. $m^* = m$, as discussed in section 2.3.2, so the high temperature total entropy in Eq. (2.51) can be reexpressed to give the entropy density,

$$s = n k_B \left\{ \frac{5}{2} - \ln \left(\frac{4}{3 \pi^{1/2}} \right) + \frac{3}{2} \ln \left(\frac{T}{T_F} \right) \right\}, \qquad T \gg T_F. \tag{2.52}$$

With both the viscosity coefficient and the entropy density fully determined, the ratio of η/s is readily calculated and the result will be presented in section 2.5.

2.4.4 Thermal Conduction

The evaluation of the thermal conductivity lifetime $\tau_{_K}$ and the thermal conductivity K is the same as the previous two transport phenomena. I focus only on the low temperature behavior of the thermal conduction as there is a lack of experimental data regarding the thermal conductivity for comparison, hence it suffices to do such to serve the purpose of this work, which is studying the low temperature transport phenomena of the strongly correlated Fermi gas from theoretical perspectives.

The zero temperature thermal conductivity lifetime $\tau_{_K}^0$ is estimated from Eq. (1.54),

$$\frac{\tau_{_K}}{\tau} = \frac{12-\pi^2}{2\pi^2} + \frac{\lambda_{_K}}{\pi^2}\frac{5}{3\,(6-2\lambda_{_K})}, \tag{2.53}$$

and $\lambda_{_K} = 1/3$ for a local Fermi liquid. Again, I have $\tau_{_K}$ in terms of the relaxation time τ as

$$\tau_{_K}^0 \approx 0.119\,\tau = \frac{0.119\times 16}{\hbar|N(0)|^2\langle W\rangle}\frac{\hbar}{k_{_B}T_{_F}}\left(\frac{T_{_F}}{T}\right)^2. \tag{2.54}$$

The leading order finite temperature correction to $\tau_{_K}^0$ is calculated to be [36]

$$\begin{aligned}\frac{1}{\tau_{_K}} - \frac{1}{\tau_{_K}^0} &= -\frac{45}{2\pi}\zeta(3)\frac{k_{_B}T_{_F}}{\hbar}\left(\frac{T}{T_{_F}}\right)^3 \\ &\times \left[-2.09(A_0^a)^3 + 2.696(A_0^a)^2 + \left(1.647 + \frac{0.549}{1+2F_0^a}\right)A_0^aF_0^a\right].\end{aligned} \tag{2.55}$$

The full low to intermediate temperature thermal conductivity lifetime is deter-

mined from the above equation,

$$\tau_K = \frac{\hbar}{k_B T_F}\left(\frac{T_F}{T}\right)^2 \left\{ \frac{\hbar |N(0)|^2}{0.119 \times 16}\langle W\rangle - \frac{45}{2\pi}\zeta(3) \right. \\ \left. \times \left[-2.09(A_0^a)^3 + 2.696(A_0^a)^2 + \left(1.647 + \frac{0.549}{1+2F_0^a}\right) A_0^a F_0^a \right] \frac{T}{T_F} \right\}^{-1}. \tag{2.56}$$

The low to intermediate temperature thermal conductivity K is given by Eq. (1.53), $K = \frac{1}{3} c_V v_f^2 \tau_K$, where τ_K is shown in Eq. (2.56).

2.5 Results and Discussion

In this section, I plot the various transport properties calculated in the previous sections with respect to temperature. The thermal conductivity lifetime τ_K is plotted in its low to intermediate temperature limit, based on which several special features of my theoretical model are explained. The spin diffusion coefficient D and the ratio of viscosity coefficient over entropy density η/s are plotted in the entire temperature range to compare with the experimental data.

2.5.1 Thermal conductivity Lifetime

Since there is a lack of experimental data on the thermal conduction of strongly interacting Fermi gases for me to compare with the calculated thermal conductivity lifetime and thermal conductivity, I present just the low temperature analysis of the thermal conductivity lifetime τ_K based on Eq. (2.56). The thermal conductivity lifetime τ_K is plotted with respect to the temperature ratio T/T_F from low to intermediate temperatures. Several different values of F_0^a are chosen to evaluate τ_K, and the results are depicted in Fig. 2.3.

In the local induced interaction model, the Landau parameter F_0^a is directly

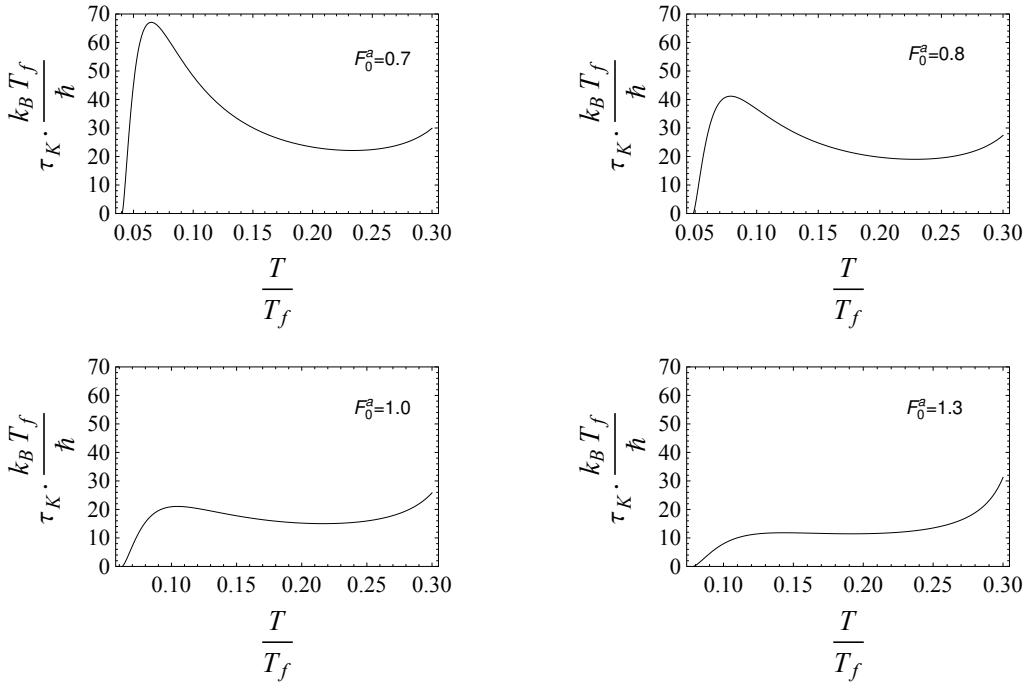

Figure 2.3: Calculated thermal conductivity lifetime τ_K vs temperature. τ_K is plotted in the low temperature limit with different values of F_0^a.

related to the interacting strength of the ultra cold Fermi gas through Eq. (2.14) and shown by Fig. 2.2, so each sub-figure in Fig. 2.3 actually shows the low temperature behavior of τ_K of an ultra cold Fermi gas with a particular interaction strength. Although the shapes of the τ_K curves vary with their corresponding values of F_0^a, several common features are shared among them. Every τ_K curve in the figure has a tendency to go up when the temperature is low and decreasing, which is characteristic for a normal Fermi liquid where the quasiparticle lifetime τ goes as $1/T^2$ at low temperatures. Meanwhile, a sharp drop in the magnitude of the lifetime τ_K is spotted in all four sub-figures of τ_K when the temperature approaches the superfluid transition temperature T_c from above. This special feature in the transport lifetime τ_K is unexpected from a normal Fermi liquid, and it is precisely due to the superfluid fluctuations taking place in the strongly interacting ultra cold Fermi gas when the temperature is very close to T_c. This phenomena is

easily understood by looking at the form of the thermal conductivity lifetime τ_K given in Eq. (2.56). The $\langle W \rangle$ term in the denominator of τ_K starts to diverge when the superfluid fluctuations begin to dominate the quasiparticle scattering amplitudes approaching T_c, therefore the magnitude of τ_K drops rapidly near T_c and vanishes at T_c. When the temperature is extended to some intermediate value, the lifetime τ_K tends to increase as the temperature increases because of the finite temperature correction to τ_K. However, when the temperature gets higher, the finite temperature correction term given in Eq. (2.55) becomes comparable to the zero temperature value $1/\tau_K^0$ rendering the relative smallness of this correction term being unjustified, which in turn introduces an artificial singularity to the lifetime τ_K at some finite temperature. Therefore, the rapid upturn in the tail of the τ_K curve for the case of $F_0^a = 1.3$ in Fig. 2.3 is unphysical and indicative of this artificial singularity. The relatively flat region in the intermediate temperatures of τ_K is interpreted as a result of the competition between the normal Fermi-liquid $1/T^2$ decay in τ_K and the finite temperature correction upturn in τ_K.

The Landau parameter F_0^a affects the shape of the thermal conductivity lifetime τ_K through the superfluid transition temperature T_c given by Eq. (2.28). Since T_c increases as F_0^a increases, the superfluid fluctuations effect kicks in at higher temperatures for higher values of F_0^a, which translates to a lower peak height in the τ_K curve at low temperatures as indicated by Fig. 2.3. The theory fails to capture the correct behavior of τ_K when F_0^a becomes too large, but it succeeds in revealing the superfluid fluctuations above T_c through τ_K, regardless of the choice of F_0^a.

2.5.2 Spin Diffusion Coefficient and Lifetime

The analysis to the spin diffusion lifetime τ_D is slightly different from what I did in the thermal conductivity lifetime τ_K. There exists a similar artificial sin-

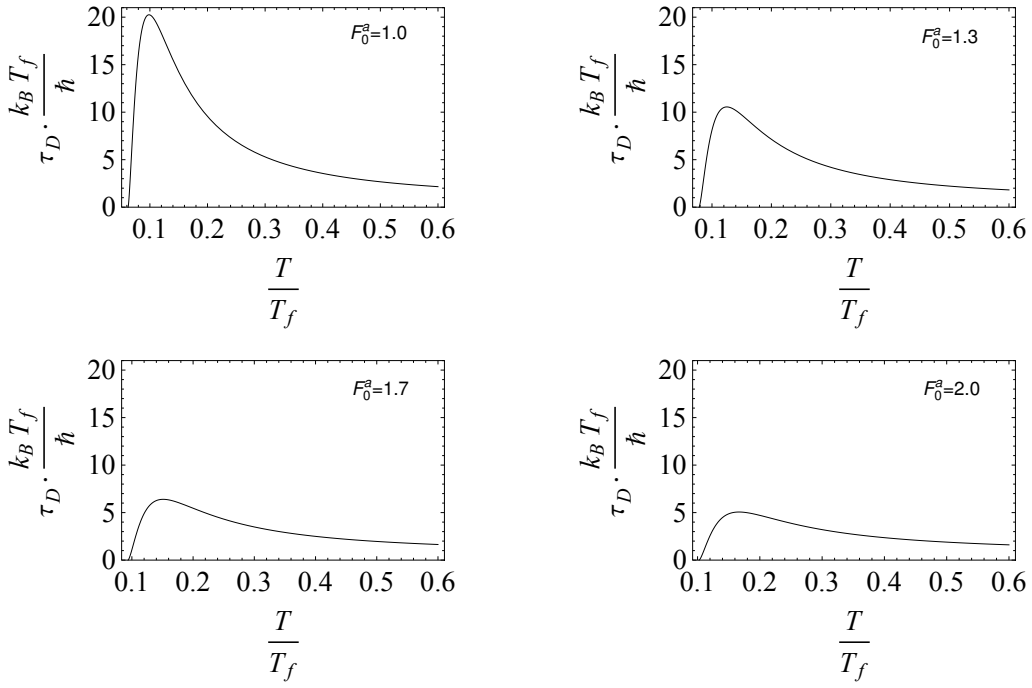

Figure 2.4: Calculated spin diffusion lifetime τ_D vs temperature. The low temperature expansion of τ_D is plotted with different values of F_0^a.

gularity in τ_D as in τ_K when the temperature increases to a point T^* where the finite temperature correction term becomes comparable to $1/\tau_D^0$, according to Eq. (2.37). Since this singularity is an artifact of overextending the correction term in temperature and causes unphysical upturns in the transport lifetimes at intermediate temperatures, I shall remove this undesired mathematical effect by expanding τ_D in powers of the ratio T/T_F and keeping terms up to the fourth powers of T/T_F in Eq. (2.37). The low temperature feature of τ_D is well approximated by the expansion for temperatures $T \ll T^*$. Hereafter, I use this expansion to describe the low to intermediate temperature behavior of τ_D. The resulting plot of τ_D with respect to temperature for several different values of F_0^a is shown in Fig. 2.4. The general features of the τ_D curves are very similar to those of τ_K, except that in the case of τ_D the unphysical upturns are now removed from the tails of these τ_D curves. Once again, the superfluid fluctuations affect greatly the behavior of τ_D

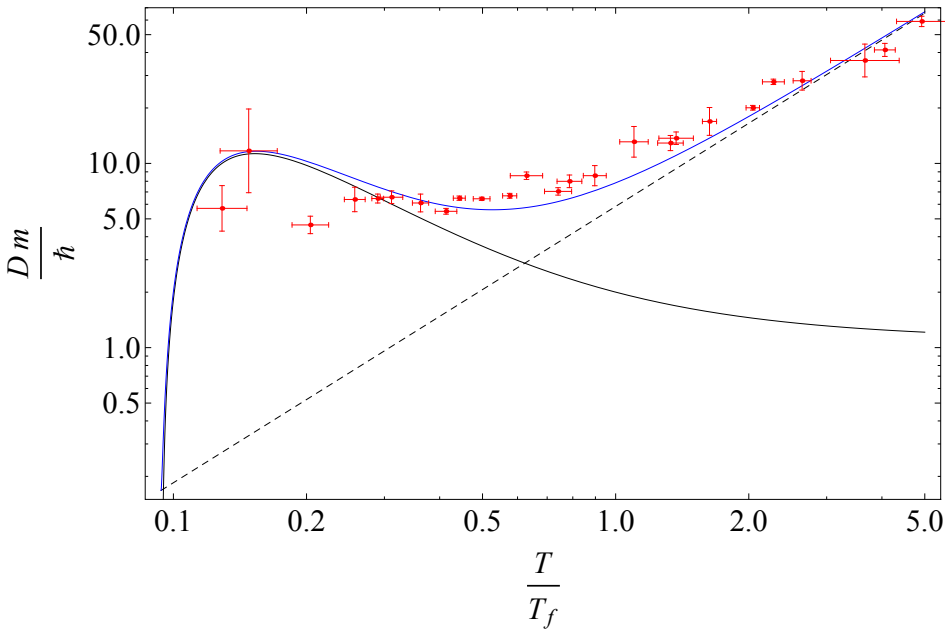

Figure 2.5: Spin diffusion coefficient D vs temperature. The black solid curve is the low temperature expansion of D at $F_0^a = 1.7$; the dashed line is the classical limit of D; the blue curve represents the sum of the two limits; the red dots with error bars are the experimental data [19].

at temperatures right above T_c, causing drastic drops in the τ_D curves.

The spin diffusion coefficient D is plotted in both the low and high temperature limits according to Eq. (2.40). By choosing $F_0^a = 1.7$, I am able to present a good match between the calculated and the measured spin diffusion coefficient [19], as depicted in Fig. 2.5. The use of the low temperature expansion of τ_D is justified since the low temperature portion (roughly at $T < 0.5\,T_F$) of the experimental data I am trying to describe falls below T^* ($T^* \approx 0.65\,T_F$ for $F_0^a = 1.7$). The superfluid transition occurs at $T_c \approx 0.167\,T_F$ in such a unitary Fermi gas [13]. Based on the calculations, the spin diffusion coefficient is suggested to experience a drastic drop when the temperature approaches T_c from above, and behaves like a normal Fermi liquid going as $1/T^2$ for $T_c < T \ll T_F$, when the temperature moves away from T_c. A naive picture is drawn to explain the role of the superfluid fluctuations in the spin diffusion. The spin diffusion coefficient D is defined as the

response of the Fermi system to a perturbation (spin gradient) in generating a net spin current according to Eq. (1.44). The superfluid fluctuations take place when up and down fermions start to pair up and move in the same direction. The Fermi system therefore generates little net spin current when subject to a spin gradient. One then ends up with a very small spin diffusion coefficient.

Since the theory in this work is built under the assumption of a uniform Fermi gas, therefore instead of introducing a scaling factor to account for the trap effect [18], I make an approximation in treating the trapped Fermi gas used in the experiment as a uniform one with an effective average density. The $F_0^a = 1.7$ is interpreted as the effective Landau parameter for the trapped gas. Although I am unable to make $F_0^a \to +\infty$ as it should be for a unitary Fermi gas according to the local induced interaction model, a Fermi system with interaction strength $k_F a_s \approx -3.3$ suggested by $F_0^a = 1.7$ is still considered as strongly interacting. In addition, the local model is constructed under zero temperature, therefore it is possible that F_0^a becomes temperature dependent and the theory deviates from its zero temperature version when temperature increases.

As the spin diffusion coefficient saturates to some finite value $D \approx 6.4\,\hbar/m$ near T_c in the experiment [19], it is interpreted as the evidence of the universal quantum limited lower bound for the spin diffusion coefficient analogous to the conjectured quantum limited viscosity in unitary Fermi gases [14]. However, as seen in Fig. 2.5, the alleged universal quantum limit in the low temperature portion of the spin diffusion coefficient may well be explained by the local minimum found in my theory by an interplay between Fermi liquid effects that want the transport coefficients to diverge, as $T \to 0$, and the superfluid fluctuations that want to drive them to zero at T_c, as $T \to T_c$, from above. The new theoretical model developed in this work brings new insights to the understanding of the transport properties of the unitary Fermi gas by taking the superfluid fluctuations into consideration.

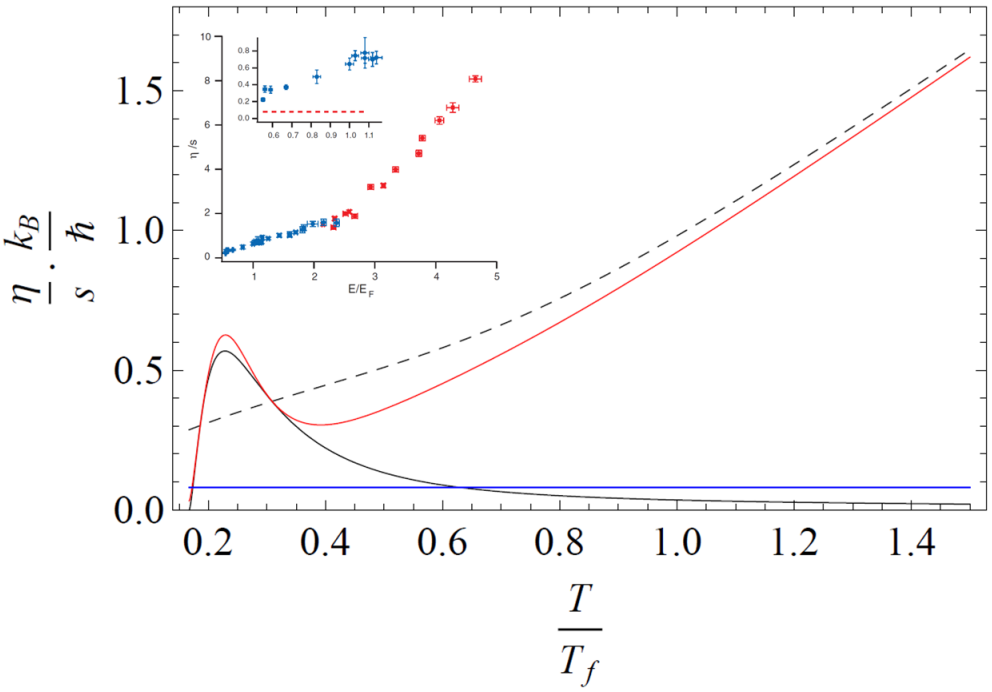

Figure 2.6: The ratio of viscosity coefficient over entropy density η/s vs temperature. The ratio η/s is evaluated at $F_0^a = 100$, i.e. the unitary limit where $F_0^a \to +\infty$ according to the local model. The black solid curve is the low temperature limit of the ratio η/s; the dashed curve is the high temperature limit of this ratio; the red curve represents the single function that captures both the low and high temperature behaviors of this ratio; the horizontal blue line on the bottom indicates the universal quantum limited lower bound of $\eta/s = \hbar/4\pi k_B$ conjectured in Ref. [14]. The inset figure shows the experimental data for the η/s ratio [21].

2.5.3 Viscosity over Entropy Density

To compare the calculations of the viscosity with the experimental findings on the viscosity properties [21], the ratio of the viscosity coefficient over entropy density η/s is plotted against the temperature in both the low and high temperature limits, as depicted in Fig. 2.6. This time, I am able to push F_0^a to infinity and achieve true unitarity in the Fermi gas based on the local induced interaction model. The inset in Fig. 2.6 shows the plot of the measured ratio η/s with respect to the energy ratio E/E_F. The ratio E/E_F could be translated to the ratio T/T_F

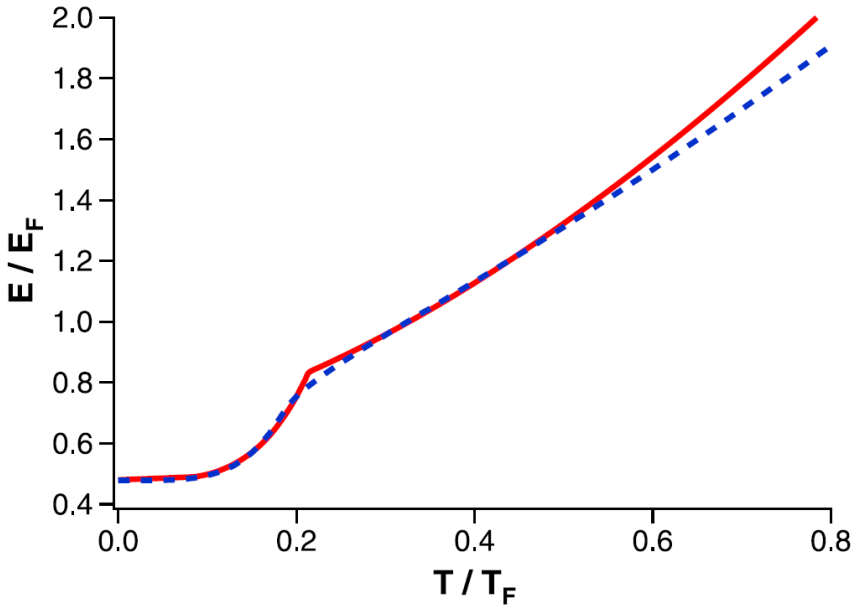

Figure 2.7: The energy of a strongly interacting Fermi gas vs temperature [43]. The red curve shows $E(T)$ as determined from the fit with a heat capacity jump in Ref. [44]. The blue dashed curve shows $E(T)$ as determined from the fit with continuous heat capacity.

as in Fig. 2.7 from Ref. [43]. An energy ratio of $E/E_{_F} = 0.6$ corresponds roughly to a temperature ratio of $T/T_{_F} = 0.17$, therefore the low temperature portions of the calculated and the measured ratio of η/s are plotted in the same temperature window.

A similar local minimum is found in the calculated ratio of η/s shown as the red curve in Fig. 2.6. This local minimum has a height, $\eta/s \approx 0.3\,\hbar/k_{_B}$ in rough agreement with the experimental saturation value of η/s for a nearly perfect Fermi gas [20, 21] in the inset of Fig. 2.6, which is not too far from the conjectured quantum limited lower bound [14], $\eta/s \approx 0.08\,\hbar/k_{_B}$. However, the minimum found in the ratio η/s is once again the result of the same interplay between the superfluid fluctuations and the normal Fermi-liquid effects as discussed in the case of the spin diffusion coefficient according to my theory. Therefore, I find the idea of universal quantum limited transport in the unitary Fermi gas not convincing based on the transport calculations presented in this work.

2.5.4 The $s-p$ Approximation

I have introduced the local approximation for the Fermi liquid description of the cold atom Fermi gases and used the local version of the induced interaction to calculate the Fermi-liquid parameters. This has been done since this provides simple analytic results that provide qualitative and reasonably good quantitative results for the Fermi-liquid parameter F_0^s and the thermodynamic scaling temperature T_s as well as T_c. In earlier publications [31, 45], the momentum dependent induced interaction is used which generated Fermi liquid parameters with $l > 0$. In the unitary limit the induced interaction gives a small mass correction, about 15% above the bare mass, and it gives an $F_0^s = -0.6$. These numbers are independent of the density at unitarity so the thermodynamic scaling is just like what I found for the local model but with a smaller value for T_s. I also found that when I use the s-p approximation [1, 45] to construct the scattering amplitude from the Landau parameters I get better fits for some of the calculated properties. These include, T_c and E_b, where $T_c \approx 0.14T_F$ and $E_b \approx -0.3E_F$. Clearly, I can get better numerical results going beyond the local model but it would not give me qualitatively new insights into some of the properties of this cold atom system. In particular this would not qualitatively change the nature of the strong superfluid fluctuation effects in the transport coefficients just above T_c.

2.6 Summary

To summarize, I have developed a complete formula for calculating the transport lifetimes and transport coefficients above T_c of an ultracold Fermi gas with arbitrary quasiparticle interaction strength through control of F_0^a. The superfluid fluctuations above T_c in the cold Fermi gas are revealed through the calculation of the quasiparticle scattering amplitude near T_c from above. Sudden decreases

in the transport lifetimes as well as the transport coefficients closely above T_c are found as the evidence of the superfluid fluctuations. Upon choosing a proper value of $F_0^a = 1.7$, I am able to describe the experimental data of the spin diffusion coefficient using my theory. The calculated ratio of the viscosity coefficient over the entropy density η/s is compared with the experiment as well. When F_0^a is pushed to infinity indicating the unitary limit, the local minimum found in the theoretical ratio agrees roughly with the minimum measured in the experiment. Unfortunately, the proposed quantum universality in the transport of the unitary Fermi gas is not confirmed by the theory developed in this work. Further work could be done by using the $s-p$ approximation with the induced interaction model for calculating the Landau parameters.

CHAPTER III

Quantum Spin Transport Through a Novel F/N Junction

3.1 Introduction

The second part of this thesis involves the study of the spin dynamics and transport in an F/N junction, one of the most basic spintronic devices. With the development of microelectronic devices based on electric charge reaching to its full capacity in the foreseeable future as the size of device features approaches the dimension of atoms, investigators have been eager to seek device applications based on electron spin, which has led to the emergence of a new research field called spintronics [46]. The central theme of spintronics involves active manipulation of the spin degree of freedom in solid-state systems, which generally requires the generation and control of nonequilibrium spin. Over the past two decades, extensive studies on spintronics have been carried out in various solid-state systems [47]. Among the many interesting spintronic systems, the F/N junction is considered to be one of the simplest and most basic, where nonequilibrium spin polarization could be generated through electrical spin injection [48, 49]. A considerable amount of work has been done studying the spin transport from the ferromagnetic metal to a normal metal in the classical diffusion dominated transport regime [47].

In this work, I focus on investigating the spin transport through the F/N junction under electrical spin injection in the low temperature regime, where the spin diffusion is dominated by spin precession rather than collision in the classical diffusion dominated transport regime as in chapter II. The relative importance of the two mechanisms has been studied both in weak ferromagnetic systems and nonequilibrium paramagnetic systems through calculating the effective spin diffusion coefficient [50]. Here, I focus on studying the propagation of spin waves and transport of magnetization through the interface of the F/N junction. To be more specific, I calculate the possible transverse spin wave modes in the ferromagnetic metal side and the spin-polarized nonequilibrium normal metal side of the F/N junction using Laudau Fermi-liquid theory. The derivation of the various spin wave modes are presented in section 3.2, and the results are shown in section 3.3. I then propose a proper set of boundary conditions at the junction interface, under which the spin waves can successfully propagate from the ferromagnet side of the F/N junction to the normal metal side. Such a phenomena could in principle be tested by a transmission conduction electron spin resonance CESR experiment performed on the F/N junction, and likely experimental results are discussed as well in section 3.3.2. Potential device applications based on this novel spin transport feature of the F/N junction are proposed in section 3.3.3. This work has been published in the journal Physical Review B [51].

3.2 Derivation of Spin Wave Modes

Under electrical spin injection, net magnetization is driven from the ferromagnet into the normal metal region of the F/N junction by a spin-polarized charge current flowing across the F/N junction, as shown in Fig. 3.1(a). For a long enough relaxation time, T_1, of the polarized spin, this would lead to a steady state in the normal metal region of the F/N junction with nonequilibrium mag-

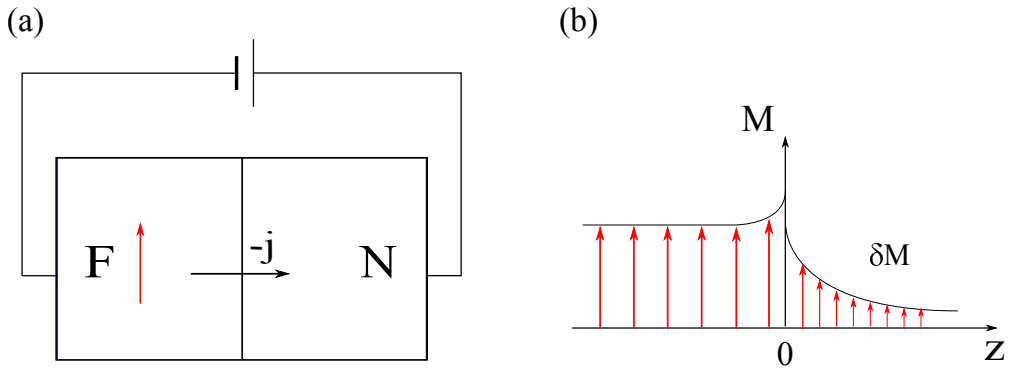

Figure 3.1: Pedagogical illustration of electrical spin injection into the F/N junction [47]. (a) Schematic experimental setup; (b) Distribution of the equilibrium and nonequilibrium magnetization along **z** direction (the direction of the charge current).

netization δM, depicted in Fig. 3.1(b), which I will, from here on, refer to as the spin-polarized quasiequilibrium (QEQ) state in the weak polarization limit [52], i.e., $\delta M \ll 1$. Therefore, in the steady state, the F/N junction could be thought of as a composition of spin-polarized equilibrium (ferromegnet side) and quasiequilibrium (normal metal side) system. I study the transverse spin wave modes that may arise in these systems, when a small transverse spin perturbation is introduced to the steady state.

Using Landau Fermi-liquid theory, spin waves for a paramagnetic Fermi liquid in the presence of a constant external magnetic field have been well understood by solving the spin kinetic equation [1, 53]. These spin wave modes are the well known Silin modes [54] for polarized Fermi liquids. A recent work has extended the study of spin waves to QEQ spin systems [52], where new gapless spin wave modes were found in a spin-polarized QEQ Fermi liquid in the absence of an external magnetic field, similar to the case of a weak ferromagnetic system. Following the same recipe as Ref. [52], I start with the study of the spin wave modes for the QEQ state of the normal metal region of the F/N junction in section 3.2.1.

3.2.1 Quasiequilibrium Fermi Liquid

Assuming the QEQ Fermi liquid having a total particle density, $n = n_\uparrow + n_\downarrow$, and a small magnetization (per unit volume), $\sigma = n_\uparrow - n_\downarrow$, where $n_\uparrow, n_\downarrow$ are the total densities of $\uparrow$, $\downarrow$ spin fermions and $\boldsymbol{\sigma}$ is polarized in an arbitrary direction, with $n = n_{\rm QEQ}$ and $\boldsymbol{\sigma} = \boldsymbol{\sigma}^{\rm QEQ}$ in the steady state, the kinetic equation for the spin density can be derived from the general Landau kinetic equation, Eq. 1.39, as [1]

$$\begin{aligned}\frac{\partial \boldsymbol{\sigma}_{\mathbf{p}}}{\partial t} + \frac{\partial}{\partial r_i}\left(\frac{\partial \varepsilon_{\mathbf{p}}}{\partial p_i}\boldsymbol{\sigma}_{\mathbf{p}} + \frac{\partial \mathbf{h}_{\mathbf{p}}}{\partial p_i} n_{\mathbf{p}}\right) + \frac{\partial}{\partial p_i}\left(-\frac{\partial \varepsilon_{\mathbf{p}}}{\partial r_i}\boldsymbol{\sigma}_{\mathbf{p}} - \frac{\partial \mathbf{h}_{\mathbf{p}}}{\partial r_i} n_{\mathbf{p}}\right) \\ = -\frac{2}{\hbar}\boldsymbol{\sigma}_{\mathbf{p}} \times \mathbf{h}_{\mathbf{p}} + \left(\frac{\partial \boldsymbol{\sigma}_{\mathbf{p}}}{\partial t}\right)_{\rm collision},\end{aligned} \tag{3.1}$$

where $\mathbf{h}_{\mathbf{p}} = \frac{2}{V}\sum_{\mathbf{p}'} f^a_{\mathbf{p}\mathbf{p}'}\boldsymbol{\sigma}_{\mathbf{p}'}$ is the effective field defined by Eq. (1.19) taking into account only the internal field in the absence of an external magnetic field, $f^a_{\mathbf{p}\mathbf{p}'}$ denotes the spin antisymmetric Landau Fermi-liquid interaction, $\varepsilon_{\mathbf{p}}$ is the quasiparticle energy and $\boldsymbol{\sigma}_{\mathbf{p}}$ is the quasiparticle spin density defined as $\boldsymbol{\sigma}_{\mathbf{p}} \equiv -\frac{\partial n^0_{\mathbf{p}}}{\partial \varepsilon_{\mathbf{p}}}\frac{\boldsymbol{\sigma}}{N(0)}$, where $n^0_{\mathbf{p}}$ is the ground state quasiparticle density distribution function (Fermi distribution function). The detailed definitions of the above quantities can be found in chapter I of this thesis, where Landau Fermi-liquid theory is reviewed. The Lorentz force term appearing in the kinetic equations of charged Fermi systems [2] vanishes here as there is no external field. According to Landau Fermi-liquid theory, the spin current is given by

$$j_{\boldsymbol{\sigma},i}(\mathbf{r},t) = 2\int \frac{d^3p}{(2\pi\hbar)^3}\left[\frac{\partial \varepsilon_{\mathbf{p}}}{\partial p_i}\boldsymbol{\sigma}_{\mathbf{p}} + \frac{\partial \mathbf{h}_{\mathbf{p}}}{\partial p_i} n_{\mathbf{p}}\right], \tag{3.2}$$

which represents the current in the $i^{\rm th}$ spatial direction of the $\boldsymbol{\sigma}$ spin polarization. When a charge current, $\mathbf{J}$, is running across the F/N junction in the steady state, I can define in the QEQ Fermi liquid an average drift velocity of electrons, $\mathbf{V}_0^{\rm QEQ}$,

as

$$\mathbf{J} = -en_{\rm QEQ}\mathbf{V}_0^{\rm QEQ}. \tag{3.3}$$

Therefore, the steady state quasiparticle velocity in the QEQ state could be approximated as

$$v_{\mathbf{p}i}^{\rm QEQ} = V_{0i}^{\rm QEQ} + v_{\mathbf{p}i}^0 = \frac{\partial \varepsilon_{\mathbf{p}}}{\partial p_i}, \tag{3.4}$$

where $v_{\mathbf{p}i}^0$ is the $i^{\rm th}$ component of the isotropic equilibrium quasiparticle velocity for the Fermi liquid. Substitute the QEQ quasiparticle velocity $v_{\mathbf{p}i}^{\rm QEQ}$ into Eq. (3.2) and follow the derivations in Appendix C, I have the QEQ spin current as

$$j_{\boldsymbol{\sigma},i}^{\rm QEQ}(\mathbf{r},t) = V_{0i}^{\rm QEQ}\boldsymbol{\sigma}(1+F_0^a) + 2\int \frac{d^3p}{(2\pi\hbar)^3} v_{\mathbf{p}i}^0 \boldsymbol{\sigma}_{\mathbf{p}}(1+\frac{F_1^a}{3}). \tag{3.5}$$

The first term on the right side of Eq. (3.5) is denoted as the drift spin current as it is caused by the electron drift,

$$j_{\boldsymbol{\sigma},i}^{\rm drift}(\mathbf{r},t) = V_{0i}^{\rm QEQ}\boldsymbol{\sigma}(1+F_0^a), \tag{3.6}$$

and the second term is then interpreted as the regular Fermi-liquid diffusive spin current [1],

$$j_{\boldsymbol{\sigma},i}^{\rm diff}(\mathbf{r},t) = 2\int \frac{d^3p}{(2\pi\hbar)^3} v_{\mathbf{p}i}^0 \boldsymbol{\sigma}_{\mathbf{p}}(1+\frac{F_1^a}{3}). \tag{3.7}$$

In the steady state, the diffusive spin current $j_{\boldsymbol{\sigma},i}^{\rm diff}$ is given by the Fick form of spin diffusion as Eq. (1.43), $j_{\boldsymbol{\sigma},i}^{\rm diff} = -D\nabla_i \boldsymbol{\sigma}^{\rm QEQ}$, where D is the collision dominated Fermi-liquid spin diffusion coefficient given by Eq. (1.44) in Landau Fermi-liquid theory. Here, I shall point out that in a normal metal with periodic ion potentials, the collision integral $I[n_{\mathbf{p}'\sigma'}]$ in Eq. (1.39) which determines the spin diffusion contains in principle both quasiparitcle scattering off impurity and quasiparticle scattering off each other, whereas only the later scattering mechanism is considered

in the derivation of the spin diffusion formula in chapter I. The decomposition of the spin current into a drift term and a diffusive term is consistent with the treatment of an earlier study on the electrical spin injection into semiconductors [55].

Let us choose the steady state polarization of the QEQ system to be in the $\boldsymbol{z}$ direction, in which case the small transverse spin distortion, $\delta\boldsymbol{\sigma}$, lies in the xy-plane and could be decomposed as, $\delta\boldsymbol{\sigma} = \delta\sigma_x\,\mathbf{i} + \delta\sigma_y\,\mathbf{j}$. The complex variable $\sigma^{\pm}$ is then defined as

$$\sigma^{\pm} = \delta\sigma_x \pm i\delta\sigma_y, \tag{3.8}$$

to track the dynamics of this small transverse spin distortion. Under such a small transverse spin distortion, a transverse spin current is $j^{\mathrm{diff}\pm}_{\boldsymbol{\sigma},i}(\mathbf{r},t)$ generated in the QEQ system through spin diffusion, and this complex spin current is given as

$$j^{\mathrm{diff}\pm}_{\boldsymbol{\sigma},i}(\mathbf{r},t) = 2\int \frac{d^3p}{(2\pi\hbar)^3} v^0_{\mathbf{p}i}\sigma^{\pm}_{\mathbf{p}}(1+\frac{F^a_1}{3}), \tag{3.9}$$

where $\sigma^{\pm}_{\mathbf{p}} \equiv -\frac{\partial n^0_{\mathbf{p}}}{\partial\varepsilon_{\mathbf{p}}}\frac{\sigma^{\pm}}{N(0)}$ measures the complex density of the transverse spin distortion. The space and time evolution of the transverse spin distortion is governed by the linearized spin conservation law derived from linearizing and summing both sides of Eq. (3.1) over the momentum $\mathbf{p}$,

$$\frac{\partial\sigma^{\pm}(\mathbf{r},t)}{\partial t} + \frac{\partial}{\partial r_i}j^{\mathrm{diff}\pm}_{\boldsymbol{\sigma},i}(\mathbf{r},t) + \frac{\partial}{\partial r_i}V^{\mathrm{QEQ}}_{0i}(1+F^a_0)\sigma^{\pm}(\mathbf{r},t) = 0, \tag{3.10}$$

where, here and through out this chapter, I have assumed a very large spin relaxation time T_1, therefore the spin relaxation term is not included. The linearized equation of motion for the transverse diffusive spin current takes a more complex

form as

$$\begin{aligned}\frac{\partial j^{\mathrm{diff}\pm}_{\boldsymbol{\sigma},i}(\mathbf{r},t)}{\partial t} &+ \frac{1}{3}(1+F_0^a)(1+\frac{F_1^a}{3})v_f^2\frac{\partial}{\partial r_i}\sigma^{\pm}(\mathbf{r},t)\\ &+ (1+\frac{F_1^a}{3})(V_{0k}^{\mathrm{QEQ}}\frac{\partial}{\partial r_k})j^{\mathrm{diff}\pm}_{\boldsymbol{\sigma},i}(\mathbf{r},t)\\ &= \pm i\frac{2}{\hbar}(f_0^a-\frac{f_1^a}{3})j^{\mathrm{diff}\pm}_{\boldsymbol{\sigma},i}(\mathbf{r},t)\sigma^{\mathrm{QEQ}}\\ &\quad -(1+\frac{F_1^a}{3})j^{\mathrm{diff}\pm}_{\boldsymbol{\sigma},i}(\mathbf{r},t)/\tau_D, \end{aligned} \tag{3.11}$$

where an extra spatial gradient term on the spin current is present on the left side of Eq. (3.11) due to the effect of the drift charge current compared to the regular Fermi-liquid result.

Eqs. (3.10) and (3.11) constitute the hydrodynamic equations for the complex transverse spin distortion which are derived in detail in Appendix C. After expanding, $\sigma^{\pm}(\mathbf{r},t)$ and $j^{\mathrm{diff}\pm}_{\boldsymbol{\sigma},i}(\mathbf{r},t)$, in their respective Fourier series as:

$$\sigma^{\pm}(\mathbf{r},t) = \int d^3q\, d\omega\, \sigma^{\pm}(\mathbf{q},\omega)e^{i(\mathbf{q}\cdot\mathbf{r}-\omega t)}, \tag{3.12}$$

$$j^{\mathrm{diff}\pm}_{\boldsymbol{\sigma},i}(\mathbf{r},t) = \int d^3q\, d\omega\, j^{\mathrm{diff}\pm}_{\boldsymbol{\sigma},i}(\mathbf{q},\omega)e^{i(\mathbf{q}\cdot\mathbf{r}-\omega t)}, \tag{3.13}$$

the Fourier transformed hydrodynamic equations lead to a single equation for the dispersion relation,

$$\begin{aligned}\omega^2 &+ \left[\omega_1^{\pm} - (1+F_0^a+1+\frac{F_1^a}{3})(\mathbf{V}_0^{\mathrm{QEQ}}\cdot\mathbf{q})\right]\omega\\ &- i(1+F_0^a)\omega_1^{\pm}(\mathbf{V}_0^{\mathrm{QEQ}}\cdot\mathbf{q}) - c_s^2q^2\\ &+ (1+F_0^a)(1+\frac{F_1^a}{3})|\mathbf{V}_0^{\mathrm{QEQ}}\cdot\mathbf{q}|^2 = 0. \end{aligned} \tag{3.14}$$

The constant term $\omega_1^{\pm}$ in the above equation is given by

$$\omega_1^{\pm} = i\left[(1+\frac{F_1^a}{3})/\tau_D \mp i\frac{2}{\hbar}(f_0^a - \frac{f_1^a}{3})\sigma^{\mathrm{QEQ}}\right], \tag{3.15}$$

and c_s^2 is interpreted as the spin wave velocity,

$$c_s^2 = \frac{1}{3}(1+F_0^a)(1+\frac{F_1^a}{3})v_f^2, \tag{3.16}$$

similar to the sound velocity with regard to the collective excitations arising from Fermi systems subject to number density distortions [1]. Eq. (3.14) is solved in the long wavelength, small $\mathbf{q}$, limit, where I keep only terms of order q^2 and below in the solutions $\omega(q)^{\pm}$. The dispersion relations of the modes found in the QEQ system are given as

$$\omega_0^{\pm}(q) = (1+F_0^a)(\mathbf{V}_0^{\mathrm{QEQ}}\cdot\mathbf{q}) - iD_{\mathrm{eff}}^{\pm}q^2, \tag{3.17a}$$

$$\omega_1^{\pm}(q) = -\omega_1^{\pm} + (1+\frac{F_1^a}{3})(\mathbf{V}_0^{\mathrm{QEQ}}\cdot\mathbf{q}) + iD_{\mathrm{eff}}^{\pm}q^2, \tag{3.17b}$$

where the term $D_{\mathrm{eff}}^{\pm}$ is interpreted as the effective spin diffusion coefficient and given by

$$D_{\mathrm{eff}}^{\pm} = \frac{ic_s^2}{\omega_1^{\pm}} = \frac{\frac{1}{3}(1+F_0^a)(1+\frac{F_1^a}{3})v_f^2}{(1+\frac{F_1^a}{3})/\tau_D \mp i\frac{2}{\hbar}(f_0^a - \frac{f_1^a}{3})\sigma^{\mathrm{QEQ}}}, \tag{3.18}$$

where the term $(1+\frac{F_1^a}{3})/\tau_D$ could be interpreted as the collision term, and $i\frac{2}{\hbar}(f_0^a - \frac{f_1^a}{3})\sigma^{\mathrm{QEQ}}$ as the spin precession term. The meaning of $D_{\mathrm{eff}}^{\pm}$ becomes clearer when Eq. (3.11) is rearranged under the steady state condition, $\partial j_{\boldsymbol{\sigma},i}^{\mathrm{diff}\pm}(\mathbf{r},t)/\partial t = 0$,

$$j_{\boldsymbol{\sigma},i}^{\mathrm{diff}\pm}(\mathbf{r},t) = -D_{\mathrm{eff}}^{\pm}\frac{\partial}{\partial r_i}\sigma^{\pm}(\mathbf{r},t) - \frac{D_{\mathrm{eff}}^{\pm}}{v_f^2(1+F_0^a)/3}(V_{0k}^{\mathrm{QEQ}}\frac{\partial}{\partial r_k})j_{\boldsymbol{\sigma},i}^{\mathrm{diff}\pm}(\mathbf{r},t). \tag{3.19}$$

For small $\mathbf{q}$, the second term on the right side of Eq. (3.19) is an order of q higher than the first term, I can thus drop the last term in Eq. (3.19) and recover the

familiar Fick form for the spin current,

$$j^{\mathrm{diff}\pm}_{\boldsymbol{\sigma},i}(\mathbf{r},t) = -D^{\pm}_{\mathrm{eff}}\frac{\partial}{\partial r_i}\sigma^{\pm}(\mathbf{r},t), \tag{3.20}$$

where $D^{\pm}_{\mathrm{eff}}$ clearly serves as the role of the effective spin diffusion coefficient.

The spin precession term, $i\frac{2}{\hbar}(f_0^a - \frac{f_1^a}{3})\sigma^{\mathrm{QEQ}}$, in the denominator of $D^{\pm}_{\mathrm{eff}}$ in Eq. (3.18), often referred to as the Leggett-Rice effect [56, 57], is solely a consequence of the interactions between quasiparticles; it would cease to exist had I treated the electronic system in the normal metal as a free Fermi gas using the simple electron band structure model, i.e., $f_0^a = f_1^a = 0$. By making the Landau parameters F_l^a go to zero, I have effectively shut off the quasiparticle interactions in the QEQ system, then the effective spin diffusion coefficient reduces to the collision dominated Fermi-liquid spin diffusion coefficient, $D = \frac{1}{3}v_f^2\tau_D$, in which case the spin diffusion lifetime τ_D derived from the collision integral $I[n_{\mathbf{p}'\sigma'}]$ is largely determined by impurity scattering in the material rather than by quasiparticle scattering caused by inter-particle interactions. The complete picture of the competition between the collision effect and the spin precession effect in the effective spin diffusion coefficient over a wide temperature range was obtained from the spin echo experiment in liquid ^{3}He [58], and was also studied theoretically in the spin polarized Fermi liquids [50].

In the low temperature limit, I take the spin diffusion lifetime $\tau_D \to \infty$, since the characteristic relaxation time τ varies as T^{-2} according to Eq. (1.45) in a clean Fermi liquid where the impurity scattering is negligible, therefore, the collision term, $(1 + \frac{F_1^a}{3})/\tau_D \to 0$, becomes negligible in $D^{\pm}_{\mathrm{eff}}$ compared to the spin precession term, leading to a purely imaginary effective spin diffusion coefficient:

$$D^{\pm}_{\mathrm{eff}} = \pm\frac{ic_s^2}{\frac{2}{\hbar}(f_0^a - \frac{f_1^a}{3})\sigma^{\mathrm{QEQ}}}. \tag{3.21}$$

Finally, by plugging Eq. (3.21) into Eq. (3.14), the dispersion relations of the modes for the QEQ system in the low temperature precession dominated regime can be expressed as

$$\omega_0^{\pm}(q) = (1+F_0^a)(\mathbf{V}_0^{\mathrm{QEQ}}\cdot\mathbf{q}) \pm \frac{c_s^2 q^2}{\frac{2}{\hbar}(f_0^a - \frac{f_1^a}{3})\sigma^{\mathrm{QEQ}}}, \tag{3.22a}$$

$$\begin{aligned}\omega_1^{\pm}(q) =& (1+\frac{F_1^a}{3})(\mathbf{V}_0^{\mathrm{QEQ}}\cdot\mathbf{q}) \mp \frac{c_s^2 q^2}{\frac{2}{\hbar}(f_0^a - \frac{f_1^a}{3})\sigma^{\mathrm{QEQ}}} \\ & \mp \frac{2}{\hbar}(f_0^a - \frac{f_1^a}{3})\sigma^{\mathrm{QEQ}}.\end{aligned} \tag{3.22b}$$

Since both dispersion relations of the modes contain only real terms, for small enough $\mathbf{q}$, I have found the transverse spin wave modes that survive from Landau damping [1] and can propagate through the QEQ system, which serve as collective excitations of the QEQ system.

3.2.2 Ferromagnetic Fermi Liquid

In this section, I proceed to derive the spin wave modes in the ferromagnetic Fermi liquid using the same method as in the QEQ system. I consider here a weak ferromagnetic Fermi liquid for the ferromagnet region of the F/N junction, where the spin dynamics could be studied in the language of Landau Fermi-liquid theory [59] in a similar fashion as the QEQ system. I should use $\bar{F}_l^a$ and $\bar{f}_l^a$ for the Landau parameters in the ferromagnetic metal side of the F/N junction to distinguish them with the Landau parameters used in the QEQ system. The derivation of the spin wave modes starts from the same spin kinetic equation, Eq. (3.1), with the various Fermi-liquid quantities being replaced by their values in the ferromagnetic state. In the precession dominated regime, the transverse spin wave modes in the ferromagnet region of the F/N junction turn out to be nearly identical to the ones found in the normal metal region of the F/N junction, i.e.,

the QEQ Fermi liquid,

$$\omega_0^{\pm}(q) = (1+\bar{F}_0^a)(\mathbf{V}_0^{\mathrm{FM}}\cdot\mathbf{q}) \mp \frac{\bar{c}_s^2 q^2}{\frac{2}{\hbar}(\bar{f}_0^a - \frac{\bar{f}_1^a}{3})\sigma^{\mathrm{FM}}}, \tag{3.23a}$$

$$\begin{aligned}\omega_1^{\pm}(q) =& (1+\frac{\bar{F}_1^a}{3})(\mathbf{V}_0^{\mathrm{FM}}\cdot\mathbf{q}) \pm \frac{\bar{c}_s^2 q^2}{\frac{2}{\hbar}(\bar{f}_0^a - \frac{\bar{f}_1^a}{3})\sigma^{\mathrm{FM}}} \\ & \mp \frac{2}{\hbar}(\bar{f}_0^a - \frac{\bar{f}_1^a}{3})\sigma^{\mathrm{FM}},\end{aligned} \tag{3.23b}$$

except for the definition of the spin wave velocity,

$$\bar{c}_s^2 = \frac{1}{3}|1+\bar{F}_0^a|(1+\frac{\bar{F}_1^a}{3})\bar{v}_f^2, \tag{3.24}$$

since, $(1+\bar{F}_0^a) < 0$, for a ferromagnetic Fermi liquid, $\bar{v}_f$ is the Fermi velocity of the electrons in the ferromagnet, σ^{FM} is the equilibrium spin polarization in the ferromagnet, and $\mathbf{V}_0^{\mathrm{FM}}$ is the drift velocity of electrons in the ferromagnet, which is related to the charge current through,

$$\mathbf{J} = -en_{\mathrm{FM}}\mathbf{V}_0^{\mathrm{FM}}, \tag{3.25}$$

with n_{FM} being the equilibrium carrier density in the ferromagnet. Again, for small $\mathbf{q}$, the transverse spin wave modes represented by Eq. (3.23) are the propagating modes in the ferromagnet region of the F/N junction.

3.2.3 Boundary Conditions

So far, I have established the propagating transverse spin wave modes in the ferromagnet region and the normal metal region of the F/N junction, respectively. Naturally, one would want to look for proper boundary conditions to make the spin wave modes propagate through the interface of the F/N junction, as it could greatly increase the functionality of the F/N junction as a spintronic device. To

simplify the analysis while keeping the underlying physics unchanged, I thereby treat the F/N junction as an effectively one dimensional structure, where only the spatial variation in the $\boldsymbol{z}$ direction of the spin density is non-zero as shown in Fig. 3.1.

In describing the steady state of the F/N junction under electrical spin injection, we have adopted the boundary conditions analogous to earlier studies on spin injection into metals [48] and semiconductors [55], where the total spin current is continuous at the interface in the absence of surface spin relaxation,

$$j^{\mathrm{FM}}_{\boldsymbol{\sigma},z}(z,t) = j^{\mathrm{QEQ}}_{\boldsymbol{\sigma},z}(z,t) \quad \text{for } z = 0, \tag{3.26}$$

where $j^{\mathrm{FM}}_{\boldsymbol{\sigma},z}(z,t)$ stands for the spin current in the ferromagnet region of the F/N junction, and $j^{\mathrm{QEQ}}_{\boldsymbol{\sigma},z}(z,t)$ stands for the spin current in the normal metal QEQ region of the F/N junction.

Contrary to the steady state spin polarization, I assume hard boundary conditions on the oscillations of the small transverse spin distortion,

$$\frac{\partial \sigma^{\pm}_{\mathrm{FM}}}{\partial z} = 0 \quad \text{for } \; z = -L_1 \text{ and } 0, \tag{3.27a}$$

$$\frac{\partial \sigma^{\pm}_{\mathrm{QEQ}}}{\partial z} = 0 \quad \text{for } \; z = 0 \text{ and } L_2, \tag{3.27b}$$

where $\sigma^{\pm}_{\mathrm{FM}}$ and $\sigma^{\pm}_{\mathrm{QEQ}}$ stand for the complex transverse spin distortions in the ferromagnet and the QEQ system, respectively. According to the boundary conditions given in Eq. (3.27), the transverse diffusive spin current arising from the transverse spin distortion vanishes at the surfaces,

$$j^{\mathrm{diff}\pm}_{\boldsymbol{\sigma},z}(z,t) = -D^{\pm}_{\mathrm{eff}} \frac{\partial \sigma^{\pm}}{\partial z} = 0 \quad \text{for } \; z = 0, -L_1 \text{ and } L_2, \tag{3.28}$$

where, L_1 and L_2, are the widths of the ferromagnet region and the normal metal

region of the F/N junction, respectively. Under the conditions of Eq. (3.27a), a series of standing wave modes with wave numbers, $q_z = n\pi/L_1$, could be excited for the transverse spin waves in the ferromagnet region of the F/N junction. These standing wave modes should appear as sidebands on the electron spin-resonance line analogous to the spin wave excitations in nonferromagnetic metals in transmission CESR experiments [60, 61], which I will discuss to some extent in section 3.3.2 of this thesis. Under spin wave excitation, transverse spin oscillations are transmitted from the left edge of the ferromagnet region to the interface of the F/N junction through the propagation of the standing wave modes, resulting in the accumulation of oscillating transverse spin signals at the interface. Recalling that I have required the total spin current to be continuous as Eq. (3.26), as well as the vanishing of the diffusive spin current in Eq. (3.28), $j^{\mathrm{diff}\pm}_{\boldsymbol{\sigma},z}(z,t) = 0$, at the interface, the drift spin current must then be continuous at the interface,

$$j^{\mathrm{drift}\pm}_{\mathrm{FM},\boldsymbol{\sigma},z}(z,t) = j^{\mathrm{drift}\pm}_{\mathrm{QEQ},\boldsymbol{\sigma},z}(z,t) \quad \text{for} \;\; z = 0. \tag{3.29}$$

Since the drift spin current is related to the electron drift velocity and the spin density through Eq. (3.6), it then leads to the following relations,

$$V^{\mathrm{FM}}_{0z}\sigma^{\pm}_{\mathrm{FM}}(1+\bar{F}^a_0) = V^{\mathrm{QEQ}}_{0z}\sigma^{\pm}_{\mathrm{QEQ}}(1+F^a_0) \quad \text{for} \;\; z = 0, \tag{3.30}$$

where I have assumed that the electron drift velocity is pointing towards the $\boldsymbol{z}$ direction in both the ferromanetic and the QEQ systems. Therefore, the transverse spin signals in the ferromagnet side of the interface are driven into the normal metal region by the external electric potential in the form of a continuous drift spin current. Consequently, propagating transverse spin wave modes are excited in the normal metal region of the F/N junction once the transverse spin distortion is driven into the normal metal region. Under the conditions of Eq. (3.27b),

similar standing wave modes with wave numbers, $q_z = n\pi/L_2$, could be excited in the normal metal region of the F/N junction as well, which makes it possible for the transmission CESR experiment to pick up the spin signals coming out of the normal metal side of the F/N junction. Therefore, Eq. (3.26) and Eq. (3.27) constitute the boundary conditions under which the spin wave modes can effectively propagate across the F/N junction.

In real systems where interface roughness is inevitable, spin-flip scattering may arise inside the contact of the F/N junction due to spin-orbit coupling or magnetic impurities. The effect of the spin non-conserving scattering is investigated in Ref. [62], where a mismatch is created between the spin currents on the left and right hand sides of the interface. Subject to the different natures of the contact and the materials making the F/N junction, the polarization of the spin current injected into the normal metal region of the F/N junction can be either larger or smaller than that of the spin current on the ferromagnet side of the junction, $j^{\rm FM}_{\boldsymbol{\sigma},z}(0,t) \lessgtr j^{\rm QEQ}_{\boldsymbol{\sigma},z}(0,t)$. In some cases, the direction of the polarization of the spin current can even be flipped across the interface, which is somewhat counterintuitive. To give account for the spin non-conserving scattering at the interface, I introduce a proportionality factor α on the left hand side of Eq. (3.30),

$$\alpha V^{\rm FM}_{0z}\sigma^{\pm}_{\rm FM}(1+\bar{F}^a_0) = V^{\rm QEQ}_{0z}\sigma^{\pm}_{\rm QEQ}(1+F^a_0) \quad \text{for } z=0, \tag{3.31}$$

where α can be both positive and negative. Therefore, as long as α is non-zero, an appreciable amount of transverse spin signals is still driven into the normal metal region of the F/N junction, and the transverse spin wave modes can still be excited in the normal metal region of the junction and propagate through the interface. Finally, I claim that as long as efficient spin injection is achieved in the F/N junction, the qualitative spin transport features of the junction stay unchanged

despite the presence of the interface roughness. The dispersions of the spin wave modes also remain the same as they are intrinsic modes of the materials forming the F/N junction under electrical spin injection.

3.3 Results and Discussion

In this section, I plot the dispersions of the spin wave modes found in the previous sections for several chosen sets of the Landau parameters. A transmission CESR experiment is proposed in the F/N junction to detect the proposed propagation of spin wave modes across the F/N junction. Potential device applications based on this spin transport phenomena is speculated in the end.

3.3.1 Spin wave modes

Aside from the collective modes developed in the previous sections for both QEQ and ferromagnetic systems, there are also a continuum of particle-hole (p-h) excitations in these systems. In spin polarized Fermi systems such as the weak ferromagnetic and the QEQ systems studied in this thesis, the p-h excitation involves spin flips, and the associated excitation energy could be calculated as $\hbar\omega_{\text{p-h}} = \varepsilon_{\mathbf{p}+\mathbf{q},\sigma} - \varepsilon_{\mathbf{p}\sigma'}$, where the quasiparticles and quasiholes participating in such excitations are all restricted near the Fermi surface. Therefore, the dispersions of the p-h excitations for the QEQ system are given as [52]

$$\omega^{\pm}_{\text{p-h}}(q) = \mp\frac{2}{\hbar}\sigma^{\text{QEQ}} f_0^a + \mathbf{q}\cdot\mathbf{v}_{\mathbf{p}}, \tag{3.32}$$

where, $\mathbf{v}_{\mathbf{p}} = \mathbf{V}_0^{\text{QEQ}} + \mathbf{v}_{\mathbf{p}}^0$, is the steady state quasiparticle velocity given by Eq. (3.4) for the QEQ system, and $|\mathbf{v}_{\mathbf{p}}^0| = v_f$. The dispersions of the p-h excitations

for the ferromagnetic systems are given by [63]

$$\omega^{\pm}_{\text{p-h}}(q) = \mp\frac{2}{\hbar}\sigma^{\text{FM}}\bar{f}^{a}_{0} + \mathbf{q}\cdot\bar{\mathbf{v}}_{\mathbf{p}}, \tag{3.33}$$

where, analogous to the QEQ system, $\bar{\mathbf{v}}_{\mathbf{p}} = \mathbf{V}^{\text{FM}}_{0} + \bar{\mathbf{v}}^{0}_{\mathbf{p}}$, is the steady state quasiparticle velocity for the ferromagnetic system, and $|\bar{\mathbf{v}}^{0}_{\mathbf{p}}| = \bar{v}_{f}$. For a given $\mathbf{q}$ in the QEQ system, with the freedom of choosing $\mathbf{v}_{\mathbf{p}}$ over the entire Fermi surface, the dispersions of the p-h excitations in Eq. (3.32) form a continuum, bounded by the maximum and minimum values of $\mathbf{q}\cdot\mathbf{v}_{\mathbf{p}}$. The same argument can be applied to the ferromagnetic system, and a similar p-h continuum exists in the ferromagnetic system as well.

The dispersions of the spin wave modes for both the QEQ and the ferromagnetic systems together with their respective p-h continuums are plotted in the low temperature precession dominated regime in Fig. 3.2. Here, I have chosen $\mathbf{q}$, $\mathbf{V}^{\text{QEQ}}_{0}$ and $\mathbf{V}^{\text{FM}}_{0}$ to be in the $\boldsymbol{z}$ direction in showing the dispersion relations of the spin wave modes, as I consider the F/N junction an effectively one dimensional system. A spin polarization of 10%, $\sigma/n = 10\%$, has been chosen for both systems for the plot. Only the upper branches $\omega^{+}(q)$ of the spin wave modes are shown in the plot, as the physics is the same for the two branches in Eqs. (3.22) and (3.23), except for the direction of the spin precession.

To evaluate the spin wave dispersion relations for the QEQ system on the normal metal region of the F/N junction, I use the set of Landau parameters F^{a}_{0} and F^{a}_{1} suitable for the simple metal aluminum derived from Ref. [64]. The Landau parameters used for evaluating the dispersion relations in the ferromagnetic system are obtained from an earlier study on the weak ferromagnetic heavy fermion material MnSi [63].

In a typical electrical spin injection experiment on the F/N junction [49] com-

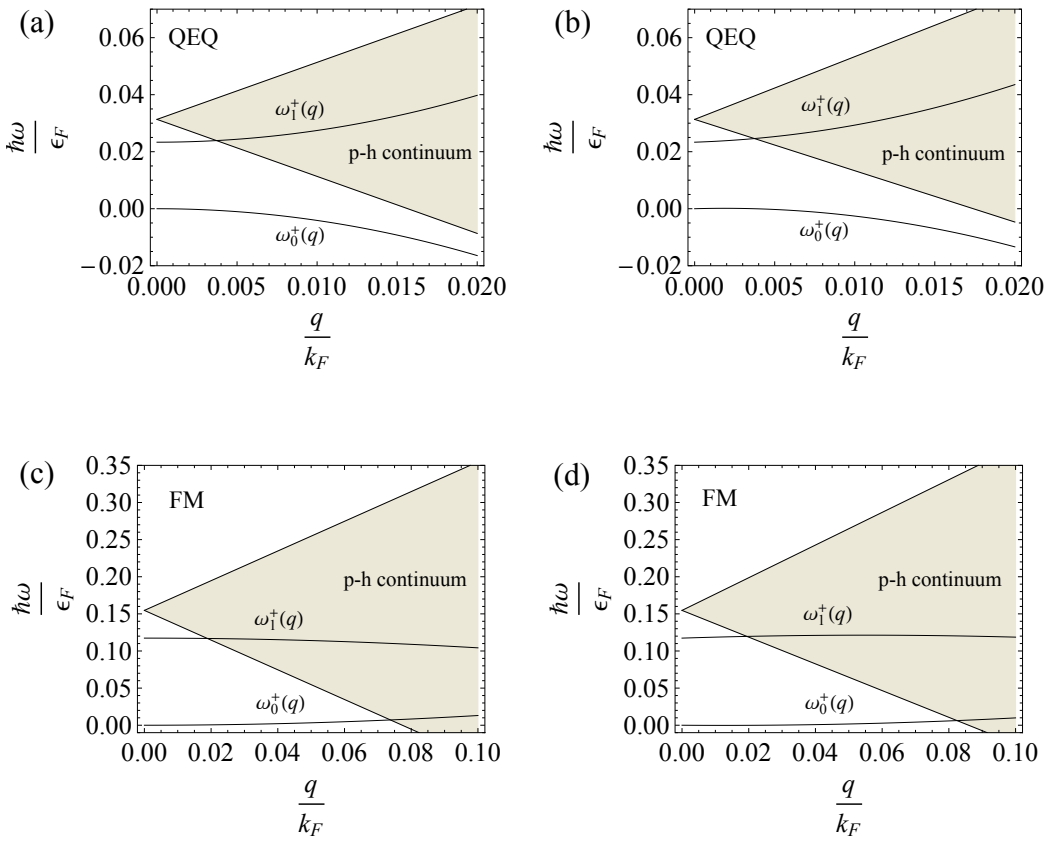

Figure 3.2: Dispersion relations of the spin wave modes and p-h continuums of the QEQ system and Ferromagnetic system. (a) QEQ system with $F_0^a = -0.235$, $F_1^a = -0.18$, $V_0^{\rm QEQ} = 0$; (b) QEQ system with $F_0^a = -0.235$, $F_1^a = -0.18$, $V_0^{\rm QEQ}/v_f = 10\%$; (c) Ferromagnetic system with $\bar{F}_0^a = -1.16$, $\bar{F}_1^a = -0.84$, $V_0^{\rm FM} = 0$; (d) Ferromagnetic system with $\bar{F}_0^a = -1.16$, $\bar{F}_1^a = -0.84$, $V_0^{\rm FM}/\bar{v}_f = 10\%$.

posed of simple metals, nickel and iron on the ferromagnet side, and aluminum on the normal metal side, the electron drift velocity $\mathbf{V}_0$ is negligible compared with the Fermi velocity v_f for a small driven current of order $10 \sim 100\,\mathrm{mA}$, however $\mathbf{V}_0$ can be appreciable with respect to the Fermi velocity when a heavy fermion material with a big effective mass is used on either side of the F/N junction, since the Fermi velocity, $v_f = p_f/m^*$, is reduced due to the big effective mass. In fact, for an F/N junction with a cross section of $1\mu m \times 1\mu m$ and a driven current of 1 A during the electrical spin injection experiment, one could have a drift velocity as close as 10% of the Fermi velocity, $\mathrm{V}_0/v_f \approx 10\%$, if the effective mass m^* of the heavy fermion material is of order $10^2 \sim 10^3\, m_e$ and the electron density is that of a typical metal [65], $n \approx 10^{23} cm^{-3}$. Hence, the spin wave dispersions for both the zero drift velocity case (simple metal F/N junctions) and the 10% drift velocity case (heavy fermion material F/N junctions) are shown in Fig. 3.2.

As is shown in Fig. 3.2(a) and 3.2(b), there exists a gapless mode as well as a gapped spin wave mode in the QEQ system despite the absence of an external magnetic field. This is because the accumulation of the nonequilibrium spin polarization in the QEQ system has effectively broken the spin symmetry in what would be originally a paramagnetic system, which makes it possible for the existence of the gapless spin wave mode — the gapless Nambu-Goldstone mode in systems with spontaneous continuous symmetry breakings. Although the dispersion relation of the gapless spin wave mode in the QEQ system is very similar to the gapless Nambu-Goldstone mode of the ferromagnetic system shown in Fig. 3.2(c) and 3.2(d), their respective origins are fundamentally different as has been discussed in detail in Ref. [52]. In a ferromagnetic system, the equilibrium magnetization in the ground state arises from the intrinsic Hamiltonian that describes the system, whereas the spin symmetry in the QEQ system is broken by imposing a nonequilibrium spin polarization on top of a paramagnetic ground state through

constant spin injections.

An intuitive picture is drawn to account for the rising of the gapless and gapped spin wave modes in both the QEQ and the ferromagnetic systems. The gapless spin wave modes in both systems are related to the uniform precessional mode of the spin polarization. This is understood through the following argument. If I take $\mathbf{q} = 0$, the spatial dependence of the transverse spin distortion disappears according to Eq. (3.12). Therefore, each individual spin of the system is polarized in the same direction, hence no uniform precession of the individual spins around the internal field will take place, and this corresponds to the case $\omega(0) = 0$, which resembles a gapless energy spectrum for the uniform spin precessional mode. Consequently, the gapped spin wave modes must be related to the precessional mode of the spin current, as the two spin wave modes are the solutions to the coupled hydrodynamic equations of the spin polarization, Eq. (3.10), and the spin current, Eq. (3.11). The gapped modes are collective excitations of the system which involve energy consuming spin flip processes, and could also be interpreted as the Higgs amplitude mode in a weak ferromagnet [63].

For a small enough $\mathbf{q}$, the dispersion curves of the spin wave modes are outside the p-h continuums (shaded areas in Fig. 3.2), therefore the collective excitations become propagating spin wave modes without getting Landau damped. It has to be pointed out that although the gapless modes seem to survive entirely from the p-h continuum, the calculation is only accurate in the small $\mathbf{q}$ limit. Corrections to the dispersion relations as well as the p-h continuums at a larger $\mathbf{q}$ need to be evaluated through calculating the complete spin response function of the system, which is beyond the scope of this thesis.

The electron drift velocity $\mathbf{V}_0$ does not change dramatically the dispersion relations of the spin wave modes found in the F/N junction. It merely introduces an additional linear $\mathbf{q}$ term to the dispersion relations, as can be seen, for example,

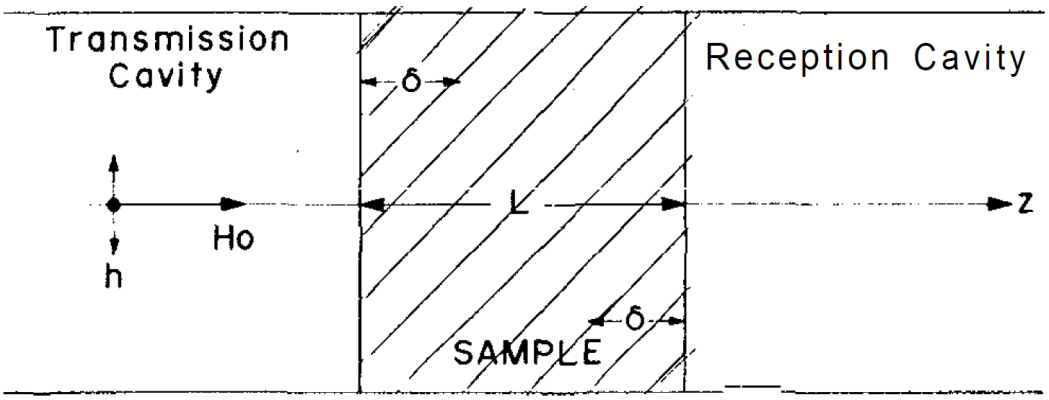

Figure 3.3: An illustrative description of a transmission CESR experiment setup [66].

in Eq. (3.22) of the low temperature spin wave dispersions for the QEQ system. The dispersion relations become anisotropic because of this linear term, which is quite understandable since the system itself is not isotropic by nature when it has a global flow of electrons drifting towards a particular direction. For a 10% drift velocity with respect to the Fermi velocity, the spin wave dispersions as well as the p-h continuums of both the QEQ and the ferromagnetic systems are tilted counterclockwise by a small angle compared to their zero drift velocity results shown in Fig. 3.2. However, the electron drift current does play a crucial rule in setting up the boundary conditions in section 3.2.3 for the propagation of the spin wave modes across the F/N junction.

3.3.2 Transmission CESR experiment

The transmission CESR experiment has long been used in investigating the spin wave excitations in paramagnetic metals [60, 61]. A simple illustrative description of the experimental setup of the sample cavity in a transmission CESR experiment is provided in Fig. 3.3, where, by coupling a microwave power to one side of the metal sample (the transmission cavity), the spin wave modes are excited in the sample and spin signals are transmitted through the sample to be detected by the

receiver on the other side (the reception cavity). For paramagnetic systems, an external magnetic field $\mathbf{H}_0$ has to be applied to the sample in order to excite spin waves.

When the frequency of the incident microwave power matches the frequency of the intrinsic standing spin wave modes of the sample, i.e., $\omega = \omega(q)$ with $q = n\pi/L$, where $\omega(q)$ is the spin wave dispersion of the sample and L is the width of the sample, the system is under spin resonance with standing spin wave modes being excited in the sample and there appears a peak in the intensity of the transmitted spin signals being collected by the receiver. A typical set of transmitted spin signal data from the transmission CESR experiment would contain multiple peaks over a range of frequency as shown in Fig. 3.4 [61]. These peaks are known as the spin resonance lines, and the central peak ($n = 0$) in the spin-wave signals is the Dysonian line [67] for the usual electron spin resonance (ESR), where the frequency of the incident microwave power is equivalent to the Larmor frequency, $\omega_0 = \gamma \mathrm{H}_0$.

Here, I propose a transmission CESR experiment on the F/N junction under electrical spin injection to probe the spin wave modes calculated in section 3.2, and to test the proposal of propagating spin wave modes across the F/N junction. According to the derivations in section 3.2, spin wave modes can be excited in the QEQ system without the introduction of an external magnetic field, which is the major difference between the QEQ state and the equilibrium paramagnetic state. Since the F/N junction contains a QEQ system on one side and a ferromagnetic system on the other, instead of applying an external magnetic field to the sample and sweeping through a range of the external magnetic fields during the measurement of a typical transmission CESR experiment on paramagnetic systems, I propose not to apply any external magnetic field to the sample, but vary the frequency of the incident microwave power, such that the idea of the QEQ

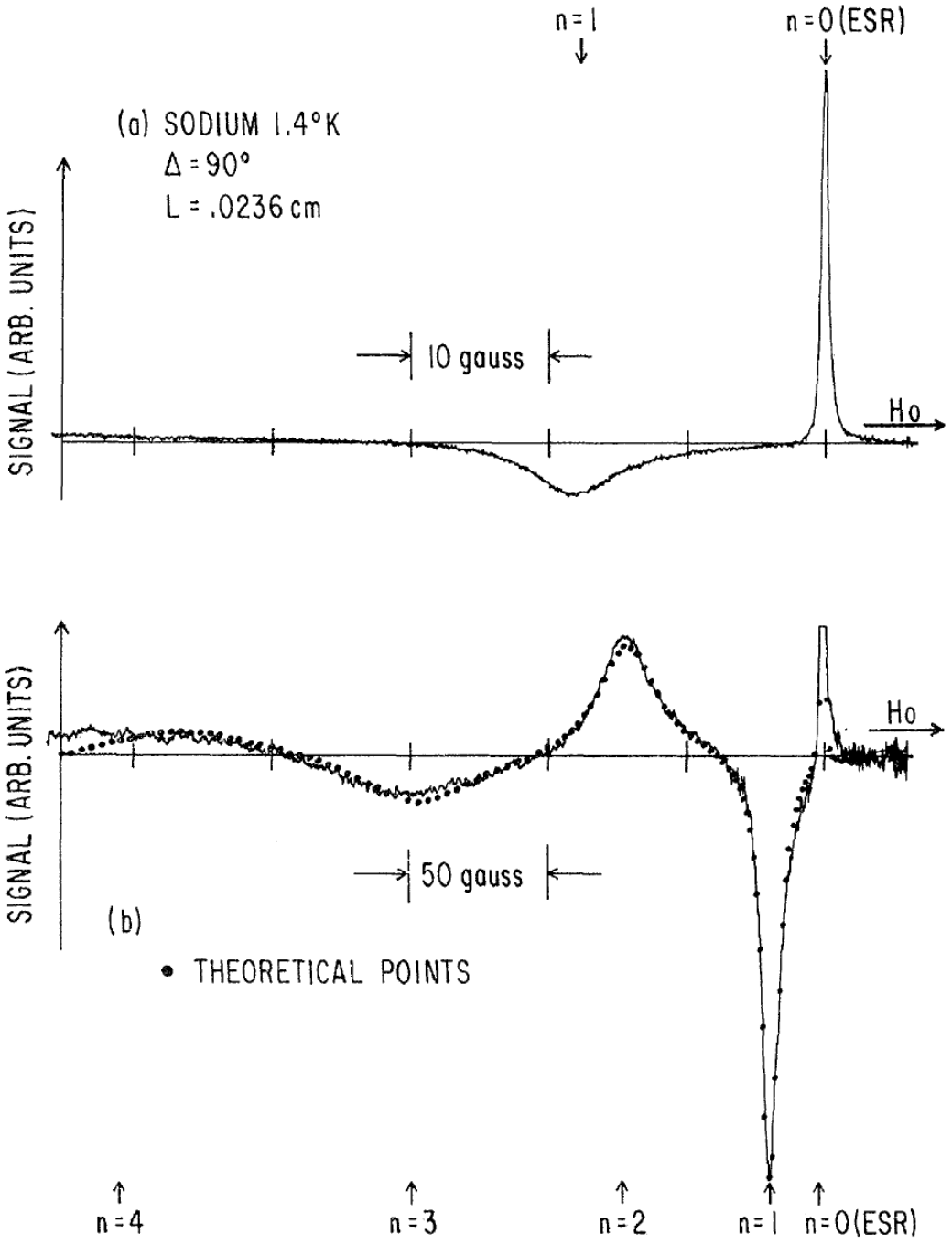

Figure 3.4: Typical spin-wave signals as a function of applied dc magnetic field [61]. (a) The $n = 0$ mode (usual CESR) and the $n = 1$ mode. (b) The first four spin-wave modes beyond the usual CESR.

state could be tested. Under the boundary conditions introduced in section 3.2.3, electron spin resonance is achieved in the F/N junction when standing spin wave modes are excited on both sides of the F/N junction. In the absence of an external magnetic field, to achieve electron spin resonance, the frequency of the incident microwave power must satisfy the following condition,

$$\omega = \omega^{\mathrm{FM}}(q_1) = \omega^{\mathrm{QEQ}}(q_2), \tag{3.34}$$

where, $q_1 = n_1\pi/L_1$ and $q_2 = n_2\pi/L_2$, are the respective wave vectors of the standing wave modes in the ferromagnetic system and the QEQ system, $\omega^{\mathrm{FM}}(q)$ and $\omega^{\mathrm{QEQ}}(q)$ stand for the spin wave dispersions of the ferromagnetic system and the QEQ system presented in Eq. (3.23) and Eq. (3.22), respectively. The spin signals measured from the transmission CESR experiment are expected to contain a series of spin resonance lines located at the frequencies derived from Eq. (3.34). Each spin resonance line represents the excitation of a standing spin wave mode on both sides of the F/N junction, the frequency of which is characterized by a distinctive pair of wave vectors $(n_1\pi/L_1, n_2\pi/L_2)$. The positions of the spin resonance lines depend on the experimental parameters such as the values of the Landau parameters of the metals forming the F/N junction, the respective widths of the two regions of the F/N junction, the degree of spin polarizations in the two regions of the F/N junction and the magnitude of the driving charge current for the electrical spin injection.

For the particular MnSi/Al junction featured in Fig. 3.2, the frequencies of the spin wave modes in the small $\mathbf{q}$ limit can be estimated. The frequencies of the gapless spin wave modes for both systems in Fig. 3.2 vary over a range of frequencies starting from zero depending on the value of $\mathbf{q}$, whereas the frequencies of the gapped modes stay relatively unchanged for small $\mathbf{q}$. For a rough estima-

tion, I find on the heavy fermion ferromagnet (MnSi) side of the F/N junction, $\nu_0 \in (0\,\mathrm{Hz}, 10^{12}\,\mathrm{Hz})$ for the frequency of the gapless mode and $\nu_1 \sim 10^{13}\,\mathrm{Hz}$ for the frequency of the gapped mode, while, $\nu_0 \in (0\,\mathrm{Hz}, 10^{14}\,\mathrm{Hz})$ and $\nu_1 \sim 10^{14}\,\mathrm{Hz}$, on the normal metal (Al) side. The frequency of the gapped mode in Al is much higher than that of both spin wave modes in MnSi, so the simultaneous excitation of the gapped mode in Al and either of the spin wave modes in MnSi by a single microwave power is impossible in principle. Therefore, under electron spin resonance, both the gapless and the gapped modes could be excited in MnSi, whereas only the gapless mode is excited in Al. A proper width of the sample could be chosen, $L \sim 1\,\mu m$, so that the wave vectors, $q = n\pi/L \sim 10^6\,m^{-1}$, of the standing spin wave modes are much smaller than the Fermi wave vector, $k_F \sim 10^{10}\,m^{-1}$, and it guarantees that we are working in the long wave length limit, $q \ll k_F$, where the spin waves survive from Landau damping and become propagating modes.

3.3.3 Potential Applications

According to the study on the spin transport phenomena of the F/N junction under electrical spin injection in this thesis, propagating spin wave modes could be excited in the normal metal side of the F/N junction without applying an external magnetic field on it, therefore the nonequilibrium nature of the spin polarization in the normal metal is protected, which is crucial for spintronic devices. Spin wave modes excited in the ferromagnetic side of the F/N junction are also proposed to be able to propagate across the interface of the junction and travel through the normal metal side of the F/N junction. This unique spin transport feature of the F/N junction makes it possible to speculate about potential device applications, in addition to whatever device applications the F/N junction may already have as a basic spintronic device [47].

Since radio frequency signals with certain frequencies can effectively tunnel

through the F/N junction when spin resonance is achieved and propagating spin waves are excited in the system, the F/N junction can be thought of as a frequency selective signal transmitter. More importantly, one can dynamically control the spin resonance conditions of the F/N junction by varying the relevant parameters of the F/N junction. As a result, one can effectively turn the transmitter on and off for a microwave signal with a particular frequency by moving the F/N junction towards and away from the spin resonance. The F/N junction then serves as a novel switch like device in terms of its ability in transmitting microwave signals. The easiest and most practical way to control the switch is varying the drift current through changing the electric bias potential applied to the F/N junction during electrical spin injection. However, as mentioned previously, the effect of the electron drift velocity is rather negligible in an F/N junction composed of simple metals, I need the F/N junction made of heavy fermion materials in order to utilize this control mechanism. Other control mechanisms such as dynamically controlling the spin polarization in the F/N junction are also worth exploring. It is also possible to realize multiple resonance conditions through changing a single or multiple parameters of the F/N junction, therefore the F/N junction could be turned into a more functional transmitter with one or more controlling dials, which could be tuned to make the device transmit microwave signals with desired frequencies.

3.4 Summary

To summarize, I have studied in this work the spin transport and spin dynamics in the F/N junction under electrical spin injection in the low temperature (precession dominated) regime using Landau Fermi liquid theory. In particular, I calculate the transverse spin wave modes on both sides of the F/N junction. The normal metal region of the F/N junction is treated as a QEQ system with nonequi-

librium spin polarization. I find both a gapless and a gapped spin wave mode in the QEQ system similar to a weak ferromagnetic system, which makes the QEQ system fundamentally different from an equilibrium paramagnetic system. Probable propagation of the spin wave modes through the F/N interface is proposed and a transmission CESR experiment on the F/N junction is suggested to test such a proposal. If the proposal is valid, one will see multiple spin resonance lines in the transmitted spin signals from the transmission CESR experiment similar to the result of a transmission CESR experiment on paramagnetic metals. In the end, potential device applications are speculated for the F/N junction, and I suggest that a novel switch like device as well as a functional microwave signal transmitter could be made out of the F/N junction with a couple of control mechanisms being mentioned as well.

CHAPTER IV

Conclusion

To conclude, this thesis is composed of two separate pieces of work both focusing on the study of the transport phenomena in correlated quantum liquids. I develop the theoretical models in both parts of the thesis using the language of Landau Fermi-liquid theory.

In the first half of this thesis, I study the transport properties of a strongly interacting ultracold Fermi gas. In particular, I have developed a complete formula for calculating the transport lifetimes and transport coefficients above T_c of an ultracold Fermi gas with arbitrary quasiparticle interaction strength through control of the Landau parameter F_0^a. This work provides new insights to the understanding of the low temperature transport properties of the strongly interacting Fermi gases, in which the superfluid fluctuation effects are integrated into the calculations of the transport lifetimes and transport coefficients. This is beyond Landau Fermi-liquid theory. The calculated spin diffusion coefficient D and ratio of the viscosity coefficient over entropy density η/s are in reasonable agreement with their respective experimental findings in a unitary Fermi gas. The theory developed in this part of the thesis poses new challenges to the conjectured universal quantum transport in the unitary Fermi gases, as I argue that the minimums found in the quantum regimes (temperatures close to T_c) of the transport coefficients are

local minimums, and they are the results of an interplay between the superfluid fluctuation effects and the normal Fermi-liquid effects in my theory.

In the second half of this thesis, I provide a systematic Fermi-liquid study of the spin transport and dynamics in the F/N junction under electrical spin injection. In particular, I calculate the transverse spin wave modes on both sides of the F/N junction in the low temperature (precession dominated) regime. A QEQ state is assumed in the paramagnetic region of the F/N junction, from which a gapless and a gapped spin wave modes are established in the normal metal region of the F/N junction without applying an external magnetic field. Under a proper set of boundary conditions, these spin wave modes are proposed to propagate through the interface of the F/N junction, which can in principle be detected in a transmission CESR experiment. This novel spin transport feature could open up potential device applications out of the F/N junction, such as a novel switch, and a functional microwave signal transmitter.

Through the course of completing this thesis, I have mastered the application of Landau Fermi-liquid theory in the areas of quasiparticle transport studies and thermodynamics analyses of various correlated quantum liquids. I have also developed a decent skill in tackling quantum field theory computations.

APPENDICES

APPENDIX A

The Cooper instability

The Cooper instability is the instability of the ground state of a noninteracting Fermi system with respect to arbitrary weak attraction between particles, which corresponds to the superfluid fluctuations studied in this thesis. The Cooper instability is related to the singularities in the particle-particle channel vertex function $\Gamma_{\alpha\beta,\gamma\delta}(p_1, p_2;\ p_3, p_4)$ for small total four-momentum $q = p_1 + p_2$, at absolute zero. In the spin singlet channel, the zero temperature vertex function $\Gamma_s(q)$ is given by Eq. (2.9) in standard quantum field theory [4]. The superfluid fluctuations above T_c is characterized by the singularities in the temperature particle-particle vertex function $\mathscr{T}_{\alpha\beta,\gamma\delta}(p_1, p_2;\ p_3, p_4)$, where in this thesis only the spin singlet temperature vertex function $\mathscr{T}_s(q)$ is considered. For simplicity, I have set the constants k_B and $\hbar$ equal to 1 in the following derivations.

The spin singlet temperature vertex function $\mathscr{T}_s(q)$ is generated from the diagram shown in Fig. A.1, which then leads to the integral equation Eq. (2.1) in section 2.2,

$$\begin{aligned}\mathscr{T}_s(p_1, p_2;\ p_3, p_4) &= \tilde{\mathscr{T}}_s(p_1, p_2;\ p_3, p_4) - \frac{T}{2(2\pi)^3}\sum_{\omega_n}\int \tilde{\mathscr{T}}_s(p_1, p_2;\ k, q-k) \\ &\quad \times \mathscr{G}(q-k)\mathscr{G}(k)\mathscr{T}_s(k, q-k;\ p_3, p_4)\mathrm{d}^3\mathbf{k}. \qquad \text{(A.1)}\end{aligned}$$

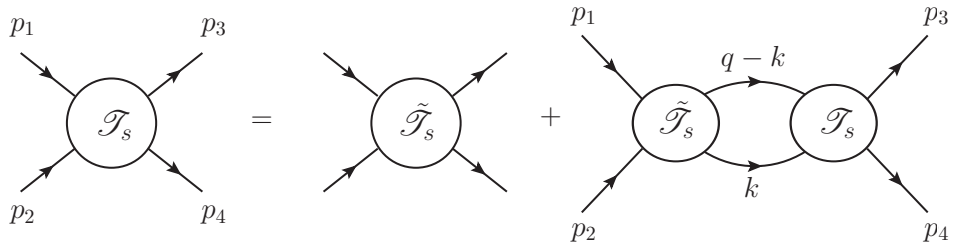

Figure A.1: Diagram for the temperature vertex function $\mathscr{T}_s$. The bubbles represent the irreducible and fully reducible particle-particle vertex function, the solid lines stand for the fermion Green's functions.

The temperature Green's function $\mathscr{G}$ takes the form

$$\mathscr{G}(k) = \frac{1}{i\omega_n - \xi(\mathbf{k})}, \quad \text{and} \quad \mathscr{G}(q-k) = \frac{1}{i(\omega_0 - \omega_n) - \xi(\mathbf{q}-\mathbf{k})}, \tag{A.2}$$

near the Fermi surface, where $|\mathbf{k}| \approx p_f$ and $|\mathbf{q}-\mathbf{k}| \approx p_f$. The energies in the diagram technique of quantum field theory are defined with respect to the chemical potential μ:

$$\xi(\mathbf{k}) = \varepsilon^0_{\mathbf{k}} - \mu \approx v_f(|\mathbf{k}| - p_f), \tag{A.3a}$$

$$\xi(\mathbf{q}-\mathbf{k}) \approx v_f(|\mathbf{k}| - p_f) - \mathbf{v}_{\mathbf{k}} \cdot \mathbf{q}, \tag{A.3b}$$

where $\mathbf{v}_{\mathbf{k}} = \frac{\partial \varepsilon^0_{\mathbf{k}}}{\partial \mathbf{k}}$ is the quasiparticle velocity, and $\varepsilon^0_{\mathbf{k}}$ is the ground state quasiparticle energy introduced in chapter I of this thesis. I can rewrite Eq. (A.1) after substituting out the Green's functions,

$$\begin{aligned} \mathscr{T}_s(q) &= \tilde{\mathscr{T}}_s(q) - \frac{T}{2(2\pi)^3} \int \mathrm{d}^3\mathbf{k} \tilde{\mathscr{T}}_s(q) \mathscr{T}_s(q) \\ &\quad \times \sum_{\omega_n} \frac{1}{i\omega_n - \xi(\mathbf{k})} \cdot \frac{1}{i(\omega_0 - \omega_n) - \xi(\mathbf{q}-\mathbf{k})}. \end{aligned} \tag{A.4}$$

The Matsubara frequency summation can be evaluated according to the fol-

lowing formula [68],

$$\sum_{\omega_n} h(\omega_n) = \sum_{z_k} \mathrm{Res}\left[h(-iz)g(z)\right]\Big|_{z=z_k}, \tag{A.5}$$

where the function $h(\omega_n) \equiv h(-iz)$ contains poles at $z = z_k$, and $g(z)$ is a complex auxiliary function defined as

$$g(z) = \begin{cases} \frac{\beta}{e^{\beta z}-1}, & \text{bosons,} \\ \frac{\beta}{e^{\beta z}+1}, & \text{fermions.} \end{cases} \tag{A.6}$$

where $\beta = 1/T$. Therefore, the summation in Eq. (A.4) is equivalent to a Matsubara frequency summation with

$$h(-iz) = \frac{1}{z - \xi(\mathbf{k})} \cdot \frac{-1}{z - [i\omega_0 - \xi(\mathbf{q}-\mathbf{k})]}, \tag{A.7}$$

the residual of which is evaluated at z equals $\xi(\mathbf{k})$ and $i\omega_0 - \xi(\mathbf{q}-\mathbf{k})$. The fermion $g(z)$ function is chosen for the summation since it is summed over the "odd" frequencies for fermions, $\omega_n = (2n+1)\pi T$. The Matsubara summation in Eq. (A.4) is then carried out to be

$$\sum_{\omega_n} h(\omega_n) = \frac{g\left(\xi(\mathbf{k})\right) - g\left(i\omega_0 - \xi(\mathbf{q}-\mathbf{k})\right)}{i\omega_0 - \xi(\mathbf{k}) - \xi(\mathbf{q}-\mathbf{k})}. \tag{A.8}$$

In the limit $\omega_0 = 0$, Eq. (A.8) is further reduced to

$$\sum_{\omega_n} h(\omega_n) = \frac{\beta}{i\omega_0 - \xi(\mathbf{k}) - \xi(\mathbf{q}-\mathbf{k})} \cdot \left(\frac{1}{e^{\beta\xi(\mathbf{k})}+1} - \frac{1}{e^{-\beta\xi(\mathbf{q}-\mathbf{k})}+1}\right). \tag{A.9}$$

In the model under discussion, the quasiparticle interactions are only defined in a narrow shell at the Fermi surface, hence a cutoff energy ω_D is imposed on the

integral in Eq. (A.4):

$$|\xi(\mathbf{k})| < \omega_D, \quad |\xi(\mathbf{q}-\mathbf{k})| < \omega_D. \tag{A.10}$$

Therefore, the integral in momentum $\mathbf{k}$ in Eq. (A.4) is replaced by the integral in energy ξ, neglecting changes of order $v_f|\mathbf{q}|$ and ω_0 in the limits of integration,

$$\int \mathbf{d}^3\mathbf{k} \to \int_{-\omega_D}^{\omega_D} m^* p_f d\xi \int_{-1}^{1} 2\pi dx, \tag{A.11}$$

where $x = \cos\theta$, and θ is the angle between $\mathbf{v_k}$ and $\mathbf{q}$, hence $\mathbf{v}_k \cdot \mathbf{q} = v_f|\mathbf{q}|\, x$. Using the definitions of the energies in Eq. (A.3), the integral equation of the temperature vertex function Eq. (A.4) is simplified to

$$\begin{aligned} \mathscr{T}_s(q) &= \tilde{\mathscr{T}}_s(q) - \frac{m^* p_f}{2(2\pi)^2} \tilde{\mathscr{T}}_s(q) \mathscr{T}_s(q) \int_{-\omega_D}^{\omega_D} d\xi \\ &\times \int_{-1}^{1} \frac{dx}{i\omega_0 - 2\xi + \mathbf{v}_k \cdot \mathbf{q}} \cdot \left(\frac{1}{e^{\beta\xi}+1} - \frac{1}{e^{-\beta(\xi - \mathbf{v}_k \cdot \mathbf{q})}+1} \right). \end{aligned} \tag{A.12}$$

In the limit of zero ω_0,

$$\frac{1}{i\omega_0 - 2\xi + \mathbf{v}_k \cdot \mathbf{q}} = \frac{\mathrm{P}}{\mathbf{v}_k \cdot \mathbf{q} - 2\xi} - i\pi\delta(\mathbf{v}_k \cdot \mathbf{q} - 2\xi), \tag{A.13}$$

where P denotes the operation of taking the principal value of an integral. Thus, the integral in Eq. (A.12) becomes

$$\int_{-\omega_D}^{\omega_D} d\xi \int_{-1}^{1} dx \, \frac{\mathrm{P}}{\mathbf{v}_k \cdot \mathbf{q} - 2\xi} \cdot \left(\frac{1}{e^{\beta\xi}+1} - \frac{1}{e^{-\beta(\xi - \mathbf{v}_k \cdot \mathbf{q})}+1} \right). \tag{A.14}$$

The above integral can be further simplified to

$$\int_{-\omega_D}^{\omega_D} d\xi \int_{0}^{1} dx \, \frac{\mathrm{P}}{2\xi - \mathbf{v}_k \cdot \mathbf{q}} \cdot \left(\tanh\frac{\beta\xi}{2} + \tanh\frac{\beta(\xi - \mathbf{v}_k \cdot \mathbf{q})}{2} \right). \tag{A.15}$$

Substituting $\mathbf{v}_k \cdot \mathbf{q}$ with $v_f|\mathbf{q}|x$, integral (A.15) is calculated to be

$$2\ln\left(\frac{2\gamma\omega_D}{\pi T}\right) - \frac{1}{3}\left(\frac{v_f|\mathbf{q}|}{2\omega_D}\right)^2 - \frac{14\zeta(3)}{3\pi^2}\left(\frac{v_f|\mathbf{q}|}{4T}\right)^2 \tag{A.16}$$

Replacing the integral in Eq. (A.12) by its result in expression (A.16), I establish a simple equation for the temperature vertex function $\mathscr{T}_s(|\mathbf{q}|, 0)$:

$$\begin{aligned}\mathscr{T}_s(\mathbf{q},0) &= \tilde{\mathscr{T}}_s - \frac{m^* p_f}{(2\pi)^2}\tilde{\mathscr{T}}_s\mathscr{T}_s(\mathbf{q},0) \\ &\times \left[\ln\left(\frac{2\gamma\omega_D}{\pi T}\right) - \frac{1}{3}\left(\frac{v_f|\mathbf{q}|}{2\omega_D}\right)^2 - \frac{14\zeta(3)}{3\pi^2}\left(\frac{v_f|\mathbf{q}|}{4T}\right)^2\right].\end{aligned} \tag{A.17}$$

For an attractive interaction, $\tilde{\mathscr{T}}_s < 0$, therefore, the result of the temperature vertex function Eq. (2.2) is recovered with T_c defined by Eq. (2.3),

$$\mathscr{T}_s(\mathbf{q},0) = \frac{1}{\frac{m^* p_f}{4\pi^2}\left[\ln\frac{T_c}{T} - \frac{1}{6}\left(\frac{v_f|\mathbf{q}|}{2\omega_D}\right)^2 - \frac{7\zeta(3)}{3\pi^2}\left(\frac{v_f|\mathbf{q}|}{4T}\right)^2\right]}. \tag{A.18}$$

APPENDIX B

Finite temperature corrections

I use the formulas derived in Ref. [36] to compute the finite temperature corrections to the various transport lifetimes. According to Ref. [36], the finite temperature corrections to the transport coefficients are given by

$$\frac{1}{DT^2} - \left(\frac{1}{DT^2}\right)_{T=0} = -18\pi\zeta(3)\frac{m^{*4}}{p_f^6}\frac{k_B^3/\hbar}{1+F_0^a}\left(\sum_{i=\mathrm{I}}^{\mathrm{III}}\gamma_i^D\Xi_i^D\right)T \tag{B.1}$$

for the spin-diffusion coefficient,

$$\frac{1}{\eta T^2} - \left(\frac{1}{\eta T^2}\right)_{T=0} = -90\pi^3\zeta(3)\frac{m^{*2}}{p_f^7}\hbar^2k_B^2\left(\gamma_{\mathrm{II}}^\eta\Xi_{\mathrm{II}}^\eta\right)\frac{T}{T_F} \tag{B.2}$$

for the coefficient of viscosity and

$$\frac{1}{KT} - \left(\frac{1}{KT}\right)_{T=0} = -810\frac{\zeta(5)}{\pi}\frac{m^{*3}}{p_f^7}\hbar^2k_B\left(\sum_{i=\mathrm{I}}^{\mathrm{II}}\gamma_i^K\Xi_i^K\right)T \tag{B.3}$$

for the thermal conductivity. Here $\zeta(n)$ are the Riemann ζ function of order n.

The Ξ functions are defined through quantities $\Xi^{s,a}$ and $\tilde{\Xi}^{s,a}$:

$$\Xi^{s,a} = \int_0^{2\pi} \frac{d\phi}{2\pi}(1-\cos\phi)\Big\{|\alpha^{s,a}(0,\phi)|^2 + \int_0^1 ds\left[\frac{|\alpha^{s,a}(0,\phi)|^2 - |\alpha^{s,a}(s,\phi)|^2}{s^2} + |\alpha^{s,a}(s,\phi)|^2\right]\Big\} \tag{B.4}$$

and

$$\tilde{\Xi}^{s,a} = \int_0^{2\pi} \frac{d\phi}{2\pi}\left\{|\alpha^{s,a}(0,\phi)|^2 + \int_0^1 ds\left[\frac{|\alpha^{s,a}(0,\phi)|^2 - |\alpha^{s,a}(s,\phi)|^2}{s^2}\right]\right\}, \tag{B.5}$$

where $\alpha^{s,a}(s,\phi) \equiv \alpha_0^{s,a}(s) + 2\alpha_1^{s,a}(s)\cos\phi$, $\alpha_0^{s,a}(s) = \frac{F_0^{s,a}+A_1^{s,a}s^2}{1+(F_0^{s,a}+A_1^{s,a}s^2)\chi(s)}$ and $\alpha_1^{s,a}(s) = \frac{F_1^{s,a}(1-s^2)}{2\left\{1+\frac{1}{2}F_1^{s,a}[(1-s^2)\chi(s)-1/3]\right\}}$ with $\chi(s) = 1 - \frac{1}{2}s\ln[(s+1)/(s-1)]$. The Ξ functions in Eqs. (B.1), (B.2) and (B.3) are given by the relations:

$$\Xi_{\rm I}^D = 2\Xi^a, \quad \Xi_{\rm II}^D = 2\tilde{\Xi}^a, \quad \Xi_{\rm III}^D = \tilde{\Xi}^s + \tilde{\Xi}^a; \tag{B.6}$$

$$\Xi_{\rm II}^\eta = \tilde{\Xi}^s + 3\tilde{\Xi}^a; \tag{B.7}$$

$$\Xi_{\rm I}^K = \Xi^s + 3\Xi^a, \quad \Xi_{\rm II}^K = \Xi_{\rm II}^\eta = \tilde{\Xi}^s + 3\tilde{\Xi}^a. \tag{B.8}$$

In the local limit, the $\Xi^{s,a}$ and $\tilde{\Xi}^{s,a}$ functions are shown to be

$$\Xi^s = (A_0^s)^2(1 - \frac{1}{4}\pi^2 A_0^s) + F_0^s A_0^s, \tag{B.9}$$

$$\Xi^a = (A_0^a)^2(1 - \frac{1}{4}\pi^2 A_0^a) + F_0^a A_0^a, \tag{B.10}$$

$$\tilde{\Xi}^s = (A_0^s)^2(1 + \frac{1}{4}\pi^2 A_0^s), \quad \tilde{\Xi}^a = (A_0^a)^2(1 + \frac{1}{4}\pi^2 A_0^a). \tag{B.11}$$

The γ functions are defined as

$$\gamma_{\rm I}^{D} = 1 - \frac{\pi^2}{6}\frac{\zeta(3)-1}{\zeta(3)}\left(\frac{\tau_{QP}}{\tau_0}\right) + 0.0297\left(\frac{\tau_{QP}}{\tau_0}\right)^2 = 0.639,$$
$$\gamma_{\rm II}^{D} = 0.0161\left(\frac{\tau_{QP}}{\tau_0}\right)^2 = 0.04,$$
$$\gamma_{\rm III}^{D} = 0.0416\left(\frac{\tau_{QP}}{\tau_0}\right)^2 = 0.103 \tag{B.12}$$

for the spin-diffusion coefficient where $\tau_{QP}/\tau_0 \equiv \frac{2}{\pi^2}\tau/\tau_D = 2/(0.129\pi^2)$ according to Eq. (2.34),

$$\gamma_{\rm II}^{\eta} = 0.042\left(\frac{\tau_{QP}}{\tau_0}\right)^2 = 0.041 \tag{B.13}$$

for the coefficient of viscosity where $\tau_{QP}/\tau_0 \equiv \frac{2}{\pi^2}\tau/\tau_\eta = 2/(0.205\pi^2)$ according to Eq. (2.41), and

$$\gamma_{\rm I}^{K} = 1 - 0.328\left(\frac{\tau_{QP}}{\tau_0}\right) + 0.037\left(\frac{\tau_{QP}}{\tau_0}\right)^2 = 0.549,$$
$$\gamma_{\rm II}^{K} = 0.043\left(\frac{\tau_{QP}}{\tau_0}\right)^2 = 0.125 \tag{B.14}$$

for the thermal conductivity where $\tau_{QP}/\tau_0 \equiv \frac{2}{\pi^2}\tau/\tau_K = 2/(0.119\pi^2)$ according to Eq. (2.53). The finite temperature corrections to the transport lifetimes can be generated from Eqs. (B.1), (B.2) and (B.3),

$$\begin{aligned}\frac{1}{\tau_D} - \frac{1}{\tau_D^0} &= -\frac{3}{2}\pi\zeta(3)\frac{k_B T_F}{\hbar}\left(\frac{T}{T_F}\right)^3\left(\sum_{i=\rm I}^{\rm III}\gamma_i^D\Xi_i^D\right)\\ &= -\frac{3}{2}\pi\zeta(3)\frac{k_B T_F}{\hbar}\left(\frac{T}{T_F}\right)^3\\ &\quad\times\left[\,-2.95(A_0^a)^3 + 1.564(A_0^a)^2 + 1.278\,A_0^a F_0^a\,\right]\end{aligned} \tag{B.15}$$

for the spin-diffusion lifetime,

$$\begin{aligned}\frac{1}{\tau_\eta}-\frac{1}{\tau_\eta^0} &= -3\pi\zeta(3)\frac{k_B T_F}{\hbar}\left(\frac{T}{T_F}\right)^3(\gamma_{\rm II}^\eta\Xi_{\rm II}^\eta)\\ &= -3\pi\zeta(3)\frac{k_B T_F}{\hbar}\left(\frac{T}{T_F}\right)^3\times\left[\,0.202(A_0^a)^3+0.164(A_0^a)^2\,\right] \quad \text{(B.16)}\end{aligned}$$

for the viscosity lifetime and

$$\begin{aligned}\frac{1}{\tau_K}-\frac{1}{\tau_K^0} &= -\frac{45}{2\pi}\zeta(3)\frac{k_B T_F}{\hbar}\left(\frac{T}{T_F}\right)^3\left(\sum_{i=\rm I}^{\rm II}\gamma_i^K\Xi_i^K\right)\\ &= -\frac{45}{2\pi}\zeta(3)\frac{k_B T_F}{\hbar}\left(\frac{T}{T_F}\right)^3\\ &\times \left[-2.09(A_0^a)^3+2.696(A_0^a)^2+\left(1.647+\frac{0.549}{1+2F_0^a}\right)A_0^aF_0^a\right]\end{aligned} \quad \text{(B.17)}$$

for the thermal-conductivity lifetime. Therefore, Eqs. (B.15), (B.16) and (B.17) resemble Eqs. (2.36), (2.43) and (2.55) in section 2.4.

APPENDIX C

Spin hydrodynamic equations

To derive the hydrodynamic equations, Eqs. (3.10) and (3.11) given in section 3.2.1, for the complex spin distortions, I start from the spin kinetic equation Eq. (3.1) given in section 3.2.1:

$$\begin{aligned}\frac{\partial \boldsymbol{\sigma}_{\mathbf{p}}}{\partial t} + \frac{\partial}{\partial r_i}\left(\frac{\partial \varepsilon_{\mathbf{p}}}{\partial p_i}\boldsymbol{\sigma}_{\mathbf{p}} + \frac{\partial \mathbf{h}_{\mathbf{p}}}{\partial p_i} n_{\mathbf{p}}\right) + \frac{\partial}{\partial p_i}\left(-\frac{\partial \varepsilon_{\mathbf{p}}}{\partial r_i}\boldsymbol{\sigma}_{\mathbf{p}} - \frac{\partial \mathbf{h}_{\mathbf{p}}}{\partial r_i} n_{\mathbf{p}}\right) \\ = -\frac{2}{\hbar}\boldsymbol{\sigma}_{\mathbf{p}} \times \mathbf{h}_{\mathbf{p}} + \left(\frac{\partial \boldsymbol{\sigma}_{\mathbf{p}}}{\partial t}\right)_{\text{collision}}. \end{aligned} \tag{C.1}$$

The spin conservation law is derived by integrating Eq. (C.1) over momentum,

$$\begin{aligned} & 2\int \frac{d^3p}{(2\pi\hbar)^3} \times \text{Eq. (C.1)} \\ \Rightarrow \quad & \frac{\partial \boldsymbol{\sigma}}{\partial t} + \frac{\partial}{\partial r_i} j_{\boldsymbol{\sigma},i}(\mathbf{r},t) = -\frac{4}{\hbar}\int \frac{d^3p}{(2\pi\hbar)^3}\boldsymbol{\sigma}_{\mathbf{p}} \times \mathbf{h}_{\mathbf{p}} = \gamma \boldsymbol{\sigma} \times \boldsymbol{\mathscr{H}}, \end{aligned} \tag{C.2}$$

where the total spin current $j_{\boldsymbol{\sigma},i}(\mathbf{r},t)$ is given by Eq. (3.2), and the total spin polarization is given by $\boldsymbol{\sigma} = 2\int \frac{d^3p}{(2\pi\hbar)^3}\boldsymbol{\sigma}_{\mathbf{p}}$. The collision term vanishes on the right hand side of Eq. (C.1) after the integral since total spin is conserved during collisions. Using the definition of the quasiparticle velocity in Eq. (3.4), the total

spin current is shown to be

$$
\begin{aligned}
j_{\boldsymbol{\sigma},i}(\mathbf{r},t) &= 2\int \frac{d^3p}{(2\pi\hbar)^3}\left(\frac{\partial\varepsilon_{\mathbf{p}}}{\partial p_i}\boldsymbol{\sigma}_{\mathbf{p}}+\frac{\partial \mathbf{h}_{\mathbf{p}}}{\partial p_i}n_{\mathbf{p}}\right) = 2\int \frac{d^3p}{(2\pi\hbar)^3}\frac{\partial\varepsilon_{\mathbf{p}}}{\partial p_i}\left(\boldsymbol{\sigma}_{\mathbf{p}}-\frac{\partial n_{\mathbf{p}}}{\partial\varepsilon_{\mathbf{p}}}\mathbf{h}_{\mathbf{p}}\right)\\
&= 2\int \frac{d^3p}{(2\pi\hbar)^3}\left(V_{0i}+v^0_{\mathbf{p}i}\right)\left(\boldsymbol{\sigma}_{\mathbf{p}}-\frac{\partial n_{\mathbf{p}}}{\partial\varepsilon_{\mathbf{p}}}\mathbf{h}_{\mathbf{p}}\right)\\
&= V_{0i}\boldsymbol{\sigma}-2V_{0i}\int \frac{d^3p}{(2\pi\hbar)^3}\frac{\partial n_{\mathbf{p}}}{\partial\varepsilon_{\mathbf{p}}}\mathbf{h}_{\mathbf{p}}+2\int \frac{d^3p}{(2\pi\hbar)^3}v^0_{\mathbf{p}i}\boldsymbol{\sigma}_{\mathbf{p}}(1+\frac{F_1^a}{3})\\
&= V_{0i}\boldsymbol{\sigma}-2V_{0i}\int \frac{d^3p}{(2\pi\hbar)^3}\frac{\partial n_{\mathbf{p}}}{\partial\varepsilon_{\mathbf{p}}}\left(\mathbf{h}^0_{\mathbf{p}}+2\int\frac{d^3p'}{(2\pi\hbar)^3}f^a_{\mathbf{p}\mathbf{p}'}\boldsymbol{\sigma}_{\mathbf{p}'}\right)\\
&\quad +2\int \frac{d^3p}{(2\pi\hbar)^3}v^0_{\mathbf{p}i}\boldsymbol{\sigma}_{\mathbf{p}}(1+\frac{F_1^a}{3})\\
&= V_{0i}\boldsymbol{\sigma}(1+F_0^a)-V_{0i}\frac{\gamma\hbar\mathscr{H}}{2}N(0)+2\int \frac{d^3p}{(2\pi\hbar)^3}v^0_{\mathbf{p}i}\boldsymbol{\sigma}_{\mathbf{p}}(1+\frac{F_1^a}{3}),
\end{aligned}
\tag{C.3}
$$

which becomes identical to Eq. (3.5) in section 3.2.1 in the absence of an external magnetic field $\mathscr{H}=0$. The procession of the total spin around the external field also vanishes in such cases and Eq. (C.2) reduces to

$$
\frac{\partial\boldsymbol{\sigma}(\mathbf{r},t)}{\partial t}+\frac{\partial}{\partial r_i}j^{\mathrm{diff}}_{\boldsymbol{\sigma},i}(\mathbf{r},t)+\frac{\partial}{\partial r_i}V_{0i}(1+F_0^a)\boldsymbol{\sigma}(\mathbf{r},t)=0. \tag{C.4}
$$

Linearizing Eq. (C.4) in $\boldsymbol{\sigma}$, I recover the spin hydrodynamic equation, Eq. (3.10) in section 3.2.1.

To derive the equation of motion for the spin current, Eq. (C.1) is rewritten to keep only terms up to second order in $\nabla, \delta n$ or $\boldsymbol{\sigma}_{\mathbf{p}}$,

$$
\frac{\partial\boldsymbol{\sigma}_{\mathbf{p}}}{\partial t}+\frac{\partial\varepsilon_{\mathbf{p}}}{\partial p_i}\frac{\partial}{\partial r_i}\left(\boldsymbol{\sigma}_{\mathbf{p}}-\frac{\partial n^0_{\mathbf{p}}}{\partial\varepsilon^0_{\mathbf{p}}}\mathbf{h}_{\mathbf{p}}\right)=-\frac{2}{\hbar}\boldsymbol{\sigma}_{\mathbf{p}}\times\mathbf{h}_{\mathbf{p}}+\left(\frac{\partial\boldsymbol{\sigma}_{\mathbf{p}}}{\partial t}\right)_{\mathrm{collision}}. \tag{C.5}
$$

Here, I am only interested in the diffusive part of the spin current since the drift part behaves essentially the same as the total spin polarization. By multiplying

the term $2\int \frac{d^3p}{(2\pi\hbar)^3} v^0_{\mathbf{p}i}(1+\frac{F_1^a}{3})$ to both sides of Eq. (C.5), I have

$$\begin{aligned} & 2\int \frac{d^3p}{(2\pi\hbar)^3} v^0_{\mathbf{p}i}(1+\frac{F_1^a}{3}) \times \text{Eq. (C.5)} \\ \Rightarrow \quad & \frac{\partial j^{\text{diff}}_{\boldsymbol{\sigma},i}(\mathbf{r},t)}{\partial t} + (1+\frac{F_1^a}{3})\, 2\int \frac{d^3p}{(2\pi\hbar)^3} v^0_{\mathbf{p}i} \frac{\partial \varepsilon_{\mathbf{p}}}{\partial p_k}\frac{\partial}{\partial r_k}\left(\boldsymbol{\sigma}_{\mathbf{p}} - \frac{\partial n^0_{\mathbf{p}}}{\partial \varepsilon^0_{\mathbf{p}}}\mathbf{h}_{\mathbf{p}}\right) \\ & = \left(\frac{\partial j^{\text{diff}}_{\boldsymbol{\sigma},i}}{\partial t}\right)_{\text{precession}} + \left(\frac{\partial j^{\text{diff}}_{\boldsymbol{\sigma},i}}{\partial t}\right)_{\text{collision}}, \end{aligned} \tag{C.6}$$

where

$$\begin{aligned} & \left(\frac{\partial j^{\text{diff}}_{\boldsymbol{\sigma},i}}{\partial t}\right)_{\text{precession}} = -\frac{2}{\hbar}(1+\frac{F_1^a}{3})\, 2\int \frac{d^3p}{(2\pi\hbar)^3} v^0_{\mathbf{p}i}\,(\boldsymbol{\sigma}_{\mathbf{p}} \times \mathbf{h}_{\mathbf{p}}) \\ & = \gamma j^{\text{diff}}_{\boldsymbol{\sigma},i} \times \boldsymbol{\mathscr{H}} - \frac{2}{\hbar}(1+\frac{F_1^a}{3})\, 2\int \frac{d^3p}{(2\pi\hbar)^3} v^0_{\mathbf{p}i}\left(\boldsymbol{\sigma}_{\mathbf{p}} \times 2\int \frac{d^3p'}{(2\pi\hbar)^3} f^a_{\mathbf{p}\mathbf{p}'}\boldsymbol{\sigma}_{\mathbf{p}'}\right). \end{aligned} \tag{C.7}$$

By keeping only the $l = 0, 1$ terms in the Legendre expansions of $\boldsymbol{\sigma}_{\mathbf{p}}$, I can write $\boldsymbol{\sigma}_{\mathbf{p}} = \boldsymbol{\sigma}_0 + \boldsymbol{\sigma}_1 \cos\theta$, and the second term on the right hand side of Eq. (C.7) becomes

$$\begin{aligned} & -\frac{2}{\hbar}(1+\frac{F_1^a}{3})\, 2\int \frac{d^3p}{(2\pi\hbar)^3} v^0_{\mathbf{p}i}\boldsymbol{\sigma}_{\mathbf{p}} \times 2\int \frac{d^3p'}{(2\pi\hbar)^3} \sum_l f^a_l P_l(\cos\langle \mathbf{p}, \mathbf{p}'\rangle)\boldsymbol{\sigma}_{\mathbf{p}'} \\ = \quad & -\frac{2}{\hbar}(1+\frac{F_1^a}{3})\, 2\int \frac{d^3p}{(2\pi\hbar)^3} v^0_{\mathbf{p}i}\,(\boldsymbol{\sigma}_0 + \boldsymbol{\sigma}_1\cos\theta) \\ & \times 2\int \frac{d^3p'}{(2\pi\hbar)^3} \sum_l f^a_l \frac{4\pi}{2l+1} \sum_{m=-l}^{l} Y^m_l(\theta',\phi')^* Y^m_l(\theta,\phi)\,(\boldsymbol{\sigma}_0 + \boldsymbol{\sigma}_1\cos\theta') \\ = \quad & -\frac{2}{\hbar}(1+\frac{F_1^a}{3})\, 2\int \frac{d^3p}{(2\pi\hbar)^3} v^0_{\mathbf{p}i}\boldsymbol{\sigma}_0 \times 2\int \frac{d^3p'}{(2\pi\hbar)^3} \frac{f^a_1}{3}\boldsymbol{\sigma}_1\cos\theta \\ & -\frac{2}{\hbar}(1+\frac{F_1^a}{3})\, 2\int \frac{d^3p}{(2\pi\hbar)^3} v^0_{\mathbf{p}i}\boldsymbol{\sigma}_1\cos\theta \times 2\int \frac{d^3p'}{(2\pi\hbar)^3} f^a_0\boldsymbol{\sigma}_0 \\ = \quad & -\frac{2}{\hbar}(f^a_0 - \frac{f^a_1}{3})(1+\frac{F_1^a}{3})\, 2\int \frac{d^3p}{(2\pi\hbar)^3} v^0_{\mathbf{p}i}\boldsymbol{\sigma}_1\cos\theta \times 2\int \frac{d^3p'}{(2\pi\hbar)^3}\boldsymbol{\sigma}_0 \\ = \quad & -\frac{2}{\hbar}(f^a_0 - \frac{f^a_1}{3})\left(j^{\text{diff}}_{\boldsymbol{\sigma},i} \times \boldsymbol{\sigma}\right). \end{aligned} \tag{C.8}$$

Therefore, the precession term reduces to

$$\left(\frac{\partial j^{\rm diff}_{\boldsymbol{\sigma},i}}{\partial t}\right)_{\rm precession} = -\frac{2}{\hbar}(f^a_0 - \frac{f^a_1}{3})\left(j^{\rm diff}_{\boldsymbol{\sigma},i} \times \boldsymbol{\sigma}\right) + \gamma j^{\rm diff}_{\boldsymbol{\sigma},i} \times \boldsymbol{\mathscr{H}}. \tag{C.9}$$

The collision term on the right hand side of Eq. (C.6) is

$$\left(\frac{\partial j^{\rm diff}_{\boldsymbol{\sigma},i}}{\partial t}\right)_{\rm collision} = (1 + \frac{F^a_1}{3})\, 2 \int \frac{d^3p}{(2\pi\hbar)^3} v^0_{\mathbf{p}i} \left(\frac{\partial \boldsymbol{\sigma}_{\mathbf{p}}}{\partial t}\right)_{\rm collision}, \tag{C.10}$$

where the collision term inside the integral is estimated using the relaxation time approximation. The relaxation time τ_D is defined as

$$\left(\frac{\partial \boldsymbol{\sigma}_{\mathbf{p}}}{\partial t}\right)_{\rm collision} = -\frac{\bar{\boldsymbol{\sigma}}_{\mathbf{p}}(\mathbf{r},t)}{\tau_D}. \tag{C.11}$$

$\bar{\boldsymbol{\sigma}}_{\mathbf{p}}(\mathbf{r},t)$ is the deviation of the spin density from its local equilibrium. Using the definitions of the quasiparticle distribution function $n_{\mathbf{p}\sigma}$ in Eq. (1.13) and the quasiparticle energy $\varepsilon_{\mathbf{p}\sigma}$ in Eq. (1.16), the local equilibrium distribution function is defined as

$$n^0_{\mathbf{p}\sigma}(\varepsilon^{\rm l.e.}_{\mathbf{p}\sigma}) = \frac{1}{e^{(\varepsilon^{\rm l.e.}_{\mathbf{p}\sigma} - \mu)/k_BT} + 1}, \tag{C.12}$$

where $\varepsilon^{\rm l.e.}_{\mathbf{p}\sigma}$ is the local quasiparticle energy. The true equilibrium distribution function is defined as

$$n^0_{\mathbf{p}\sigma}(\varepsilon^0_{\mathbf{p}\sigma}) = \frac{1}{e^{(\varepsilon^0_{\mathbf{p}\sigma} - \mu)/k_BT} + 1}, \tag{C.13}$$

where $\varepsilon^0_{\mathbf{p}\sigma}$ is the equilibrium quasiparticle energy. The deviation $\bar{\boldsymbol{\sigma}}_{\mathbf{p}}(\mathbf{r},t)$ is calcu-

lated as

$$\begin{aligned}
\bar{\boldsymbol{\sigma}}_{\mathbf{p}}(\mathbf{r},t) &= \frac{1}{2}\sum_{\sigma}\left(n_{\mathbf{p}\sigma}(\varepsilon^{\text{l.e.}}_{\mathbf{p}\sigma}) - n^{0}_{\mathbf{p}\sigma}(\varepsilon^{\text{l.e.}}_{\mathbf{p}\sigma})\right)\boldsymbol{\tau}_{\sigma\sigma} \\
&= \frac{1}{2}\sum_{\sigma}\left[\left(n_{\mathbf{p}\sigma}(\varepsilon^{\text{l.e.}}_{\mathbf{p}\sigma}) - n^{0}_{\mathbf{p}\sigma}(\varepsilon^{0}_{\mathbf{p}\sigma})\right) - \left(n^{0}_{\mathbf{p}\sigma}(\varepsilon^{\text{l.e.}}_{\mathbf{p}\sigma}) - n^{0}_{\mathbf{p}\sigma}(\varepsilon^{0}_{\mathbf{p}\sigma})\right)\right]\boldsymbol{\tau}_{\sigma\sigma} \\
&= \boldsymbol{\sigma}_{\mathbf{p}}(\mathbf{r},t) - \frac{\partial n^{0}_{\mathbf{p}}}{\partial \varepsilon^{0}_{\mathbf{p}}}\mathbf{h}_{\mathbf{p}}(\mathbf{r},t). \qquad \text{(C.14)}
\end{aligned}$$

Plugging Eqs. (C.11) and (C.14) into Eq. (C.10), I end up with

$$\begin{aligned}
\left(\frac{\partial j^{\text{diff}}_{\boldsymbol{\sigma},i}}{\partial t}\right)_{\text{collision}} &= -(1+\frac{F^{a}_{1}}{3})\,2\int\frac{d^{3}p}{(2\pi\hbar)^{3}}v^{0}_{\mathbf{p}i}\left(\boldsymbol{\sigma}_{\mathbf{p}} - \frac{\partial n^{0}_{\mathbf{p}}}{\partial\varepsilon^{0}_{\mathbf{p}}}\mathbf{h}_{\mathbf{p}}\right)/\tau_{D} \\
&= -(1+\frac{F^{a}_{1}}{3})\,\frac{j^{\text{diff}}_{\boldsymbol{\sigma},i}}{\tau_{D}}. \qquad \text{(C.15)}
\end{aligned}$$

The second term on the left hand side of Eq. (C.6) is evaluated with the quasiparticle velocity $v_{\mathbf{p}i}$ defined by Eq. (3.4),

$$\begin{aligned}
&(1+\frac{F^{a}_{1}}{3})\,2\int\frac{d^{3}p}{(2\pi\hbar)^{3}}v^{0}_{\mathbf{p}i}\left(V_{0k}+v^{0}_{\mathbf{p}k}\right)\frac{\partial}{\partial r_{k}}\left(\boldsymbol{\sigma}_{\mathbf{p}} - \frac{\partial n^{0}_{\mathbf{p}}}{\partial\varepsilon^{0}_{\mathbf{p}}}\mathbf{h}_{\mathbf{p}}\right) \\
= \;& (1+\frac{F^{a}_{1}}{3})\left(V_{0k}\frac{\partial}{\partial r_{k}}\right)j^{\text{diff}}_{\boldsymbol{\sigma},i}(\mathbf{r},t) + \frac{v_{f}^{2}}{3}(1+F^{a}_{0})(1+\frac{F^{a}_{1}}{3})\frac{\partial}{\partial r_{i}}\left(\boldsymbol{\sigma} - \frac{\gamma\hbar}{2}\frac{N(0)\mathscr{H}}{1+F^{a}_{0}}\right). \qquad \text{(C.16)}
\end{aligned}$$

Putting together Eqs. (C.6), (C.9), (C.15) and (C.16), I have the equation of motion for the diffusive spin current in the absence of the external magnetic field $\mathscr{H} = 0$:

$$\begin{aligned}
&\frac{\partial j^{\text{diff}}_{\boldsymbol{\sigma},i}(\mathbf{r},t)}{\partial t} + \frac{1}{3}(1+F^{a}_{0})(1+\frac{F^{a}_{1}}{3})v_{f}^{2}\frac{\partial}{\partial r_{i}}\boldsymbol{\sigma}(\mathbf{r},t) + (1+\frac{F^{a}_{1}}{3})\left(V_{0k}\frac{\partial}{\partial r_{k}}\right)j^{\text{diff}}_{\boldsymbol{\sigma},i}(\mathbf{r},t) \\
&\qquad = -\frac{2}{\hbar}(f^{a}_{0} - \frac{f^{a}_{1}}{3})j^{\text{diff}}_{\boldsymbol{\sigma},i}(\mathbf{r},t)\times\boldsymbol{\sigma}(\mathbf{r},t) - (1+\frac{F^{a}_{1}}{3})j^{\text{diff}}_{\boldsymbol{\sigma},i}(\mathbf{r},t)/\tau_{D}, \qquad \text{(C.17)}
\end{aligned}$$

Linearizing the above equation in $\boldsymbol{\sigma}$, I recover the spin hydrodynamic equation

Eq. (3.11) in section 3.2.1.

BIBLIOGRAPHY

BIBLIOGRAPHY

[1] G. Baym and C. J. Pethick, *Landau Fermi-Liquid Theory: Concepts and Applications* (John Wiley & Sons, New York, 1991).

[2] D. Pines and P. Nozieres, *The Theory of Quantum Liquids, Volume I: Normal Fermi Liquids* (W. A. Benjamin, New York, 1966).

[3] P. Nozieres, *Theory of Interacting Fermi Systems* (W. A. Benjamin, New York, 1964).

[4] A. A. Abrikosov, L. P. Gorkov, and I. E. Dzyaloshinski, *Methods of Quantum Field Theory in Statistical Physics* (Dover, New York, 1975).

[5] M. H. Anderson, J. R. Ensher, M. R. Matthews, C. E. Wieman, and E. A. Cornell, "Observation of Bose-Einstein condesation in a dilute atomic vapor," Phys. Rev. B **269**, 198 (1995).

[6] C. C. Bradley, C. A. Sackett, J. J. Tollett, and R. G. Hulet, "Evidence of Bose-Einstein condesation in an atomic gas with attractive interactions," Phys. Rev. Lett. **79**, 1687 (1997).

[7] K. B. Davis, M. O. Mewes, M. R. Andrews, N. J. van Druten, D. S. Durfee, D. M. Kurn, and W. Ketterle, "Bose-Einstein condensation in a gas of sodium atoms," Phys. Rev. Lett. **75**, 3969 (1995).

[8] I. Bloch, J. Dalibard, and W. Zwerger, "Many-body physics with ultracold gases," Rev. Mod. Phys. **80**, 885 (2008).

[9] S. Giorgini, L. P. Pitaevskii, and S. Stringari, "Theory of ultracold atomic Fermi gases," Rev. Mod. Phys. **80**, 1215 (2008).

[10] H. Feshbach, "Unified theory of nuclear reactions," Ann. Phys. **5**, 357 (1958).

[11] H. Feshbach, "A unified theory of nuclear reactions. II," Ann. Phys. **19**, 287 (1962).

[12] T. L. Ho, "Universal thermodynamics of degenerate quantum gases in the unitarity limit," Phys. Rev. Lett. **92**, 090402 (2004).

[13] M. Ku, A. T. Sommer, L. W. Cheuk, and M. W. Zwierlein, "Revealing the superfluid lambda transition in the universal thermodynamics of a unitary Fermi gas," Science **335**, 563 (2012).

[14] P. K. Kovtun, D. T. Son, and A. O. Starinets, "Viscosity in strongly interacting quantum field theories from black hole physics," Phys. Rev. Lett. **94**, 111601 (2005).

[15] T. Schafer, "Ratio of shear viscosity to entropy density for trapped fermions in the unitarity limit," Phys. Rev. A **76**, 063618 (2007).

[16] T. Enss, R. Haussmann, and W. Zwerger, "Viscosity and scale invariance in the unitary Fermi gas," Ann. Phys. **326**, 770 (2011).

[17] T. Enss, "Quantum critical transport in the unitary Fermi gas," Phys. Rev. A **86**, 013616 (2012).

[18] T. Enss and R. Haussmann, "Quantum mechanical limitations to spin diffusion in the unitary Fermi gas," Phys. Rev. Lett. **109**, 195303 (2012).

[19] A. Sommer, M. Ku, G. Roati, and M. W. Zwierlein, "Universal spin transport in a strongly interacting Fermi gas," Nature **472**, 201 (2011).

[20] J. E. Thomas, "The nearly perfect Fermi gas," Phys. Today **63(5)**, 34 (2010).

[21] C. Cao, E. Elliott, J. Joseph, H. Wu, J. Petricka, T. Schafer, and J. E. Thomas, "Universal quantum viscosity in a unitary Fermi gas," Science **331**, 58 (2011).

[22] J. R. Engelbrecht and K. S. Bedell, "Robustness of a local Fermi liquid against ferromagnetism and phase separation," Phys. Rev. Lett. **74**, 4265 (1995).

[23] J. A. Jackiewicz and K. S. Bedell, "Quantum fluctuation driven first order phase transition in weak ferromagnetic metals," Philos. Mag. Lett. **85**, 1755 (2005).

[24] H. Li, J. Jackiewicz, and K. S. Bedell, "Superfluid amplitude fluctuations above T_c in a unitary Fermi gas," Phys. Rev. B **91**, 075107 (2015).

[25] V. K. Samalam and J. W. Serene, "Zero-sound attenuation from order-parameter fluctuations in liquid ^{3}He," Phys. Rev. Lett. **41**, 497 (1978).

[26] L. P. Gorkov and T. K. Melik-Barkhudarov, "Contribution to the theory of superfluidity in an imperfect Fermi gas," Sov. Phys. JETP **13**, 1018 (1961).

[27] S. Babu and G. E. Brown, "Quasiparticle interaction in liquid ^{3}He," Ann. Phys. **78**, 1 (1973).

[28] T. L. Ainsworth, K. S. Bedell, G. E. Brown, and K. F. Quader, "A model for paramagnetic Fermi systems," J. Low Temp. Phys. **50**, 319 (1983).

[29] K. S. Bedell and K. F. Quader, "p-wave superconductivity in heavy-fermion systems: An induced-interaction approach," Phys. Rev. B **32**, 3296 (1985).

[30] T. L. Ainsworth and K. S. Bedell, "Momentum-dependent scattering-amplitude model for liquid ^{3}He," Phys. Rev. B **35**, 8425 (1987).

[31] S. Gaudio, J. A. Jackiewicz, and K. S. Bedell, "Fermi liquid behavior and Luttinger's theorem close to a diverging scattering length," Philos. Mag. Lett. **89**, 1823 (2009).

[32] C. J. Pethick and H. Smith, *Bose-Einstein Condensation in Dilute Gases* (Cambridge University Press, New York, 2008).

[33] S. Nascimbene, N. Navon, K. J. Jiang, F. Chevy, and C. Salomon, "Exploring the thermodynamics of a universal Fermi gas," Nature **463**, 1057 (2010).

[34] J. Carlson, S. Y. Chang, V. R. Pandharipande, and K. E. Schmidt, "Superfluid Fermi gases with large scattering length," Phys. Rev. Lett. **91**, 050401 (2003).

[35] L. D. Landau and E. M. Lifshitz, *Quantum Mechanics: Non-relativistic Theory* (Elsevier, Amsterdam, 1977).

[36] K. S. Dy and C. J. Pethick, "Transport coefficients of a normal Fermi liquid: Application to liquid He^3," Phys. Rev. **185**, 373 (1969).

[37] C. J. Pethick, "Finite temperature corrections to the transport coefficients of a normal Fermi liquid," Phys. Rev. **177**, 391 (1969).

[38] V. J. Emery, "Solution of Boltzmann equation for degenerate Fermi systems," Phys. Rev. **175**, 251 (1968).

[39] V. J. Emery and D. Cheng, "Transport coefficients in degenerate Fermi systems," Phys. Rev. Lett. **21**, 533 (1968).

[40] J. C. Rainwater and R. Mohling, "Transport properties of Fermi fluids at finite temperatures," J. Low Temp. Phys. **23**, 519 (1976).

[41] G. M. Brunn, "Spin diffusion in Fermi gases," New J. Phys. **13**, 035005 (2011).

[42] R. K. Pathria, *Statistical Mechanics*, 2nd ed. (Butterworth-Heinemann, Oxford, 1996).

[43] L. Luo and J. E. Thomas, "Thermodynamic measurements in a strongly interacting fermi gas," J. Low Temp. Phys. **154**, 1 (2009).

[44] M. Houbiers, H. T. C. Stoof, W. I. McAlexander, and R. G. Hulet, "Elastic and inelastic collisions of ^{6}Li atoms in magnetic and optical traps," Phys. Rev. A **57**, R1497 (1998).

[45] S. Gaudio, J. A. Jackiewicz, and K. S. Bedell, "Many body exchange effects close to the *s*-wave Feshbach resonance in two-component Fermi systems: is a triplet superfluid possible?" Philos. Mag. Lett. **87**, 713 (2007).

[46] S. Das Sarma, "Spintronics," Am. Sci. **89**, 516 (2001).

[47] I. Zutic, J. Fabian, and S. Das Sarma, "Spintronics: Fundamentals and applications," Rev. Mod. Phys. **76**, 323 (2004).

[48] A. G. Aronov, "Spin injection in metals and polarization of nuclei," JETP Lett. **24**, 32 (1976).

[49] M. Johnson and R. H. Silsbee, "Spin-injection experiment," Phys. Rev. B **37**, 5326 (1988).

[50] H. P. Dahal and K. S. Bedell, "Effective spin diffusion in spin-polarized equilibrium and quasiequilibrium Fermi liquids," Phys. Rev. B **87**, 174406 (2013).

[51] H. Li and K. S. Bedell, "Quantum spin transport and dynamics through a ferromagnetic/normal metal junction," Phys. Rev. B **92**, 224437 (2015).

[52] K. S. Bedell and H. P. Dahal, "Spin waves in quasiequilibrium spin systems," Phys. Rev. Lett. **97**, 047204 (2006).

[53] K. S. Bedell and D. E. Meltzer, "Spin waves and spin diffusion in Fermi liquids: Bounds on effective diffusion coefficients," Phys. Rev. B **33**, 4543 (1986).

[54] V. P. Silin, "On the theory of a dengenerate electron fluid," JETP **6**, 387 (1958).

[55] A. G. Aronov and G. E. Pikus, "Spin injection into semiconductors," Sov. Phys. Semicond. **10**, 698 (1976).

[56] A. J. Leggett and M. J. Rice, "Spin echoes in liquid ^{3}He and mixtures: a predicted new effect," Phys. Rev. Lett. **20**, 586 (1968).

[57] A. J. Leggett, "Spin diffusion and spin echoes in liquid ^{3}He at low temperature," J. Phys. C **12**, 448 (1970).

[58] L. R. Corruccini, D. D. Osheroff, D. M. Lee, and R. C. Richardson, "Spin-wave phenomena in liquid ^{3}He systems," J. Low Temp. Phys. **8**, 229 (1972).

[59] K. S. Bedell and K. B. Blagoev, "Quantum spin hydrodynamics and a new spin-current mode in ferromagnetic metals," Philos. Mag. Lett. **81**, 511 (2001).

[60] P. M. Platzman and P. A. Wolff, "Spin-wave excitation in nonferromagnetic metals," Phys. Rev. Lett. **18**, 280 (1967).

[61] S. Schultz and G. Dunifer, "Observation of spin waves in sodium and potassium," Phys. Rev. Lett. **18**, 283 (1967).

[62] E. I. Rashba, "Diffusion theory of spin injection through resistive contacts," Eur. Phys. J. B **29**, 513 (2002).

[63] Y. Zhang, P. Farinas, and K. S. Bedell, "The "Higgs" amplitude mode in weak ferromagnetic metals," Acta Phys. Pol. A **127**, 153 (2015).

[64] T. M. Rice, "Landau Fermi-liquid parameters in Na and K," Phys. Rev. **175**, 858 (1968).

[65] N. W. Ashcroft and N. D. Mermin, *Solid State Physics*, 1st ed. (Harcourt, San Diego, 1976).

[66] S. Coutinho and R. Luzzi, "Conduction electron spin resonance - I," Revista Brasileira de Fisica **4**, 447 (1974).

[67] F. J. Dyson, "Electron spin resonance absorption in metals. II. Theory of electron diffusion and the skin effect," Phys. Rev. Lett. **98**, 349 (1955).

[68] A. Altland and B. Simons, *Condensed Matter Field Theory* (Cambridge University Press, New York, 2006).